1-1-2009

Signal Analysis For Cardiac Electrical Activation Studies

Elnaz Shokrollahi
Ryerson University

SIGNAL ANALYSIS FOR CARDIAC ELECTRICAL ACTIVATION STUDIES

Elnaz Shokrollahi, B.Eng
Ryerson University, 2007

A thesis
presented to Ryerson University
in partial fulfillment
of the requirements for the degree of
Master of Applied Science in the Program of Electrical Engineering

Toronto, Ontario, Canada, 2009

Author's Declaration

I hereby declare that I am the sole author of this thesis.
I authorize Ryerson University to lend this thesis to other institutions or individuals for the purpose of scholarly research.
Signature

I further authorize Ryerson University to reproduce this thesis by photocopying or by other means, in total or in part, at the request of other institutions or individual for the purpose of scholarly research.
Signature

Abstract

Signal Analysis for Cardiac Electrical Activation Studies

©Elnaz Shokrollahi, 2009

Masters of Applied Science
Electrical and Computer Engineering
Ryerson University

The aim of this study is to determine if some of the characteristics of reconstructed unipolar electrograms from the noncontact mapping system can be used to detect epicardial and to differentiate it from endocardial electrical activation in a canine heart. This would help the electrophysiologist know where exactly the origin of ventricular tachycardia or the critical point in tissue is located. Following this, arrhythmia can be successfully treated by ablating that part of the tissue of heart. Virtual electrograms were recorded while pacing the right ventricle of an open-chest dog at multiple endocardial and epicardial sites using the commercially available noncontact mapping system (EnSite Array^{TM} Catheter 3000). The endocardial and epicardial paced virtual electrograms from the juxtaposing sites allow for analyzing systematically the differences in their morphologies. Maximal dV/dt, area under the depolarization curve and latency extracted from unipolar electrograms demonstrated significant difference between epicardial and endocardial pacing sites with a p-value of less than 0.01 in all three cases. The above features were fed to a linear discriminant analysis based classifier and high classification accuracy was achieved. Therefore, reliable criteria can be proposed to allow for discrimination of an endocardial versus epicardial origin of electrical activation.

And also the endocardial and epicardial paced virtual electrograms from the juxtaposing sites allows for an estimate of the transfer function of the myocardium in different positions of the right ventricles of a canine heart. The transfer function estimation will aid in better mathematical modeling of myocardium and could be a sensitive measure of myocardial homogeneity and arrhythmic foci localization.

Another study was done on human heart. This study was to evaluate the ability of virtual electrograms to predict abnormal bipolar electrograms. We tested the hypothesis of max dV/dt, filtering and optimized DSM threshold. This allow better identification of abnormal myocardial substrate traditionally defined by contact bipolar mapping in human RVOT.

Acknowledgment

I would like to acknowledge Dr. Sri Krishnan for his continuous support and mentoring throughout my undergraduate and postgraduate experiences. His guidance and moral support has helped me to succeed beyond my imagination. I am indeed grateful to him for this. I would sincerely like to acknowledge Dr. Nanthakumar for his important contribution, kind encouragement, enlightening comments and suggestions and his compassionate support throughout the course of this thesis.

I would like to thank my parents and family for their continuous support and encouragement, which has given me the ability to pursue my goals with confidence and full determination. Special thanks goes to my sister, Mehrnaz Shokrollahi, who has also been my colleague and best friend from the first day of school at Ryerson University. With her around I always felt supported and encouraged.

I would also thank my fellow colleagues from Signal Analysis Research (SAR) group, especially Dr. Karthi Umapathy for the enlightening and informative discussions he had with me about my research. His timely research tips and motivation was helpful in different stages of my research. And I would also thank my fellow colleagues from The Toby Hull Cardiac Fibrillation Management Laboratory, Toronto General Hospital (TGH) for providing a stimulating research environment.I would acknowledge Stéphane Massé. Without his generous assistance and feedback the research work would have been impossible. I would like to thank Luc Soucie, Andrew Ramadeen, Dr. Tony and Talha Farid for their great help.

I would like to acknowledge St. Jude Medical for providing financial support during my graduate study. Last but not least, I would like to thank everyone at Ryerson University who provided me with the highest level of educational experience, which I will never forget.

Dedication

To my parents, Shohreh Kamali and Hadi Shokrollahi, to my brother Peyman Shokrollahi and my sister Mehrnaz Shokrollahi for their love, support and encouragement.

Contents

List of Figures

List of Tables

List of Acronyms

3D	3-Dimensional
AC	Alternating Current
ACT	Activated Clotting Time
AIC	Akaike Information Criteria
AR	Autoregressive
ARVC	Arrhythmogenic Right Ventricular Cardiomyopathy
AV	Atrioventricular
BEM	Boundary Element Method
BPM	Beat per Minuate
CS	Coronary Sinus
DF	Dominant Frequency
DSM	Dynamic Substrate Mapping
DWT	Discrete Wavelet Transform
EAM	Electroanatomic Mapping
ECG	Electrocardiogram
EMG	Electromyogram
EP	Electrophysiology
EMG	Electromyogram
FFT	Fast Fourier transform
FP	False Positive
FN	False Negative
ICD	Implantable Cardioverter Defibrillators
LDA	Linear Discriminant Analysis
LV	Left Ventricle
MEA	Multi Electrode Array
MRI	Magnetic Resonance Imaging
NS	None Significant
PNV	Peak Negative Voltage
PVC	Premature Ventricular Contraction
RA	Right Ventricle
RF	Radio Frequency
RMS	Root Mean Square
ROC	Receiver Operating Characteristics
RV	Right Ventricle
RVOT	Right Ventricular Outflow Track
SNR	Signal to Noise Ratio
TGH	Toronto General Hospital
TN	True Negative
TP	True Positive
VAG	Vibroarthrogram
VF	Ventricular Fibrillation
VT	Ventricular Tachycardia

Chapter 1

Introduction

FOR much of recorded history, humans have viewed cardiac arrest as irreversible. For religious and scientific reasons it was considered impossible, to attempt to reverse death. It was not until the latter part of the eighteenth century that humans began to believe that resuscitation was possible. Another 200 years passed before the skills for resuscitation were developed to a degree that made the reversibility of cardiac arrest a practical reality in the 1960s. Many important observations and much real progress had nevertheless been made during the intervening years. But the clinical problems were poorly understood, the implications of new discoveries were not always appreciated, single components of life-saving were attempted in isolation, procedures that were potentially effective were often displaced by those of no value, and suitable technology was lacking. Resuscitation had to await its time. As medicine advanced and people lived longer, heart disease became a serious health issue. In fact, according to the Heart and Stroke Foundation, every 7 minutes, someone dies from heart disease or stroke in the USA. Sudden cardiac arrest (SCA) is a major public health concern, as it claims the lives of more than 350,000 Americans every year more than breast cancer, accidents, homicide, AIDS and, stroke (Figure 1.1) [12]. The last 70 years have seen considerable refinement of our understanding of the electrophysiology, hemodynamics, and metabolic consequences of ventricular fibrillation. Despite intensive study, however, our understanding of the pathophysiology of this lethal ventricular arrhythmia is far from complete. Knowing exactly how the heart functions and utilize the technology available may

help in discoveries of lethal arrhythmias.

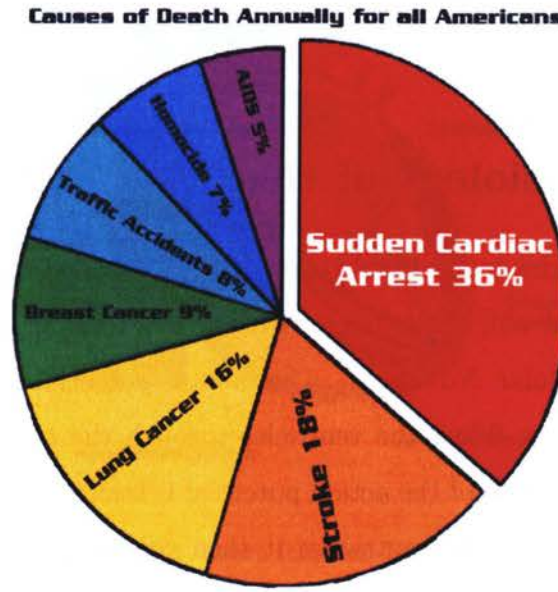

Figure 1.1: Death rate in the USA [1].

1.1 Motivation Behind this Study

The study of sustained ventricular tachycardia is often frustrating and frequently unsuccessful. Recently, considerable emphasis in the therapy of this arrhythmia has been placed on surgical, pacemaker modalities and drug therapy. Also the modern mapping systems, like the electroanatomic mapping system and the noncontact mapping has significantly improved the understanding of complex atrial and ventricular arrhythmias by allowing the direct association of electrical activity at a particular location with the corresponding anatomic structures. This combination finally resulted in a more effective targeting of RF energy applications in patients with atrial reentrant tachycardias and VTs. Both systems allow for reliable proof of the completeness of the induced RF current lesion lines, a major prerequisite for a successful procedure. Another decisive factor for a successful RF ablation procedure, beside the exact

identification of the critical zone for initiation and perpetual of the tachycardia, is the localization of the anatomic substrate within the atrial or ventricular wall. In this thesis, studying both temporal and spectral characteristics of the reconstructed unipolar electrograms may predict the origin of electrical activation with in ventricular walls.

1.2 Electrophysiology of Heart

Rhythmic contraction begins in the Sino-Atrial Node (also called the Sinus Node located on the superior posterolateral wall of the Right Atrium) due to its leaky membrane and larger concentration of extracellular Na^+ ions. This action potential is conducted throughout the atria; the atria contract filling the ventricles through the atrioventricular (mitral and tricuspid) valves. Transmission of the action potential is stalled at the atrioventricular node (AV node) to allow filling of the ventricles; it then proceeds quickly along the Purkinje fibers to the entire left and right ventricular walls, triggering coordinated contraction of the ventricles (Figure 1.2). This part of the cycle, which forces blood out of the heart to both the general and the pulmonary circulation is called Systole.

Heart is a muscular organ responsible for pumping blood through the blood vessels by repeated and rhythmic contractions. The average human heart beats 72 beats per minute (BPM). The function of right side of the heart is to collect de-oxygenated blood, in the right atrium, from the body and pump it, via the right ventricle, into the lungs so that the carbon dioxide can be dropped off and oxygen picked up. The left side of the heart collects oxygenated blood from the lungs into the left atrium. From the left atrium the blood moves to the left ventricle, which pumps it out to the body. This blood pumping is all electrical activities that help the heart muscles to contract and pass blood through the body (Figure 1.3).

Every living cardiac cell undergoes a regular sequence of electrical changes that initiate the contractile activity (systole) and the relaxation (diastole) of the cell. Thus, the contraction of the heart is associated with a compound action potential that is initiated at the sinus

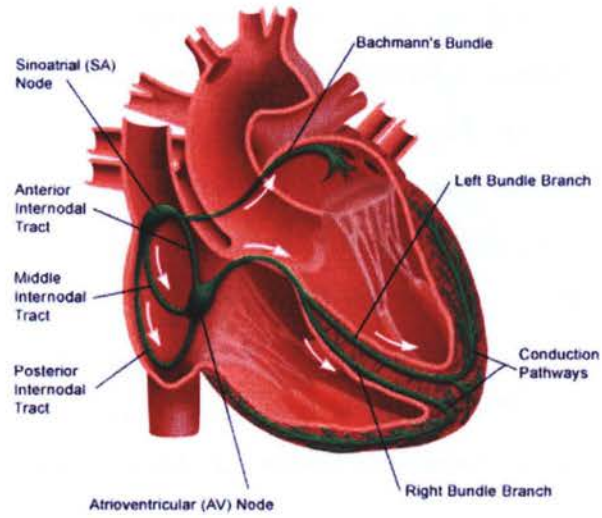

Figure 1.2: Heart Rhythm Structure [2].

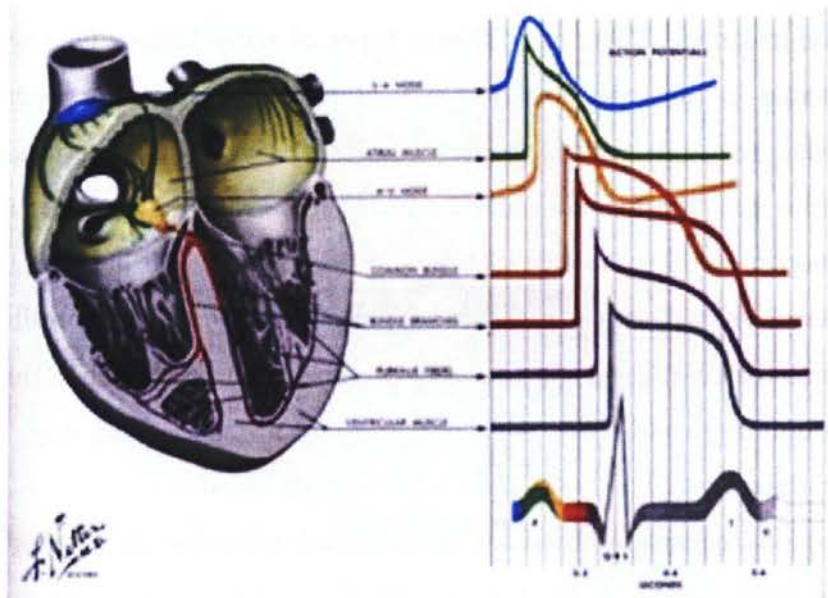

Figure 1.3: Heart Electrical Activity. Relation of action potential from the various cardiac regions to the body surface ECG [3].

node and sweeps over the conduction path of the heart, preceding the mechanical contraction of the cardiac fibers. During this depolarization and repolarization of the myocardium, a potential difference is created between different regions on the surface of the heart. A separation of charge or potential difference is called a dipole. The electrical potential of the dipole is conducted through an electrolyte solution, such as the interstitial fluid and blood plasma, and eventually reaches the surface of the skin. By placing electrodes on the skin surface, we are able to detect and record the electrical activity over the heart surface prior to its contraction. The electrocardiogram (EKG/ECG) is a graphic record of the action potentials of the heart. It is recorded with an electrocardiograph, and the study of this cardiac electrical activity is called electrocardiography. By measuring the potential changes in various directions across the heart, it is possible to detect abnormalities.

1.3 Heart Arrhythmia

If the conduction path does not work properly it will produce different types of life-threatening abnormalities, which are called arrhythmias. An irregular heart beat is an arrhythmia. Heart rates can also be irregular. There are different types of arrhythmias. One type of arrhythmia that originated in the ventricles of the heart is called ventricular tachycardia (VT). This happens when the lower part of the heart starts beating faster than usual (Figure 1.4). Therefore, blood is not pumped efficiently through the body and even heart itself. So heart won't deliver enough blood to its own muscle and heart attack will happen.

The heart beats when electrical signals move through it. Ventricular fibrillation (VF) is a condition in which the heart's electrical activity becomes disordered. When this happens, the heart's lower (pumping) chambers contract in a rapid, unsynchronized way. The ventricles "flutter" rather than beat. The heart pumps little or no blood.

VF is very serious, collapse and sudden cardiac death will follow in minutes unless medical help is provided immediately. If treated in time, VF and VT (extremely rapid heartbeat) can be converted into normal rhythm. This requires shocking the heart with a device called a defibrillator.

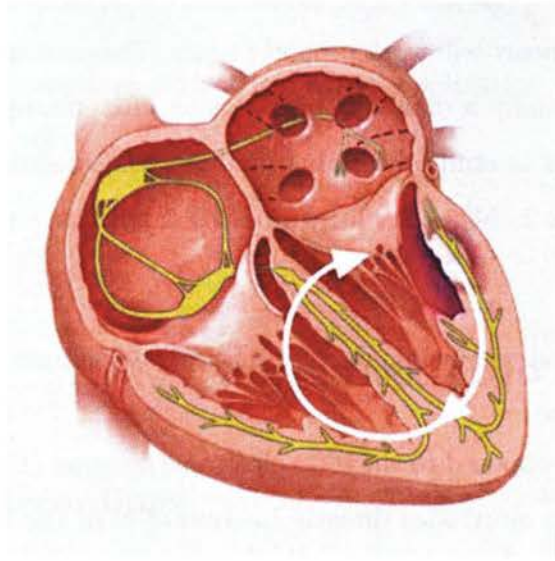

Figure 1.4: Ventricular Tachycardia [4].

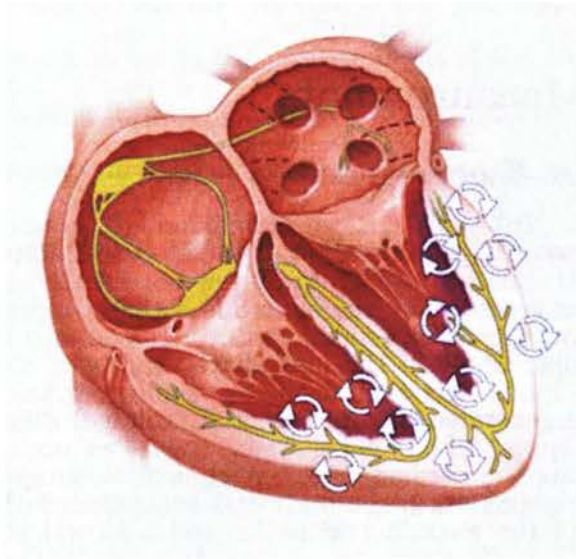

Figure 1.5: Ventricular Fibrillation [4].

Physicians and electro-physiologist are working on these abnormalities to find out where exactly these abnormalities start. If they know where exactly is its origin, they can burn that part of the tissue so heart will work properly again. Diagnosing this tachycardia usually is troublesome as it is usually a diagnosis of exclusion after multiple ablation attempts on the endocardium. In order to study these abnormalities some definitions needs to be covered here.

1.4 Definition of Electrogram

The term electrogram, as opposed to the term electrocardiogram (ECG), denotes a recording of cardiac potentials from electrodes directly in contact with the heart [13]. Electrograms form the raw data for cardiac mapping, which has been defined as: "a method by which potentials recorded directly from the surface of the heart are spatially depicted as a function of time in an integrated manner," and which is important as both a research tool and a method for guiding therapy.

1.5 Baseline Measurements

1.5.1 Intra-cardiac Electrograms

While the surface ECG records, a summation of the electrical activity of the entire heart, intra-cardiac electrograms recorded by the electrode catheter represent only the electrical activity of the local cardiac tissue in the immediate vicinity of the catheter's electrodes. Cardiac electrograms are generated by the potential (voltage) differences recorded at two recording electrodes during the cardiac cycle. A clinical electrogram is connected to the anodal (positive) input of the recording amplifier and a second source that is connected to the cathodal (negative) input [14]. Recorded electrograms can provide three important pieces of information:

1. The local activation time that is, the time of activation of myocardium immediately adjacent to the recording electrode relative to a reference;

2. The direction of propagation of electrical activity activation within the field of view of the recording electrode;

3. The complexity of myocardial activation within the field of view of the recording electrode.

There are two major cardiac electrogram recordings which their definitions are covered in the following section.

1.5.2 Unipolar Recordings

Unipolar recordings are obtained by positioning the exploring electrode in the heart and the second electrode (usually referred to as the indifferent electrode) distant from the heart so that is has little or no cardiac signal. The precordial ECG leads, for example, are unipolar recordings that use an indifferent electrode created by connecting the arm and left leg electrodes through high-impedance resistors. By convention, the exploring electrode in contact with the cardiac tissue is connected to the positive input of the recording amplifier. In this configuration, an approaching wavefront creates a positive deflection that quickly reverses itself as the wavefront passes directly under the electrode, generating an RS complex. In a normal homogeneous tissue, the maximum negative slope (dV/dt) of the signal coincides with the arrival of the depolarization wavefront directly beneath the electrode, because the maximal negative dV/dt corresponds to the maximum Na^+ channel conductance.

The unfiltered unipolar recordings provide information about the direction of impulse propagation; positive deflections (R waves) are generated by propagation toward the recording electrode, and negative deflections (QS complexes) are generated by propagation away from the electrode. The unipolar electrograms are generally unfiltered (0.05 to 300 Hz), but are usually filtered at comparable settings to those of bipolar electrograms (10 to 40 to 300 Hz or more) when an abnormal tissue (scars or infarct areas) is studied, for which

local electrograms can have very low amplitude and can be masked by larger far-field signals. Filtering the unipolar electrograms can help eliminate far-field signals; however, filtered unipolar recordings lose the ability to provide directional information [14], [15], [16].

The major disadvantage of unipolar recordings is that they contain substantial far-field signals generated by depolarization of tissue remote from the recording electrode. Another disadvantage is the inability to record an undisturbed electrogram during or immediately after pacing [17].

1.5.3 Bipolar Recordings

Bipolar recordings are obtained by connecting two electrodes that are exploring the area of interest to the recording amplifier. At each point in time, the potential generated is the sum of the potential from the positive input and the potential at the negative input. The potential at the negative input is inverted; this is subtracted from the potential at the positive input so that the final recording is the difference between the two. Unlike unipolar recordings, bipolar electrodes with short interpolar distance are relatively unaffected by far−field events. The bipolar electrogram is simply the difference between the two unipolar electrograms recorded at the two poles. Because the far-field signal is similar at each instant in time, it is largely subtracted out, leaving the local signal [14], [16]. Therefore, compared with unipolar recordings, bipolar recordings provide an improved signal-to-noise ratio, and high-frequency components are well picked-up.

Several factors can affect bipolar electrogram amplitude and width, including conduction velocity (the greater the velocity, the higher the peak amplitude of the filtered bipolar electrogram), the mass of the activated tissue, the distance between the electrode and the propagating wavefront, the direction of propagation relative to the bipoles, the inter-electrode distance, the amplifier gain, and other signal processing techniques that can introduce artifacts [14], [16].

The direction of wavefront propagation cannot be reliably inferred from the morphology of the bipolar signal. Moreover, bipolar recordings do not allow simultaneous pacing and

recording from the same location. The difference in unipolar and bipolar recordings can be used to assist in mapping by simultaneously recording bipolar and unipolar signals from the mapping catheter. Although bipolar recordings provide sufficient information for most mapping purposes in clinical EP laboratories, simultaneous unipolar recordings can provide an indication of the direction of wavefront propagation and a more precise measure of the timing of local activation [17].

1.6 Electrophysiology (EP) Studies

Electricity flows throughout the heart in a regular measured pattern. As mentioned earlier, this electrical system brings about heart muscle contractions. A problem anywhere along the electrical pathway causes an arrhythmia, or healthy rhythm disturbance. Arrhythmias, by their very nature, are unpredictable and intermittent, which makes it unlikely that an ECG will capture the underlying electrical pathway problem. An electrophysiologic, or EP, is somewhat invasive and provides information that is key to diagnosing and treating arrhythmias. During this study a specially trained cardiac specialist may provoke arrhythmia events and collect data about the flow of electricity during actual events.

The study is performed after giving local anesthesia and conscious sedation (twilight sleep) to keep the patient as comfortable as possible. The procedure involves inserting a catheter - a narrow, flexible tube- attached to electricity monitoring electrodes, into a blood vessel, often through a site in the groin or neck, and winding the catheter wire up into the heart. The journey from entry point to heart muscle is navigated by images created by a fluoroscope, an x−ray−like machine that provides continuous, "live" images of the catheter and heart muscle. Once the catheter reaches the heart, electrodes at its tip gather data and a variety of electrical measurements are made (Figure 1.6). These data pinpoint the location of the faulty electrical site. During this "electrical mapping", the cardiac arrhythmia specialist, an electrophysiologist, may instigate, through pacing (the use of tiny electrical impulses), some of the very arrhythmias that are the crux of the problem. The events are safe, given the range of experts and resources close at hand and are necessary to ensure the precise

location of the problematic tissue.

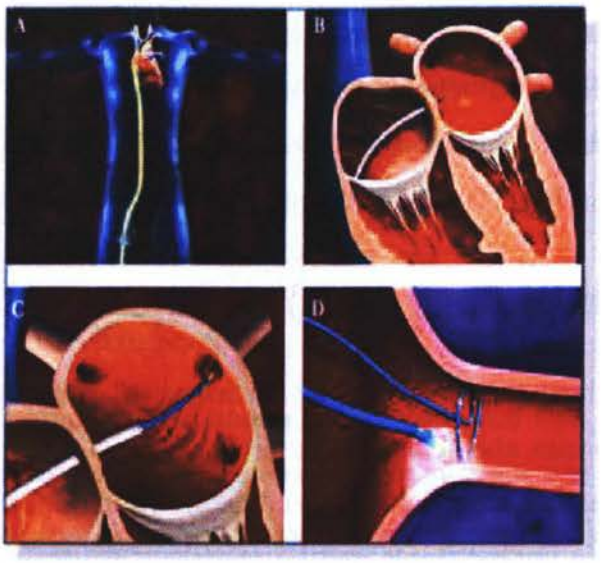

Figure 1.6: Electrophysiology Study on Human Heart.

Current techniques of mapping potentials directly from the endocardium present certain difficulties. Limited in the number of recording sites, intravascular multi−electrode catheter mapping is time consuming, and data are collected over many beats. Therefore, this approach cannot be used on a beat by beat basis to study dynamic changes in the activation process [18]. Multi−electrode endocardial balloons or sponges, although capable of mapping the entire endocardium, occlude the cavity and require open heart surgery, heart−lung bypass, and other complicated and risky procedures [18], [19], [20]. Conventional contact catheter mapping procedure is dependent on myocardial contact and the multiple regions sampled as it relies on recording of endocardial electrograms sequentially from a small, localized area of myocardium. The noncontact mapping system, using the inverse solution, can create a voltage map based on reconstructed far−field signals from the noncontact catheter.

1.7 Noncontact Mapping

In recent studies, a mathematical method is used to reconstruct the endocardial potential distribution from cavitary potential measured with a multi−electrode array (MEA) that is not in direct contact with the endocardium. The mapping system (EnSite; Endocardial Solutions Inc., St. Paul, Minnesota, USA) is a computerized (Silicon Graphics, Mountain View California) and custom−built amplifier electrophysiology recording system that consists of a 9 French catheter with a distally located braided 64 electrode array that is deployed by a 7.5 mL balloon filled with a mixture of saline and contrast medium (Figure 1.7). The probe was inserted via a femoral vein (9 French sheath) and advanced into the right atrium (RA) and into the right ventricle (RV). Each wire has a 0.025−in break in insulation, producing a noncontact unipolar electrode [21]. The raw far−field electrographic data from the MEA are acquired and fend into a multichannel recorder and amplifier system, sampled at 1.2 kHz, and filtered with a bandwidth of 0.1 to 300 Hz. The amplifier also has 16 channels for contact catheters and 12 for surface ECG. A ring electrode located on the proximal shaft of the MEA catheter in the descending aorta is used as a reference for both noncontact and contact unipolar electrogram recordings. Intravenous heparin is infused to keep activated clotting time (ACT) at 250 − 300 seconds.

The system can locate any conventional mapping−ablation catheter in space with respect to the array catheter (and thus with respect to the cardiac chamber being mapped). A low current (5.68 Hz) locator signal is passed between the contact catheter electrode being located and reference electrodes on the noncontact array. This creates a potential gradient across the array electrodes, which is then used to position the source. This locator system is also used to construct the 3−D computer model of the endocardium that is required for the reconstruction of endocardial electrograms and isopotential maps. This model is acquired by moving a conventional contact catheter around the endocardial surface of the cardiac chamber; the system collects the location information, building up a series of coordinates for the endocardium, and generating a patient−specific, anatomically contoured model of its geometry. During geometry creation, only the most distant points visited by the roving

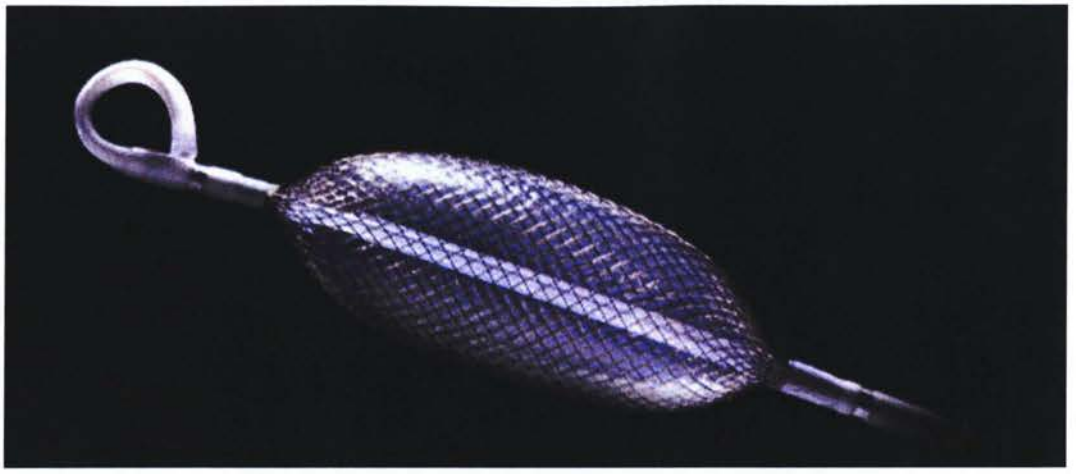

Figure 1.7: Noncontact mapping catheter. The noncontact mapping catheter is shown with its braided microelectrode array and 7.6 ml balloon deployed [5].

catheter are recorded to ignore those detected when the catheter is not in contact with the endocardial wall.

Using mathematical techniques to process potentials recorded from the array, the system is able to reconstruct more than 3000 unipolar electrograms simultaneously and superimpose them on the virtual endocardium, producing isopotential maps with a color range representing voltage amplitudes (Figure 1.8). Additionally, the locator signal can be used to display and track the position of any catheter on the endocardial model and allows marking of anatomical locations identified using fluoroscopy and electrographic characteristics. Therefore, by moving the ablation catheter around endocardium with respect to the MEA, low−current "locator" signal between the catheter being located and alternately between ring electrodes proximal and distal to the MEA on the noncontact catheter, multiple spatial points are identified.

These points were collected from multiple RV endocardial sites, and a three−dimensional (3−D) RV geometry was generated by interpolation between the mapped sites and defining boundaries. Anatomic structures were labeled on the 3−D geometry by determining the

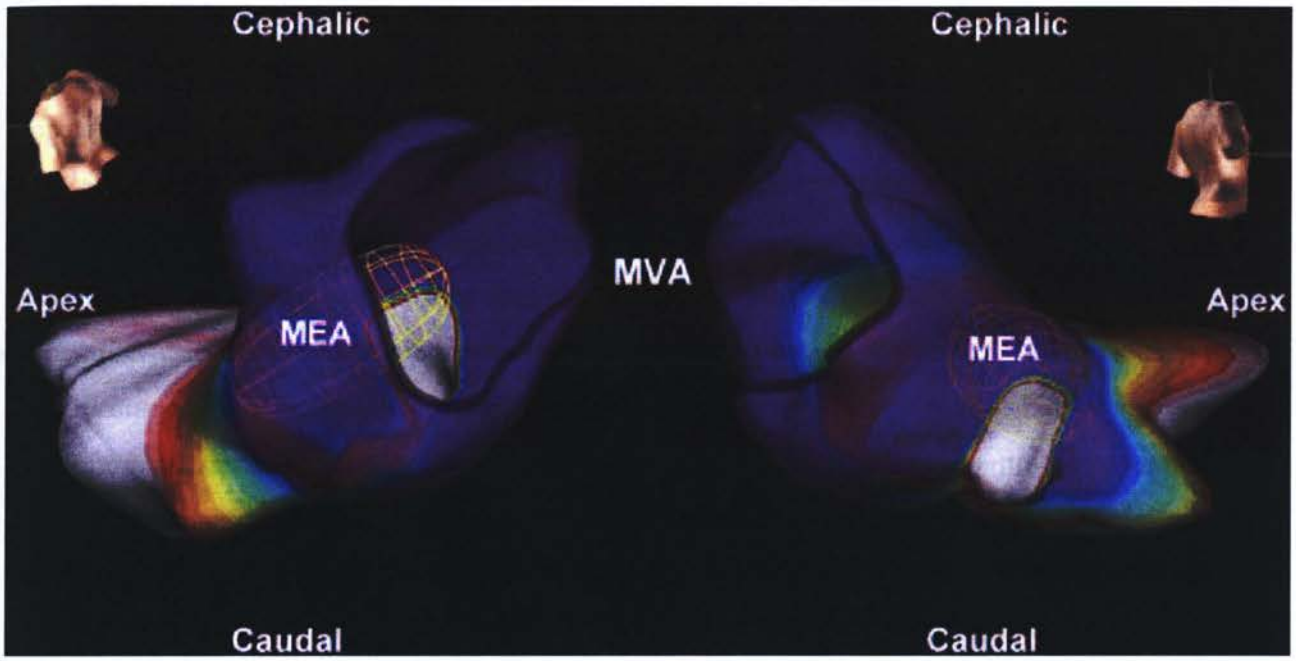

Figure 1.8: Isopotential maps recorded during ventricular tachycardia. The virtual endocardium may be rotated and the orientation in 3D space is depicted by the torso in the corner of the image. These maps are translucent allowing visualization of the entire activation map and the MEA [6].

catheter position from fluoroscopy and electrogram recordings, and defining those structures on the 3−D geometry at those sites. Using inverse solution mathematics, the system calculates the real−time endocardial potentials simultaneously at more than 3000 virtual sites these electrograms are of lower amplitude and frequency than the source on the endocardium. The technique to enhance and resolve these far−field potentials has been devised based on an inverse solution to Laplace's equation by use of a boundary element method (BEM). The inverse solution considers how a signal detected at a remote point will have appeared at the source, and the BEM is a method for applying the inverse solution to resolve a matrix of such signals from a source at a known boundary (e.g. the blood−endocardial boundary). Laplace equation can describe the potential distribution on the MEA created by potentials at the blood−endocardial boundary. The potential field at any 1 electrode is influenced to a degree by the potentials from the entire endocardium, the degree of influence being inversely proportional to the distance between the electrode and each endocardial point.

The potential field created on the MEA surface is therefore related to the MEA−endocardial geometry matrix. When the geometry matrix is known, it is possible to compute with inverse solution of Laplace's equation the endocardial electrograms from the MEA potentials. Because inverse solution is inherently ill posed which means inaccuracy in the MEA−endocardial geometry matrix results in large errors, regularization technique based on Tikhonov is used [22]. The accuracy of reconstruction of endocardial electrograms is therefore dependent on the solution to Laplace's equation, the regularization technique used, and the accuracy of the geometry matrix. Errors in geometry will still occur and may be related to the number of endocardial points sampled and the complexity of the geometry of the chamber.

In addition, the most recent version of the EnSite software provides the capability of point by point contact mapping, allowing the creation of activation and voltage maps by acquiring serial contact electrograms and displaying them on the virtual endocardium. This is useful for adding detail, familiarity, and validation of the information obtained by the noncontact method [23].

1.7.1 Clinical Implications with EnSite

The MEA has been successfully deployed in all four chambers. The biggest advantage of noncontact endocardial mapping is its ability to recreate the endocardial activation sequence from simultaneously acquired multiple data points over a few tachycardia beats, without requiring sequential point−to−point acquisitions, obviating the need for prolonged tachycardia episodes that the patient might tolerate poorly. The animated spread of the depolarization wave can be visualized by the isopotential maps generated at successive cross sections of time. These maps are particularly useful for identifying slowly conducting macroreentrant pathways.

Mapping multiple cardiac cycles in real time is also the advantage of noncontact mapping. Mapping cardiac cycles will disclose changes in the activation sequence from one beat to the next. Because mapping data are acquired without conventional electrode catheters being in direct contact with the endocardium, use of noncontact mapping can help avoid the mechanical induction of ectopic activity that is frequently seen during conventional mapping. The device enables interpolation and analysis of unipolar electrograms. It also provides information on focus localization and signal morphology. These parameters are set with different filter settings.

1.8 Signal Filtering

The signal sampling processing may require filter settings that are sensitive and selective to enable visualization of early low amplitude signal components and suppress repolarization related far−filed signal elements. The surface ECG is usually filtered at 0.1 Hz to 100 Hz. The bulk of the energy is in the 0.1 Hz to 20 Hz range. Because of interference from alternating current (AC), muscle twitches, and similar relatively high−frequency interference, it is sometimes necessary to record the surface ECG over a lower frequency range or to use notch filters. Amplifiers are also used to filter the low and high frequency content of

the intracardiac electrograms. Intracardiac electrograms are usually filtered to eliminated far−field noise, typically at 30 Hz to 500 Hz.

High−Pass Filtering: High−pass filtering helps attenuate the frequencies that are slower than the specified cutoff of the filter. If intracardiac recording were not filtered, the signal would oscillate up and down as this potential fluctuated with respiration, catheter movement, and variable catheter contact.

For bipolar electrograms, high−pass filters with corner frequencies between 10 and 50 Hz are commonly used. Filtering can distort the electrogram morphology and reduce its amplitude. Unipolar signals are commonly filtered at 0.05 to 0.5 Hz to remove baseline drift. Filtering at higher cutoff frequencies (e.g. 30 Hz) alters the morphology of the signal so that the morphology of the unipolar signal is no longer an indication of the direction of wavefront propagation. However filtering the unipolar signal does not affect its usefulness as a measure of the local activation time.

Low−Pass Filtering: Low−pass filters attenuate frequencies that are faster than the specified cutoff frequency (usually 250 to 500 Hz). This is useful for reducing high−frequency noise and, at these frequencies, does not substantially affect electrograms recorded with clinical systems because most of the signal content is lower than 300 Hz.

Band−Pass Filtering: Defining a band of frequencies to record, such as setting the high-pass filter to 30 Hz and the low−pass filter to 300 Hz, defines a band of frequencies from 30 to 300 Hz that are not attenuated (i.e. band−pass filtering). A notch filter is a special case of band pass filtering, with specific attenuation of frequencies at 50 or 60 Hz to reduce electrical noise introduced by the frequency of common AC current.

Identification of true local activation and its differentiation from far−filed signals or repolarization waves is essential to successful utilization of EnSite system. This problem may be emphasized with unipolar, noncontact mapping because signals detected by the array initially are amplified to derive the endocardial map. Thus, low−frequency noise, repolarization waves, or far−field signals in the measured cavity will be magnified into larger signals on the reconstructed chamber. Therefore, filter setting is required to enable visualization

of early low amplitude signal components and suppress repolarization related to far−field signal elements.

1.9 Organization of the Thesis

This project mostly focuses on the differentiating the endocardial and epicardial electrical activation. This will help find the origination of arrhythmia (mostly VT) and thus a selection of appropriate therapeutic intervention and ablation strategies. To this end, Chapter 2 explains the fundamental and some of the algorithms. The remainder of this report is organized as shown in Figure 1.9.

In this thesis, two sets of data were collected. One set was gathered at TGH where combined contact and noncontact mapping are performed in 6 consecutive patients with symptomatic right ventricle outflow track (RVOT) morphology premature ventricular beats and structurally normal beats. All procedures were performed in the fasting, non−sedated state with continuous electrocardiograph and noninvasive haemodynamic monitoring. The signal analysis on this data will construct Chapter 3. The other set was gathered at St. Michael's hospital on a canine heart. This was an open chest experiment in which both endocardially paced and epicardially paced electrograms were recorded for further analysis. The signal analysis in both time and frequency domain on the data will construct Chapter 4. Chapter 5, the last chapter, presents the conclusions, recommendations, and future works resulting from the presented studies.

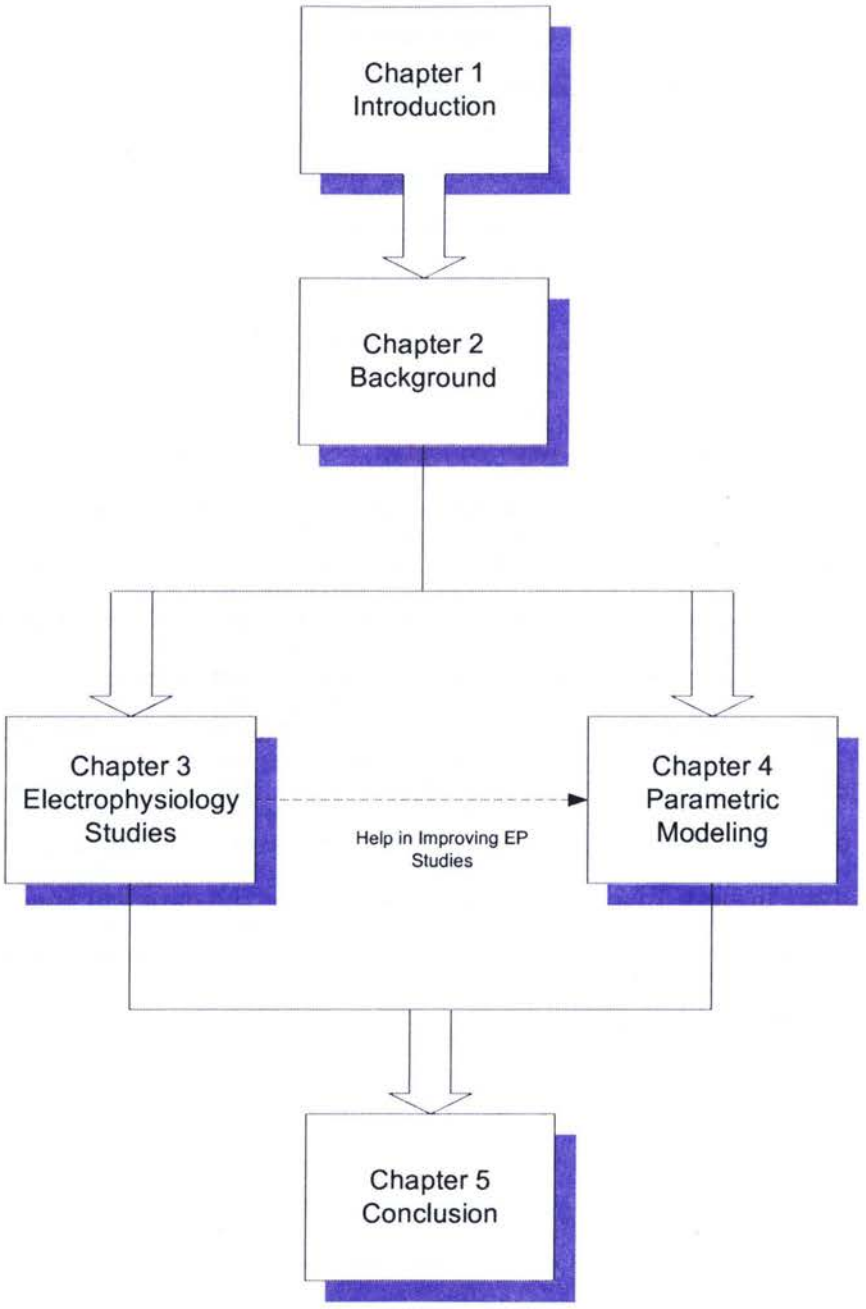

Figure 1.9: Organization of thesis.

Chapter 2

Background

PATIENTS who survive sudden cardiac death are often then found to have ischaemic heart disease (a disease characterized by reduced blood supply to the heart muscle) and inducible VT. Treatment of these patients is difficult. Pharmacologic treatment suppresses less than half of them [24]. Implantable defibrillators only offer partial treatment of arrhythmia and as such are not ideal particularly for patients with frequent arrhythmias, slow VT, or atrial fibrillation with a rapid ventricular response. Catheter ablation is an attractive alternative treatment as it offers the potential for long term prevention of VT with a lower risk than surgical ablation [25]. Catheter ablation is an invasive procedure used to remove a faulty electrical pathway from the hearts of those who are prone to developing cardiac arrhythmias. Only 10% of patients with re−entrant VT have been considered suitable for catheter ablation using conventional techniques [26], mainly because of hemodynamic intolerance of the tachycardia which limits the time available for mapping by conventional sequential catheter techniques. This is reflected in the success rate of catheter ablation using conventional techniques. Although 69−90% of VT are not inducible immediately after catheter ablation, long term recurrence rates are high.

Mapping of endocardial potential is an important procedure for studying normal and pathologic characteristics of the cardiac excitation process. Mapping the endocardial potential distribution and its evolution in time is useful for analyzing activation patterns, locating arrhythmogenic sites, and identifying areas of abnormal activity and slow conduction. Accu-

rate localization of the arrhythmogenic site in patients with ventricular arrhythmias is critical to the success of non−pharmacologic interventions, such as catheter ablation, to abolish the arrhythmia. Furthermore, analyzing the activation pattern is critical to understanding the underlying mechanism of an arrhythmia and thus to the selection of appropriate therapeutic intervention and ablation strategies [12].

Much has been learned from animal models using multielectrode arrays attached to the epicardial surface of the heart and optical mapping; however, these techniques cannot be easily applied in humans. Mapping the human arrhythmia has been limited to multielectrode arrays applied to small ares of one of the chambers of the hearts during nonphysiological conditions of cardiac surgery [27],[28]. In this Chapter, two mapping techniques will be covered but before that, the motivation behind this study and fundamental concepts should be covered.

2.1 Fundamental Concepts

Essential to the effective management of any cardiac arrhythmia is: thorough understanding of the mechanisms of its initiation and maintenance. Conventionally, this has been achieved by careful study of the surface ECG and correlation of the changes therein with data from intra−cardiac electrograms recorded by catheters at various key locations within the cardiac chambers (i.e., activation mapping). A record of these electrograms documenting multiple sites simultaneously is studied to determine the mechanisms of an arrhythmic event.

The main value of intra−cardiac and surface ECG tracings is the timing of electrical events and determining the direction of impulse propagation. Additionally, electrogram morphology can be of significant importance during mapping. Interpretation of recorded electrograms is fundamental to the clinical investigation of arrhythmias during EP studies. Establishing electrogram criteria, which permits accurate determination of the moment of myocardial activation at the recording electrode, is critical for construction of an area map of the activation sequence. Bipolar recordings are generally used for activation mapping.

Unipolar recordings are used to supplement the information obtained from bipolar recordings. The recordings can be used to assist in mapping by simultaneously recording bipolar and unipolar signals from the mapping catheter [23], [14].

2.1.1 Unipolar Recordings

Unipolar electrograms represent electrical activity form the entire heart, although contribution from distant events decreases in proportion to the square of the distance from the unipolar electrode.

Timing of Local Activation. The major component of the unipolar electrogram allows determination of the local activation time, although there are exceptions. The point of maximum amplitude, the zero crossing, the point of maximum slope (maximum first derivative), and the minimum second derivative of the electrogram have been proposed as indicators for underlying myocardial activation. The maximum negative slope (i.e., maximum change in potential, dV/dt) of the signal coincides best with the arrival of the depolarization wavefront directly beneath the electrode because the maximal negative dV/dt corresponds to the maximum sodium channel conductance [15]. In normal tissue the maximum negative slope is a good indication of local depolarization. In abnormal regions, such as infarct scars, the tissue beneath the recording electrode may be small relative to the surrounding myocardium outside the scar.

Direction of Local Activation. The morphology of the unfiltered unipolar recording indicates the direction of wavefront propagation. By convention, the mapping electrode that is in contact with the myocardium is connected to the positive input of the recording amplifier. In this configuration, positive deflections (R waves) are generated by propagation toward the recording electrode, and negative deflections (QS complexes) are generated by propagation away from the electrode. If a recording electrode is at the source from which all wavefronts propagate (at the site of initial activation), depolarization produces a wavefront that spreads away from the electrode, generating a monophasic QS complex. When the unipolar is not in contact with the myocardium but floating in the cavity, the initial negative

slope of the recording is typically slow. This will suggest that the electrogram is a far−field signal, generated by tissue some distance from the recording electrode.

Filtering at higher corner frequencies (e.g. 30 Hz) alters the morphology of the signal, so that the morphology of the unipolar signal is no longer an indication of the direction of wavefront propagation and the presence or absence of a QS complex cannot be used to infer proximity to the site of earliest activation [15], [29].

Advantages of Unipolar Recordings. One important value of unipolar recordings is that they provide a more precise measure of local activation. This is true for filtered and unfiltered unipolar electrograms. In addition, unfiltered unipolar recordings provide information about the direction of impulse propagation. Using the unipolar configuration also eliminates a possible anodal contribution to depolarization and allows pacing and recording at the same location. This generally facilitates the use of other mapping modalities.

Disadvantages of Unipolar Recordings. The major disadvantage of unipolar recordings is that they have poor signal−to−noise ratio and contain substantial far−field signal generated by depolarization of tissue remote from the recoding electrode. Therefore, distant activity can be difficult to separate from local activity. This is especially true when recording from areas of prior myocardial infarction, where the fractionated ventricular potentials are ubiquitous and it is often impossible to select a rapid negative dV/dt when the entire QS potential is slowly inscribed−that is, cavity potential [15], [29].

2.1.2 Bipolar Recordings

Bipolar recording is useful for recording local activity and fractionated potentials.

Timing of Local Activation. Algorithms for detecting local activation time from bipolar electrograms have been more problematic, partly because of generation of the bipolar electrogram by two spatially separated recording poles. In homogeneous sheet of tissue, the initial peak of a filtered (30 to 300 or more Hz) bipolar signal, the absolute maximum electrogram amplitude, coincides with depolarization beneath the recording electrode,

appears to correlate more consistently with local activation time, and corresponds to the maximal negative dV/dt of the unipolar recording. To acquire true local electrical activity, a bipolar electrogram with an interelectrode distance less than 1 cm is desirable. Smaller interelectrode distances record increasingly local events. Elimination of far−field noise is usually accomplished by filtering the intracardiac electrograms typically at 30 to 500 Hz [15], [29].

Direction of Local Activation. The morphology and amplitude of bipolar electrograms are influenced by the orientation of the bipolar recording axis to the direction of propagation of the activation wavefront. A wavefront that is propagating in the direction exactly perpendicular to the axis of the recording dipole produces no difference in potential between the electrodes, and hence no signal [15], [29]. The direction of wavefront propagation however cannot be reliable to the morphology of the bipolar signal although a change in morphology can be useful findings [15], [29]. For example, when recoding from the lateral aspect of the cavotricuspid isthmus during pacing from the coronary sinus (CS), a reversal in the bipolar electrogram polarity from positive to negative at the ablation line indicates complete isthmus block.

Advantage of Bipolar Recordings. Bipolar recordings provide an improved signal−to−noise ratio, and high frequency components are more accurately seen, which facilitates identification of local depolarization, especially in abnormal areas of infarction or scar.

Disadvantages of Bipolar Recordings. In contrast to unipolar signals, the direction of wavefront propagation cannot be reliably inferred from the morphology of the bipolar signal. Furthermore, bipolar recordings do not allow simultaneous pacing and recording from the same location.

Example of unipolar and bipolar electrogram is in Figure 2.1.

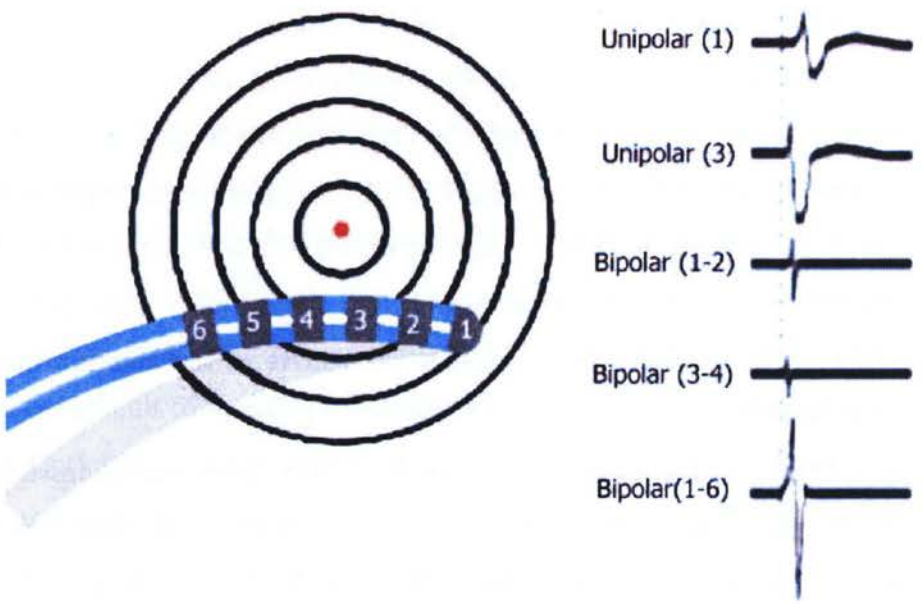

Figure 2.1: Example of Unipolar and Bipolar Electrogram Recorded with Multipolar Electrode Catheter. The red dot is the point source of activation [7].

2.1.3 Comparison During Cardiac Mapping

Both unipolar and bipolar configurations have been used by various investigators to record cardiac electrical activity [30], [31]. However, controversy exists as to which is the preferred electrode configuration for the detection of local cardiac activation. The characteristics of the two electrode configurations suggest that they may provide complementary information during cardiac mapping studies, although direct comparisons of the relative merits of unipolar and bipolar recordings have not been undertaken in the clinical setting. Therefore, different mapping techniques use either of the two configurations.

2.2 Two Different Mapping Techniques

Accurate mapping is the corner stone to successful ablative therapy of cardiac arrhythmias because it provides insight into the arrhythmia mechanism and identifies the location of a suitable target for ablation. Ablation of these arrhythmias is critically dependent on locating the abnormal depolarization that completes the diastolic pathway. Using conventional mapping techniques it has been possible to treat a wide range of arrhythmias with high success and low complication rates. However, identification of the target diastolic pathway is difficult and time consuming because conventional methods of mapping involve sequential recording from a limited number of sites by moving a deflectable catheter. The concept of noncontact mapping was introduced by Taccardi [32]. This technique employs mathematical methods to compute electrograms simultaneously and produce high resolution color maps of activation in the intact beating heart.

2.2.1 Conventional Mapping

Bipolar electrograms can also be recorded from the distal electrode pair sequentially during sinus rhythm along the endocardial noncontact geometry. Detecting low amplitude bipolar signals and creating myocardial surrogate maps have become a corner stone in interventional electrophysiology [33]. This technique has some disadvantages one is that, it is time

consuming as endocardial bipolar electrograms are recorded sequentially and is also heavily dependent on density of areas interrogated. Second, focal lesion creation may not be sufficient to ablate VT conducting through a broad isthmus region. And also, with the linear ablation technique, confirming continuity of linear lesion and identification of points of breakthrough may be challenging. However, conventional mapping offers the advantage of direct voltage mapping to identify regions of low voltage or scar area.

2.2.2 Dynamic Substrate Mapping

Noncontact mapping uses the dynamic substrate mapping (DSM) to mark the areas of low voltage. DSM marks the areas of substrate of activation by observing how isopotential maps display the wavefront moving around lines of block, anatomic barriers, zones of slow conduction, or diseased tissue. After 3−D geometry is created a high−density virtual electrograms is displayed as sequential isopotential maps. Electrograms are filtered between 2 Hz and 100 Hz. Noncontact mapping uses the unipolar virtual electrograms to define the areas of abnormal myocardial substrate. This is unlike the conventional contact mapping which defines substrate using the amplitude of bipolar electrograms. Substrate is defined as area of consistently low peak negative voltage (PNV) (< 50 % of the largest peak negative).

DSM is one such algorithm that is thought to identify abnormal myocardial substrate using electrogram amplitude feature. DSM is color coded voltage display on the mapping system. DSM defines a certain percentage of the maximum recorded virtual electrograms amplitude as abnormal myocardium. In DSM in order to focus on the interval encompassing local activation and the receding wave−front, all positive potential are coded purple. As the voltage becomes more negative, the display progresses through the color scheme and back after the peak negative voltage has occurred. The color range is set by the operator, with white being the most negative and purple the most positive. If an electrogram does not generate a sufficiently low peak negative voltage, it will not progress to white but peaks at an intermediate color.

During one cardiac cycle a negative peak voltage which is the largest unipolar deflection on the endocardium during the duration of the surface QRS, is recorded. This PNV is then used to normalize all other voltages. If 20%, 30% or 50% of the PNV is set as threshold to define areas of substrate voltages less than these threshold values will be the areas of low voltage. Therefore, DSM uses a ratio−metric comparison of the PNV of unipolar virtual electrogram to the maximal PNV of unipolar virtual electrogram recorded over a single beat. The areas of substrate are defined by an adjustable ratio (percentage) of all unipolar virtual electrogram compared to the maximal PNV of unipolar virtual electrogram. A distinct cutoff value of abnormal myocardium has not been clearly defined [34].

An example of DSM figure can be found in Figure 2.2 the color scale on the left represents a voltage descriptor. The white line delineates the low−voltage area identified during sinus rhythm. These markers were placed on the 3−D volume to identify the borders of the low voltage regions. Because noncontact mapping uses the inverse solution to generate electrograms, filtering must be employed to eliminate high amplitude repolarization signals.

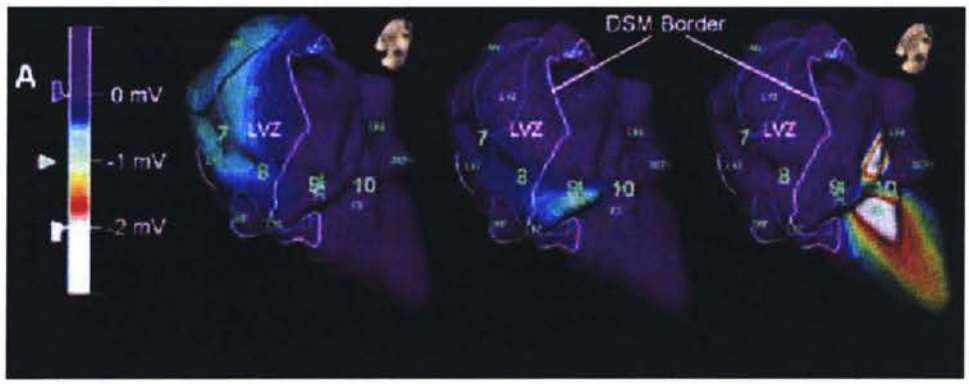

Figure 2.2: Dynamic substrate mapping defining scar within the light blue border.

Zou et al. [34] were one of the first to study and define abnormal anatomical VT substrate using DSM. In this paper, they mapped the abnormal EP with DSM and marked the areas of substrate to understand the mechanism of tachycardia and ablation strategy. They concluded

that noncontact mapping and linear ablation appears to be an effective strategy for the management of recurrent VT.

2.3 Localizing the Site of Origin

Noncontact mapping has been demonstrated to facilitate radio frequency (RF) ablation of ventricular arrhythmias, but the reproducibility in localization of endocardial exit sites during focal VT originating from defined myocardial layers has not been systematically studied. Therefore, to optimize the success rate of VT ablation, the ability to assign the source of an arrhythmia to a specific myocardial layer would be of major interest [35]. The potential to identify foci located deep in the myocardium would be particularly valuable. Theoretically, unipolar electrograms obtained from the subendocardium should display an initial positive waveform like a broad, low−amplitude leasing R−wave morphology in case of a subepicardial focus. Lacroix et al. [36] who tried to identify epicardial VTs from the endocardium with unipolar electrograms, analyzed 111 tachycardias and found R wave morphologies only in two subepicardial and five subendocardial VTs.

Voss et al.[37] experimented to verify whether noncontact mapping can distinguish between endo− or epicardial foci. Constant pacing was applied through octopolar needle electrodes in the left ventricle to mimic VT of subendocardial, midmyocardial or subepicardial origin. Using the noncontact mapping they measured the site of origin of 50 consecutive beats of all VTs and also the variation between respective exit sites. They concluded that morphological criteria such as the transition of virtual waveforms appear inappropriate to identify epicardial foci with noncontact mapping. In contrast, a former study [32] investigating the feasibility of noncontact mapping already shows that the site of origin could be determined relating to spatial location and intramural depth. The deeper in the myocardium a focus is located, the greater the distance between the site of origin and the endocardial exit site.

Ching man et. al [38] studied the accuracy of the unipolar ventricular electrogram in identifying the site of origin of a ventricular depolarization. They realized the absence of

R−wave in the unipolar electrogram is not likely to be an accurate indicator of the site of origin of ventricular tachycardia of right ventricle.

The present study is first to evaluate the ability of virtual electrograms to predict abnormal bipolar electrograms in human RVOT. And also to report on what is the optimized threshold of DSM that traditionally defines the areas of substrates by bipolar contact mapping. Because, characteristics of recorded unipolar virtual electrograms have not been related to traditional contact bipolar mapping in right ventricular outflow tract (RVOT). The following sections in this Chapter is dedicated to the explanation of backbone mathematics of this thesis. Chapter 3 is more on the clinical findings, therefore some of the tests and diagnostic computations is explained in the following sections.

2.4 t−Test

The t−Test assesses whether the means of two groups are *statistically* different from each other. Statistically different means: when we are looking at the differences between values for two groups, we have to judge the difference between their means relative to the spread or variability of their values. Figure 2.3 below shows three cases with same mean but different t−Test result because the overlap between the bell-shaped curves are different. Therefore, the most different or distinct case would be the low-variability case.

The formula for the test is as follows:

$$\frac{\text{Signal}}{\text{Noise}} = \frac{\text{Difference\_between\_Group\_Means}}{\text{Variability\_of\_Groups}}$$
$$t = \frac{\bar{X}_T - \bar{X}_C}{\sqrt{\frac{\text{var}_T}{n_T} + \frac{\text{var}_C}{n_C}}} \tag{2.1}$$

The top part of the ratio is the difference between the two means/averages. $\bar{X}_T$ is the mean of one group and $\bar{X}_C$ is the mean of another group. The denominator is a measure of the variability or dispersion of the values. To calculate the denominator, we take the variance of each group and divide it by the number of people in that group. var_T variance

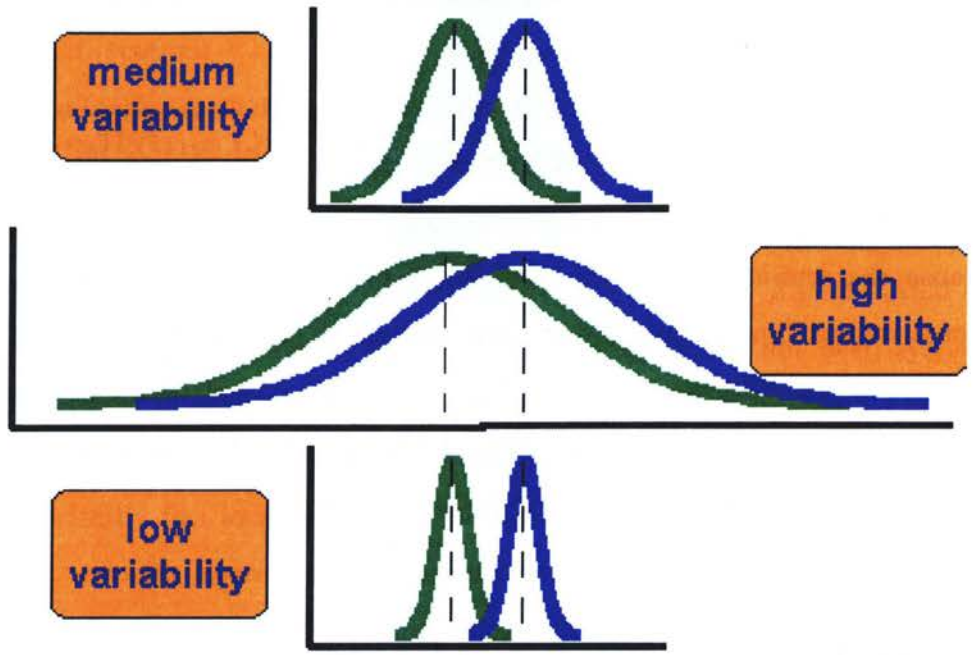

Figure 2.3: Three scenarios for differences between means [8].

of one group and n_T is number of people in that group. Then we add these two values and then take their square root as in Equation 2.1.

We also need to determine the degrees of freedom (df) for the test. In the t−test, the degrees of freedom is the sum of the number of in both groups minus 2. Given the df, and the t−value, one can look the t−value up in a standard table of significance (available as an appendix in the back of most statistics texts) to determine whether the t−value is large enough to be significant.

2.5 Measure of Diagnostic Accuracy

Perhaps the simplest measure of diagnostic decision quality in the medical world is the fraction of cases for which the classification is correct; this is called "accuracy". ROC curve was calculated based on the percentage of hits and false alarms. In other words, ROC curve

describes the inherent tradeoff between sensitivity and specificity of a diagnostic test by plotting the sensitivity vs. specificity points obtained for a decision threshold or cut points of the decision stage of the proposed algorithm. Measure of effectiveness of an algorithm is then given by the area under the ROC curve. The closer the value of area under ROC curve to 1, the higher the diagnostic accuracy.

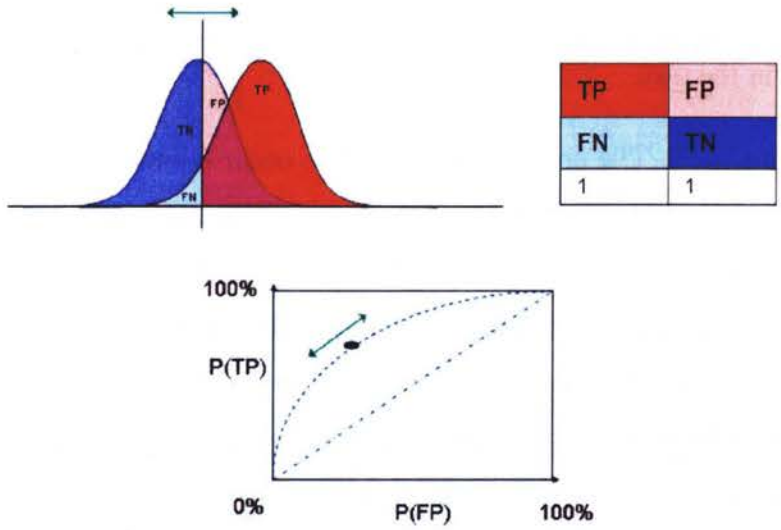

Figure 2.4: Fundamental Concept of ROC

2.5.1 Sensitivity and Specificity

Let p_i be the probability that patient i will get a positive diagnosis (i.e., the patient is ill) and q_i be the patient i's probability of a positive test. The prevalence, P of the positive diagnosis in the population is theoretically P = mean (p_i). The level of the test, Q, is Q = mean (q_i). And also $P^{'} = 1$ - P and $Q^{'} = 1$ - Q

In general, four possible decisions and two types of errors are made when comparing a test result with a diagnosis as shown in Table 2.1. If both diagnosis and test are positive, it

	Test Positive	**result** Negative	
Diagnosis Positive	TP	FN	P
Negative	FP	TN	P'
	Q	Q'	1

Table 2.1: Relationships between the measurement probabilities of the outcome, prevalence, and level of a test defined in the text.

is called a *true positive* (TP). The probability of a TP to occur is estimated by counting the true positives in the sample and divide by the sample size. If the diagnosis is positive and the test is negative it is called a *false negative* (FN). *False positive* (FP) and *true negative* (TN) are defined similarly. The values described are used to calculate different measurements of the quality of the test. The first one is *sensitivity*, SE, which is the probability of having a positive test among the patients who have a positive diagnosis. *Specificity*, SP, is the probability of having a negative test among the patients who have a negative diagnosis. The SE and SP is defined below.

$$Sensitivity = \frac{TP}{TP + FN} \tag{2.2}$$

$$Specificity = \frac{TN}{TN + FP} \tag{2.3}$$

ROC curve therefore is a plot of the sensitivity vs. (1 − specificity) for a binary classifier system as its discrimination threshold is varied. Figure 2.5 shows a typical example of a ROC curve. As it is seen from the Figure 2.5, conventional ROC curves of the kind described here inevitably must pass through lower left corner of the graph because all test can be called negative, and through the upper right corner of the graph because all tests can be called positive.

Especially the ROC curve was used in this thesis for Chapter 3. Because, the character-

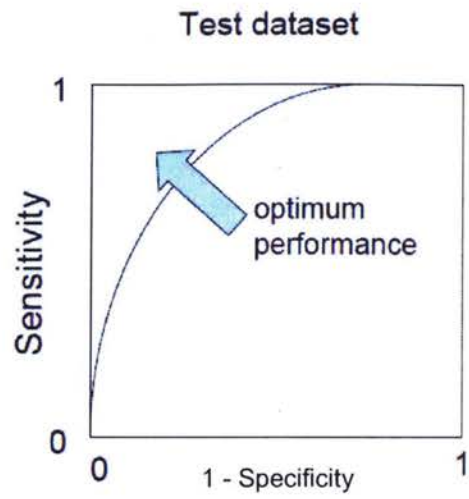

Figure 2.5: Example of ROC curve with Optimum Performance

istics of recorded unipolar virtual electrograms have not been related to traditional contact bipolar mapping in RVOT. In order to identify an optimal value of DSM threshold that can best describe the substrate localization comparable to bipolar electrogram, the ROC was drawn. ROC curve represents a pattern of responding values expected for a particular but arbitrary bipolar threshold (BT) at the range values of DSM threshold. Recognizing the arbitrary nature of decision threshold selection might seem to complicate out problem. We resolve this dilemma by intentionally forcing the decision threshold to vary and by observing the resulting changes in the various decision fractions.

2.6 Spectral Analysis

Relating signals in time domain is intuitively grasped by most people, whether it be an ECG tracing or a company's stock rate. In time domain, the x−axis represents time, while

the y−axis represents amplitude. Frequency domain plots, where the x−axis represents frequency, are less commonly used in everyday life. However, spectral analysis of biomedical signals is of considerable interest in the investigation and understanding of the workings of human physiology. The detection and resolution of frequencies, which may be time varying due to mechanical actions correlated to the electrical signals of the body, is a major motivation for this analysis. Conventional analysis in the time domain has important limitation [39]. Spectral analysis, most commonly with fast Fourier transform (FFT) has been proposed which overcomes major limitations of time domain techniques [39], [40]. This transform takes advantage of the fact that continuous signals can be decomposed to a sum weighted sinusoidal functions. Equation 2.4 calculates the frequency component of each segment using FFT.

$$X(k) = \sum_{j=1}^{N} x(j)\omega_N^{(j-1)(k-1)} \tag{2.4}$$

2.6.1 Autoregressive Modeling

FFT has a major drawback in that they require large quantities of data to produce significant results. As a result, any variation or perturbation in frequency can be smoothed out by the action of the algorithm; for example, the FFT will give a 'broad' spectral peak centered at the frequency of interest, particularly if using zero padding. To resolve these problems, the most attractive method is to use autoregressive analysis. The algorithms have proven to be effective in many fields, including biomedicine.

Autoregressive modeling (AR) has been used in various applications, including classification of physiological signals like ECG, EEG, heart rate etc. The advantage of AR modeling is its simplicity and is suitable for real−time classification monitoring. AR models are popular due to the linear form of the system, simultaneous equations involving the unknown AR model parameters and the availability of efficient algorithm for computing the solution [41]. AR modeling has been used extensively for power spectrum estimation of ECG signals [42].

In an AR process of order (p_i) the output x_n at time n depends linearly, via coefficients

a_i, on the previous p outputs and an additive white noise excitation. Specially, the process is modeled as

$$x_n = \omega_n - \sum_{i=1}^{i=p} a_i x_{n-i} \tag{2.5}$$

In the given interval the signal requires to be stationary for AR modeling. The recorded electrograms are stationary signals. There are various proposed methods for determining the coefficients in an autoregressive process. We chose to use Burg method to fit[43] a *pth* order autoregressive model to the input signal by minimizing (least squares) the forward and backward prediction errors while constraining the AR parameters to satisfy the Levinsone Durbin recursion. The Burg method was preferred over the YuleWalker[43] and the covariance methods, as it has been documented that it provides higher frequency resolution, and avoids frequency estimation biases and spectral line splitting problems that are associated with one or more of the above power spectral estimators [43]. Vector a contains the normalized estimate of the AR system parameters, $A(z)$, in descending powers of z.

$$H(z) = \frac{\sqrt{e}}{A(z)} = \frac{\sqrt{e}}{1 + a_2 z^{-1} + ... + a_{p+1} z^{-p}} \tag{2.6}$$

The spectrum of the model can also be estimated from Equation 2.7 as:

$$P_{AR}(\omega) = \frac{1}{|1 + \sum_{k=1}^{p} \alpha_k e^{j\omega k}|^2} \tag{2.7}$$

Since the method characterizes the input data using an all−pole model, the correct choice of the model order p is important. The Akaike information criterion (AIC) [44], was used for estimating the optimum AR model order. The model order which minimized the criterion function was selected. The formula for this criterion is as follows:

$$AIC(p) = N \ln(\hat{\rho}_p) + 2p \tag{2.8}$$

where $\hat{\rho}_p$ is the estimated linear prediction error variance for the model with order p. Low orders result in smoothed spectra, whereas high orders might introduce spurious detains to the spectrum [45].

AR models effectively capture spectral peaks and model the correlation in sequences. After calculating the AR coefficients, the AR model parameters can be used as features of the classifier. AR spectral parameters may also reflect the underlying difference in the structure. AR coefficients can be used to calculate the following measurement described below: 1) Cepstral Coefficients. 2) Spectral Estimation. 3) Classification.

2.6.2 Cepstral Analysis

Cepstral Analysis is an inverse Fourier transform of the logarithm of the magnitude of the Fourier transform (or power spectrum of the signal). This value is real and nonnegative which is not invertible because the phase is missing. Cepstral coefficients can be derived directly from the AR coefficients using the formula below [46]:

$$\begin{aligned} c_1 &= -a_1 \\ c_n &= -a_n - \sum_{k=1}^{n-1} (1 - k/n) a_k c_{n-k} \quad \text{for } 1 < \text{n} \leq \text{p} \\ c_n &= -\sum_{k=1}^{n-1} (1 - k/n) a_k c_{n-k} \quad \text{for n} > \text{p} \end{aligned} \tag{2.9}$$

where a_n and c_n denote the *nth* AR and cepstral coefficients respectively. Cepstral coefficients have rather different dynamics, the higher coefficients showing the smallest variances. In fact cepstral approach requires fewer coefficients than traditional approaches such as FFT and discrete wavelet transform (DWT). The discrimination, using analysis of temporal spectral and cepstral parameters of unipolar virtual electrograms may determine relevant parameters needed for the classification of endocardial vs epicardial electrical activation. There appear to be no reports directly comparing spectral with cepstral features for classification. It is possible that spectral moments may perform better than cepstral features for classifying some classes of segments. If so, this could lead to improvements in feature extraction and would also serve to validate the use of spectral moments analysis in the clinical literature. On the other hand, should cepstral features prove equally or more effective for classifying obstruent spectra, it may lead to recommendations to alter analysis techniques common among clinical phoneticians and speech language pathologists. To examine this

issue, the present study directly compared cepstral features and spectral moments features for the classification of burst spectra.

Computer aided signal processing saves time, standardizes the measurements and enables the extraction of features which could not be calculated manually. Considerable work has been carried out in time domain for classification and identification of electrical activity of unipolar virtual electrogram. Quantitative signal analysis in the frequency domain using classical power spectrum analysis techniques has been well documented over recent years for biomedical signals. However, spectral analysis and parametric modeling techniques such as AR has not as yet been investigated in detail for clinical diagnostics. AR modeling is currently by far the most popular method of time series analysis. It has several advantages:

1. Generally, any signal can be modeled as an AR process as long as an appropriate model order is selected.

2. Availability of many algorithm to estimate the model parameters and find a solution to the linear system equations.

3. Shows better resolution than traditional Fourier spectrum (explained more in the AR modeling section).

As mentioned in previous section of this Chapter, the estimation of AR parameters were derived by the Burg method[43]. Burg method has some advantages as well. First, it results in high frequency resolution. Second, yields a stable AR model. And third, it is computationally efficient. Furthermore, cepstral analysis that has been applied to speech recognition for a long time and more recently to surface electromyograms (EMG) movement patterns [47], has not yet been applied to unipolar virtual electrogram. The objective of this work was to investigate the usefulness of AR and cepstral analysis in the diagnostic assessment of recorded electrograms from both endocardial and epicardial paced myocardium.

2.7 Pattern Classification

Pattern classification by definition is the organization of patterns into groups of patterns sharing the same set of properties. The motivation for the pattern classification is to automatically group signals of same characteristics using the discriminatory features derived as explained in previous section. In classification and other data analytical tasks it is often necessary to utilize pre−processing on the data before applying the algorithm at hand and it is common to first extract features suitable for the task to solve. Feature extraction for classification differs significantly from feature extraction for describing data. Discriminant analysis addresses the following question: Given a data set with two classes, say, which is the best feature or feature set (either linear or non−linear) to discriminate the two classes?

Pattern classification was carried out by a linear discriminant analysis (LDA) based classifier [48]. LDA is used in machine learning to find the linear combination of features which best separates two or more classes of object or event. The resulting combinations may be used as a linear classifier before later classification. The following is review of discriminant analysis.

Let $X_1 = x_1,...,x_{l1}$ and $X_2 = x_1,...,x_{l2}$ be samples from two different classes we have (i.e. endocardially paced vs. epicardially paced (more explanation in chapter 4.)) and with some abuse of notation $X = X_1 \bigcup X_2 = x_1,...,x_l$. Fisher's linear discriminant is given by the vector ω which maximizes [49]

$$J(\omega) = \frac{\omega^T S_B \omega}{\omega^T S_W \omega} \tag{2.10}$$

where

$$S_B := (m_1 - m_2)(m_1 - m_2)^T and \tag{2.11}$$

$$S_W := \Sigma_{i=1,2} \Sigma_{x \varepsilon X_i} (x - m_i)(x - m_i)^T \tag{2.12}$$

are the between and within class scatter matrices respectively and m_i is defined by

$$m_i := \frac{1}{t_i} \Sigma_{j=1}^{t_i} x_j^i \tag{2.13}$$

where m_i is the mean of each class. The intuition behind maximizing $J(\omega)$ is to find a direction which maximizes the projected class means (the numerator) while minimizing the classes variance in this direction (the denominator).

The classification accuracy was estimated using the leave−one−out method, which is known to provide a least bias estimate [50]. In leave−one−out−method, one sample is excluded from the data−set and the classifier is trained with the remaining samples. Then the excluded signal is used as the test data and the classification accuracy is determined. This is repeated for all samples of the data−set. Since each signal is excluded from the training set in turn, the independence between the test and the training sets are maintained.

Leave−one−out cross−validation is normally restricted to applications where the amount of training data available is severely limited, such that even a small perturbation of the training data is likely to result in a substantial change in the fitted model. In this case, it makes good sense to adopt a leave−one−out cross−validation strategy as it minimizes the perturbation to the data in each trial. Leave−one−out cross−validation is rarely adopted in large−scale applications simply because it is computationally expensive. The training algorithms for kernel machines, including that for the Fisher kernel discriminant, typically have a computational complexity of $O(l^3)$, where l is the number of training patterns. In this case, the leave−one−out cross−validation process has a computational complexity of $O(l^4)$, which quickly becomes impractical as the number of training patterns increases. Note however that minimizing an upper bound on the leave−one−out error has proved an effective means of model selection for support vector machines (e.g. [51]).

2.8 Transfer Function Studies

Now that a mathematical function or model that accurately produces myocardial time−frequency curves from the right ventricle (RV) is presumed to contain information specific to RV−myocardial transport processes [52]. The transport processes would help to better estimate the existing mathematical models of the heart and aid in better localization of arrhythmia focus.

Transfer function can provide information on the physical properties of the regionally ischemic right and left ventricle. In addition, transfer function method can reveal changes of the instantaneous physical properties of both the normal and ischemic myocardium moment by moment during the cardiac cycle. When we consider the clinical importance of regional myocardial ischemia, it would be of value to add new information on the pathophysiology of regional ischemia that has been gained by this transfer function method.

Therefore, our aim for the study of transfer function is to characterize the basic features of RV (explained in Chapter 4) during cardiac cycle. "Transfer function" is a widely used technical term. If a stimulation (sinusoidal) is applied to a linear system, the output is also sinusoidal. If $X(\omega)$and $Y(\omega)$ are Fourier transforms of the input and output respectively, at angular frequency ω, then the ratio $Y(\omega)/X(\omega)$ is the transfer function at that frequency. A full description of the transfer function includes both its magnitude and phase; in this thesis, however, we restrict our attention only to the magnitude. The transfer function completely characterizes the system and includes the viscoelastic properties of the myocardium.

The validity of the transfer function approach is dependent upon the assumption that the system being described is linear and stationary. The linearity of the system was confirmed that right ventricle could be taken as linear if the magnitude of acceleration in input oscillation was kept constant and small throughout the frequency range from 50 to 200 Hz. Stationarity can only be evaluated in terms of the repeatability of the measurements and the extent to which the transfer functions, calculated in the frequency domain, can be used to retrieve the original information. The transfer function approach described here has several distinct advantages over conventional methods of measuring myocardial physical properties:

First if nearly identical sampling systems are used, the calculated transfer function will be independent of the characteristics of the sampling apparatus itself and thus represent only the dispersion that occurs in the vascular system under study [53].

Second the transfer function method possesses higher temporal resolution. This is probably the greatest advantage of the method because in that transfer function contain information which is not normally seen in the recorded electrogram.

Third the transfer function method can be used in the ejecting heart preparation, even though additional signal processing is required to eliminate the effects of heart sounds [54], [55].

Fourth the transfer function can be applied to the heart with heterogeneous myocardial properties such as regional ischemia with clear differences in the curve characteristics, whereas the interpretation of more classical methods in the heterogeneous setting is more difficult [55].

Therefore, transfer function completely characterizes the system and it may include the viscoelastic properties of the myocardium of the RV. The transport processes would help to better estimate the existing mathematical models of the heart and aid in better localization of arrhythmia focus. Because the important feature is that in the frequency domain, the input and output of a linear system are multiplicatively related via the transfer function. A full description of the transfer function includes both its magnitude and phase; in this thesis, however, we restrict our attention only to the magnitude.

Chapter 4 will cover all this analysis and classifications in detail. Chapter 3 and 4 is the contribution of my work and applying the explained mathematics on the gathered data.

Chapter 3

Signal Analysis for Cardiac Studies in Human Heart

3.1 Motivation Behind the Study

MOST electrophysiologists are familiar with unipolar or bipolar voltage mapping to reflect underlying tissue integrity and pathophysiology in patients with a prior myocardial infarction. Characteristics of recorded unipolar virtual electrograms (noncontact mapping) have not been related to traditional contact bipolar mapping in RVOT. A distinct cutoff value of abnormal myocardium has not been clearly defined [34]. This study was performed on humans. DSM during sinus rhythm was performed on 6 patients with symptomatic RVOT tachycardia. Within the same electroanatomic geometry bipolar electrograms were recorded with peak−to−peak voltages as a reference for substrate identification. The optimal threshold for DSM, the effect of high−pass filter, and the role of dV/dt were determined for accurately identifying bipolar defined substrate using noncontact mapping. In order to identify a range of fixed values of bipolar threshold, different relative threshold values to peak negative voltages (PNV) of DSM were appointed to draw the ROC.

3.2 Catherization Lab (Cath−Lab)

The cardiac catheterization laboratory provides the region's highest level of diagnostic and treatment options in interventional cardiology. During a catheterization procedure, the patient is lying on a bed and a thin, flexible tube, or catheter, is inserted into an artery or vein in the patient's arm or leg. The catheter is then gently moved further into the arteries and then to the heart. It can be used as a diagnostic tool to figure out what is wrong with a patient's cardiovascular system or it can also be used as a form of treatment for coronary artery disease.

The technique of noncontact mapping has been described previously in Chapter 2. For this analysis, the 9−French 64 electrode balloon catheter was passed over a guide wire into RVOT. Heparin was used to maintain the activated clotting time (ACT) to be 250 seconds. A quarto polar ablation (Biosense Webster) catheter was roved around the MEA and multiple spatial points along the endocardial surface of the RVOT were annotated on the electroanatomic geometry. Key anatomic landmarks such as the pulmonary valve annulus were marked on the geometry. The 64 recording electrodes of the MEA pick up far field electrogram information during sinus rhythm. The system calculates real−time endocardial potentials at more than 3000 virtual sites by using inverse solution mathematics. Simultaneous virtual unipolar electrograms were mathematically reconstructed and displayed on the anatomic model, capable of producing isopotential or isochronal color maps at the operator's discretion. Unipolar electrograms were filtered with a bandwidth of 1 Hz to 300 Hz. It is possible, at any given interval of the cycle, to display the virtual unipolar endocardial electrograms from a chosen site of the endocardial surface [56].

The most recent version of the EnSite software provides the capability of point−by−point contact mapping, allowing the creation of activation and voltage maps by acquiring serial contact electrograms and displaying them on the virtual endocardium. This has utility in adding detail, familiarity, and validation of the information obtained by the noncontact method. Bipolar electrograms from the distal electrode pair were then recorded sequentially during sinus rhythm along the endocardial noncontact geometry. Peak−to−peak voltage

amplitude of the bipolar electrograms were automatically calculated and displayed in an adjustable color isopotential map.

All procedures were performed in the fasting, non−sedated state with continuous electrocardiograph and noninvasive hemodynamic monitoring. In this study three male and three female had premature ventricular beat of RVOT origin were included. Premature ventricular contractions (PVCs) are premature heartbeats originating form the ventricles of the heart. PVCs are premature because they occur before the regular heartbeat. During PVCs, the ventricle electrically discharges (and contracts) prematurely before the normal electrical discharges arrive from the SA node. These premature discharges are due to electrical 'irritability' of the heart muscle of the ventricles, and can be caused by heart attacks, lack of oxygen, or medications. Immediately after a PVC, the electrical system of the heart resets. Example of a PVC in Figure 3.1.

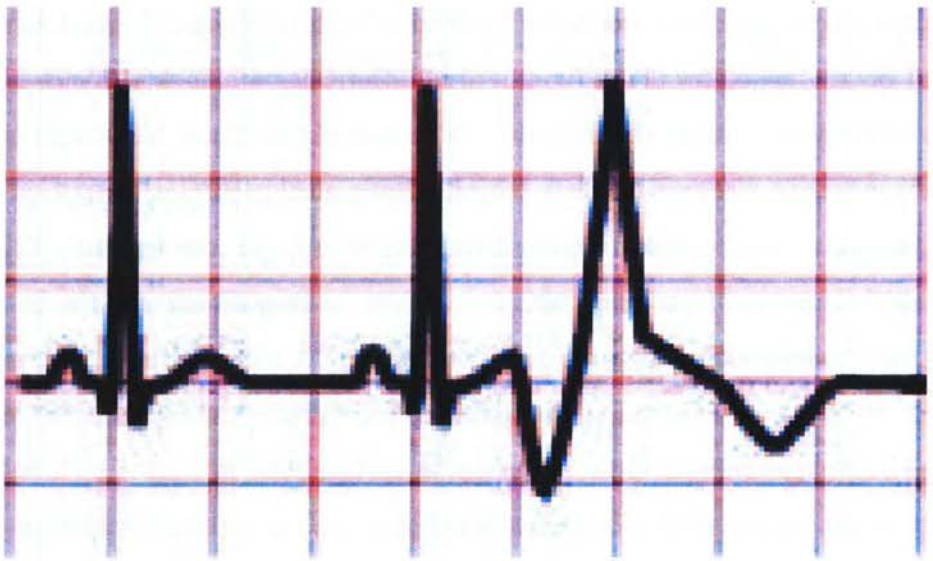

Figure 3.1: Example of a premature ventricular contraction [9].

3.3 Data Preparation

The comparison analysis between contact and noncontact mapping to define abnormal endocardium was performed in all 6 patients. The clinical and electrophysiological characteristics of the patients are shown in Table 3.1. Establishing the RVOT landmarks on the constructed geometry was accomplished in 20 ± 9 minutes. Figure 3.2 is a snap shot of a three dimensional geometry of the RVOT generated by noncontact mapping of a typical patient. Fluoroscopy and anatomic markers confirmed that there was no significant movement of the MEA during each procedure. The mean numbers of the bipolar contact electrograms were 100 ± 15.

Patients	Age years	Gender	VT CL msec	Diagnosis	Medications
1	51	F	366	PVB Paroxysmal Atrial Flutter	Beta Blocker Aspirin
2	53	M	378	PVB of RVOT	Beta Blocker ACE Inhibitor & Aspirin
3	61	M	389	PVB of RVOT(high) Anteroseptal	Beta Blocker Aspirin
4	41	F	323	PVB of RVOT(basal) Postrerolateral	Estrogen & Aspirin
5	35	F	277	PVB & non− Sustained VT of RVOT	None
6	30	M	342	PVB & non− Sustained VT RVOT	None

Table 3.1: VT = Ventricular Tachycardia; CL = Cycle Length; PVB = Premature Ventricular Beats; RVOT = Right Ventricular Outflow Track .

Figure 3.2: Example of the geometry and DSM map of one of the patients. DSM marks the areas of low voltage. By using an ablation catheter the geometry of heart for each patient is constructed. Color represents relative unipolar voltage level at each chamber location. The DSM tool can be used to place adjustable isopotential substrate markers based on either relative or absolute voltages. DSM locates the most negative signal within a user–defined caliper range and can often organize voltage information from a single beat of each rhythm. This figure is a snap shot of the third patient three dimension geometry before ablation. The low voltage areas are colored as white up to blue which has the largest voltage value.

3.4 Signal Processing

Based on early work from the University of Pennsylvania, bipolar voltage mapping has become the standard for substrate localization in the electrophysiology laboratory. Statistical analysis of patients with normal left ventricles suggested that a bipolar electrogram voltage of $< 3mV$ was abnormal [57]. With the advent of 3−D electroanatomic mapping (EAM) systems, refinement of the voltage threshold for scar has been performed in both animals and humans. Callans et al [58] have compared bipolar voltage mapping with intracardiac echocardiography in porcine infarctions with the CARTO system, finding that an electrogram < 2.0 mV correlated with akinetic areas. The same group went on to evaluate EAM with CARTO in humans, finding 95% of all LV electrograms were > 1.55 mV [59]. Therefore, a threshold of 1.5 mV was set for definition of abnormal myocardium and a value of < 0.5 mV was arbitrarily set for the definition of dense scar.

DSM as explained in Chapter 2 is a method of marking the areas of substrate of activation by observing how isopotential maps display the wavefront moving around lines of block, anatomic barriers, zones of slow conduction, or diseased tissue. Noncontact mapping uses unipolar virtual electrograms to define these areas of substrate, unlike conventional contact mapping which defines substrate using the amplitude of bipolar electrograms. Marking these substrates can be useful in identifying a critical isthmus of VT conduction and determining an ablation strategy. This study investigates whether "virtual electrograms" from a noncontact mapping system (EnSite 3000) can identify abnormal myocardial substrate boundary defined by bipolar contact mapping in the human right ventricular outflow tract (RVOT).

3.4.1 Preprocessing

The signals recorded from the noncontact mapping system as well as the contact electrograms were exported from the EnSite system for further analysis. The contact and noncontact electrograms were simultaneously displayed and analyzed. The number of the contact electrograms was much less than the number of unipolar virtual electrograms. Therefore,

for each bipolar contact electrode a corresponding virtual electrode was identified for comparison. This was achieved by calculating the Euclidean distance, given in the Equation 3.1, of any bipolar contact electrode to any of the virtual electrode based on their spatial coordinates. The virtual electrode that has the minimum distance to a given bipolar contact electrode would be its corresponding virtual electrode. This was achieved because EnSite system extract relevant features from electrograms such as the exact coordinates of each of the electrograms.

$$D = \sqrt{(x_1 - x_2)^2 + (y_1 - y_2)^2 + (z_1 - z_2)^2} \tag{3.1}$$

x_1, y_1, z_1 = the Cartesian coordinate of a bipolar electrogram.

x_2, y_2, z_2 = the Cartesian coordinate of a virtual unipolar electrogram.

The bipolar electrograms with their corresponding virtual electrograms were saved for further analysis. The following parameters of unipolar virtual electrograms were examined to determine optimal settings for identifying contact defined scar.

1. DSM was performed during the sinus rhythm with thresholds from $10 - 90\%$ of the maximal PNV unipolar virtual electrograms.

2. Max dV/dt of all unipolar electrograms was identified.

3. The high−pass filter was adjusted between 1 and 32 Hz.

3.4.2 Peak Negative Voltage of Unipolar Electrograms

DSM was performed during sinus rhythm. The peak negative voltages of all virtual electrograms were identified. Abnormal EP substrate were defined as regions with voltage magnitude less than defined percentage of the peak negative voltage. Markers were placed on the three−dimensional volume to identify the borders of these low voltage regions. Scar area by virtual geometry depends on threshold adjustments. As MEA measures cavity potential and the fact that unipolar electrograms have a large "field of view", an absolute voltage threshold for scar definition is not accurate for noncontact mapping [60]. Therefore, a threshold from

10 to 90% of maximum negative voltage was used to define the areas of low voltage. More specifically the DSM thresholds were [0.1 0.2 0.25 0.28 0.3 0.45 0.5 0.6 0.7 0.8 0.9] of the maximum negative voltage. Figure 3.3 shows the fundamental definitions underlying the operating mode of the DSM algorithm.

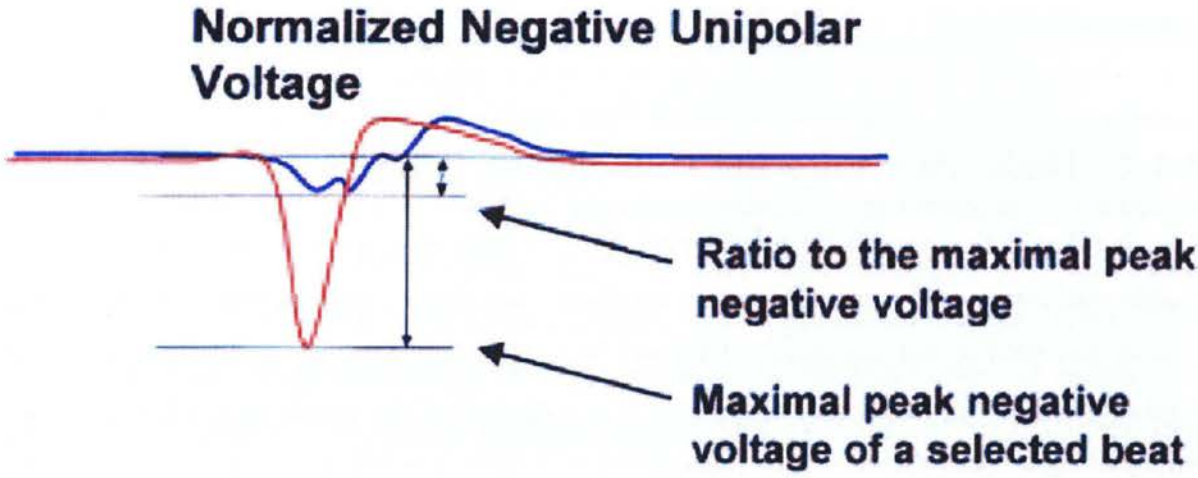

Figure 3.3: Schematic illustration of unipolar electrograms and the fundamental operating mode of dynamic substrate mapping (DSM). PNV = peak negative voltage [10].

3.4.3 First Derivative of Unipolar Electrograms

The first derivative of the unipolar electrogram (dV/dt) represents the velocity of local activation. Usually analysis of initial dV/dt of unipolar ventricular electrograms may enhance the specificity of earliest site of activation. The slope, dV/dt, is been used quantitatively to assess the distance from ventricular activation [38]. However, the application of dV/dt may not be clinically useful for determining ventricular activation in the ventricle in patients with structural disease. Because, in diseased states the slope of the unipolar electrogram is decreased, the duration prolonged and the maximal negative value of the derivative is reduced. For substrate mapping these features provide additional details of tissue viability compared to electrogram voltage.

The voltage deflection was measured by subtracting the lowest voltage value from the highest. The electrogram slope (first differential of the electrogram) was calculated for each value by subtracting the data point from its adjacent data point. In the literature unipolar electrograms, signals associated with high conduction velocity (i.e., His–Purkinje system) possess a greater slope ($-dV/dt$), and thus are characterized by higher–frequency components ($> 32\ Hz$) [61].

3.4.4 High–Pass Filtering Unipolar Electrograms

The signal sampling processing may require filter settings that are sensitive and selective to enable visualization of early low amplitude signal components and suppress repolarization related far–field signal elements. Adjusted low high–pass filtering enables an improved display of early and slow rising activation and a display of the wavefronts, whereas higher values of high–pass filters reduce repolarization related signal components and noise. At high–pass filtering of 1 to 2 Hz, slow and fast activation wavefronts are displayed including potential repolarization components. At about 4 to 12 Hz high–pass filter setting, the wavefront is sharpened, unwanted signal component become more suppressed. A high–pass filter of 16 Hz and more displays mainly wavefront changes. The objective of the study was to evaluate the potential impact of different high–pass filter on the accuracy of mapping of abnormal myocardium using DSM. Table 4.4 shows the high–pass filter settings used in noncontact mapping system.

It is widely known that changing the filter settings used to display virtual electrograms can have a profound effect on the morphology of the electrogram (as it can do to contact electrograms). Adjustment of filtering is necessary to differentiate true electrical activity from noise especially when trying to identify and display the low amplitude unipolar signals associated with diastolic potentials. It is widely accepted that the maximum negative first derivative defines local activation on a unipolar electrograms. However, the effect of inverse solution and reconstruction of electrograms appears to lower the frequency of low amplitude

Signal Type	Repolarization atrial/ventricular	Slow Conduction scar border	Normal Myocardium atrial or ventricular	Fascicular His–Purkinje
Spectral Components	$0.05 - 4Hz$	$1 - 4Hz$	$4 - 16Hz$	$8 - 32Hz$
High-Pass Filter				
Typical	$> 4\ Hz$	$1\ Hz$	$8\ Hz$	$16\ Hz$
Range	$8 - 12Hz$	$1 - 4Hz$	$4 - 6Hz$	$8 - 32Hz$
Advantage	eliminates far field	visualize slow conduction	minimal repolarization	eliminates far field, myocardial cond.
Disadvantage	eliminates slow conduction	potential repolarization artifact	eliminates slow conduction	eliminates myocardial conduction

Table 3.2: High–pass filter settings by signal type (Estimated for unipolar virtual electrograms.).

potentials somewhat, therefore it would be difficult to distinguish the deflections of a unipolar virtual electrogram from baseline wander. Increasing the value of high–pass filter would help distinguish such noise from true electrical activation on the isopotential maps but it may filter out the virtual electrograms associated with true activation for this reason. It is therefore needed to try different filter settings with the operator looking at the electrograms produced at region of interest on the isopotential map rather than relying on the isopotential map alone to guide ablation.

The effect of filtering is shown as an example in Figure 3.4. In this figure each row shows waveforms and its corresponding isopotential map. The blue waveform is the surface ECG, the red waveform is the right ventricular electrogram and the yellow waveforms are the virtual electrograms generated from the MEA. The virtual electrogram recording sites may be positioned retrospectively by the operator anywhere on the virtual endocardium. The positions of the selected recording sites in this instance are shown by numbers on the upper isopotential map. These correspond to the virtual electrograms with the same number on the waveform views (*dashed oval*).

3.4.5 Bipolar Contact Electrograms

Contact mapping system allows ventricular scars to be identified by measuring the voltage of bipolar electrograms during sinus rhythm. Peak–to–peak voltage values of bipolar electro-

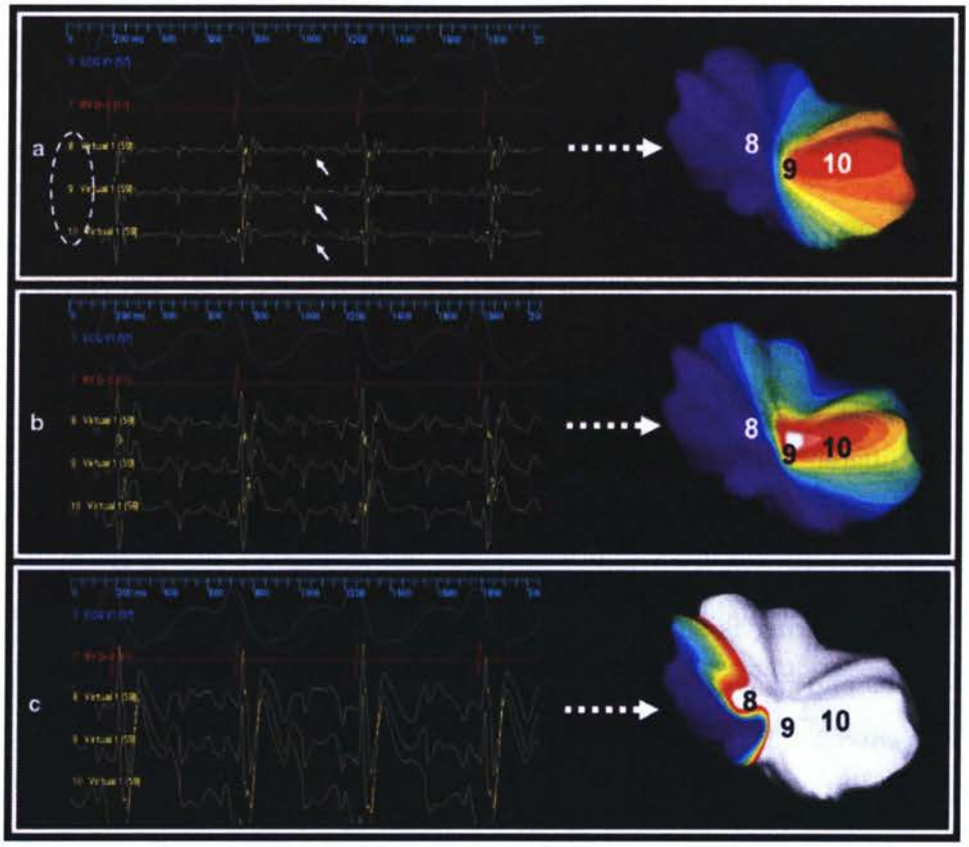

Figure 3.4: In panel **a**, the high−pass filter is set at 32 Hz, low−pass filter at 300 Hz. A deflection can be seen on the virtual electrograms between QRS during the diastolic interval which could be a diastolic potential. Panel **b** high−pass filter is 12 Hz. In panel **b** it is more difficult to identify a discernible potential. High−pass filter is set to 2 Hz and low−pass of 300 Hz for panel **c**. The virtual electrogram amplitude are changed again which is reflected in the isopotential map also [11].

gram is needed to identify the areas of low voltage or scar. Usually, a bipolar peak−to−peak voltage value of $< 0.5mV$ is considered a dense scar and $> 1.5mV$ normal myocardium [62]. The threshold value for defining the scar voltage may slightly change in different studies. In this study, for comparing the bipolar threshold of [0.15 0.25 0.5 0.75 1 1.25 1.5] mV was used both to compare with the DSM threshold and to draw the ROC (Figure 3.5).

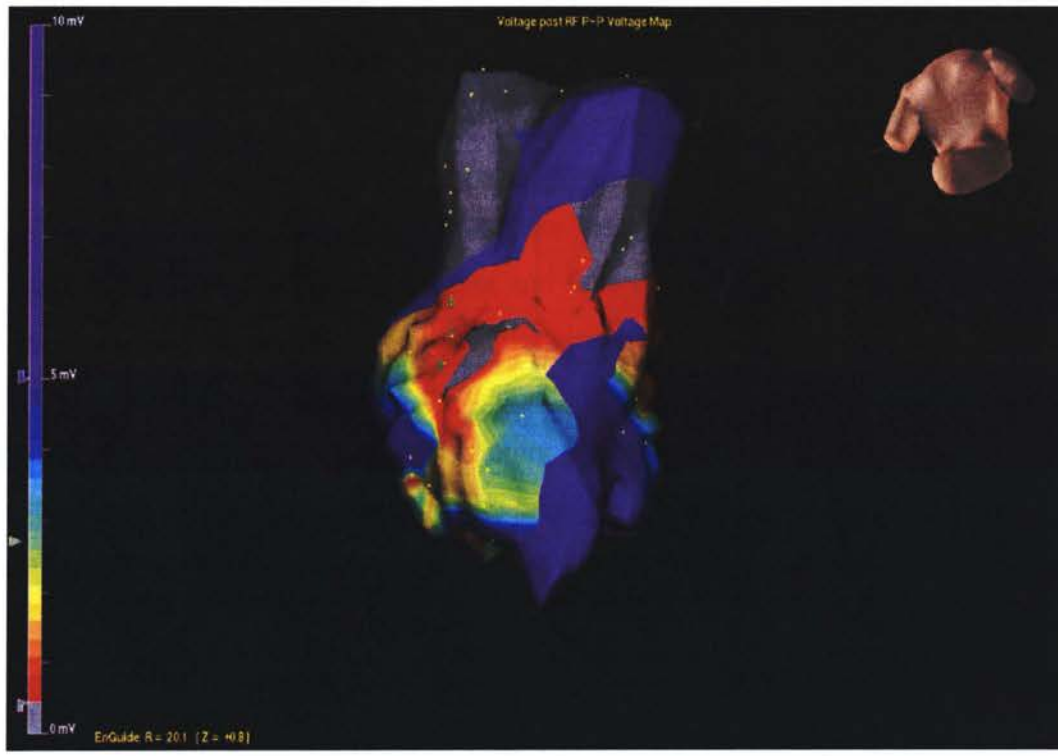

Figure 3.5: Bipolar color scale extracted from one the patients. Color scale is set with dense scar ($<$ 0.5 mV) red, and normal myocardium ($>$ 1.5 mV) magenta. The yellow dots are the bipolar recording points.

Figure 3.6 gives the clear definition of areas of scar defined by unipolar or bipolar electrograms.

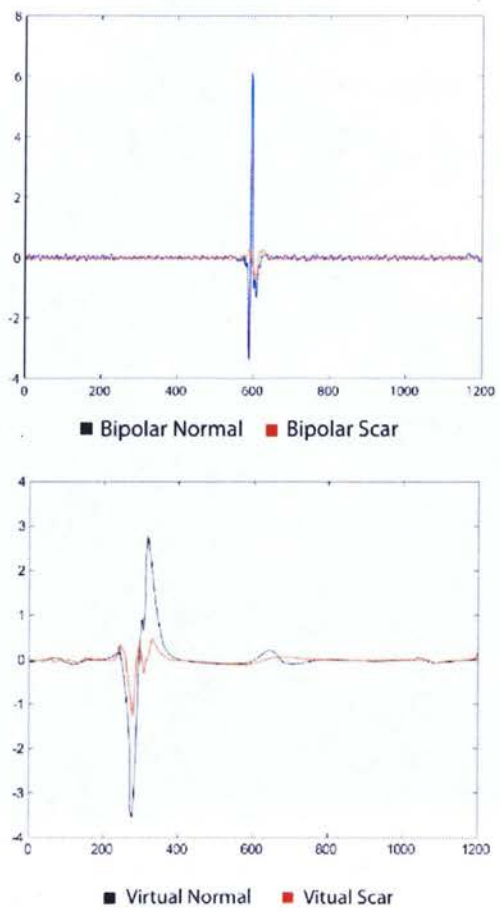

Figure 3.6: Illustration of scar electrogram by both unipolar and bipolar recordings.

3.4.6 Receiver Operating Characteristics

ROC curves were constructed to identify the optimal decision threshold for the slow conduction zone in the derivation sets (a fixed PNV or normalized voltage), defined as the value on the ROC curve with the best sensitivity–specificity trade–off. The ROC curve plots the true–positive rate (sensitivity) against the false positive rate (1 – specificity) over a range of cut points. The points along the diagonal indicate results that are no better than chance. When comparing tests, the test with the largest area under the ROC curve is preferred, assuming that the goal is to balance the sensitivity and specificity.

In order to draw ROC curve a fixed value of bipolar threshold with different value of DSM threshold were appointed. ROC curve represents a pattern of responding values expected for a particular bipolar threshold at the entire values of DSM threshold. ROC curve was calculated based on the percentage of hits and false alarms. In this case, a hit was defined as finding the points in which both the bipolar electrogram and unipolar virtual electrogram have found a scar (TP). A false was defined as finding points of which both the bipolar and unipolar virtual electrograms define the point to be normal (TN). Similarly, FN is when bipolar electrogram define the points to be scar but the unipolar virtual electrogram define the points to be healthy. The result for the ROC curve is in the following sections.

3.5 Clinical Findings

3.5.1 ROC of Virtual Electrogram DSM to predict bipolar amplitude

To identify abnormal endocardium with the noncontact mapping system, we used previously described techniques that suggest the area where local electrogram amplitude is less than a pre–defined percentage of the maximum peak negative voltage. Analyzing the ROC curve in Figure 3.7, abnormal myocardial substrate defined by contact bipolar mapping can be optimally identified when we selected a cutoff of 25% of the maximum peak negative voltage

as the criteria for low voltage area. In all the ROC curves plotted with different bipolar threshold 25% DSM threshold was considered to be statistically significant (Figure 3.8).

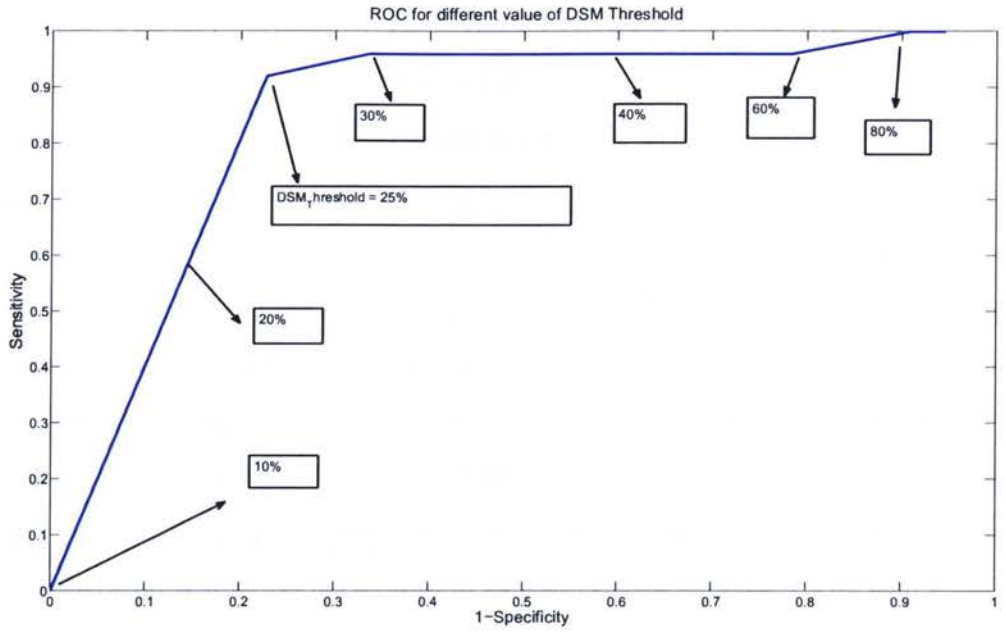

Figure 3.7: ROC curve for 0.25 mV of bipolar threshold: To better understand the ROC curve plotted in for this study; different values of unipolar threshold that allows plotting the ROC curve is marked in this ROC.

The calculate area under the ROC curver for the optimum value of the DSM threshold (=25%) is presented in Table 4.5. The largest area under the ROC curve was seen when the bipolar threshold was $0.25mV$.

3.5.2 ROC of Virtual Electrogram dV/dt to predict bipolar amplitude

The minimum unipolar electrogram slope is the most useful indices for distinguishing the presence of myocardial scar. From the noncontact mapping electrode, the value and location

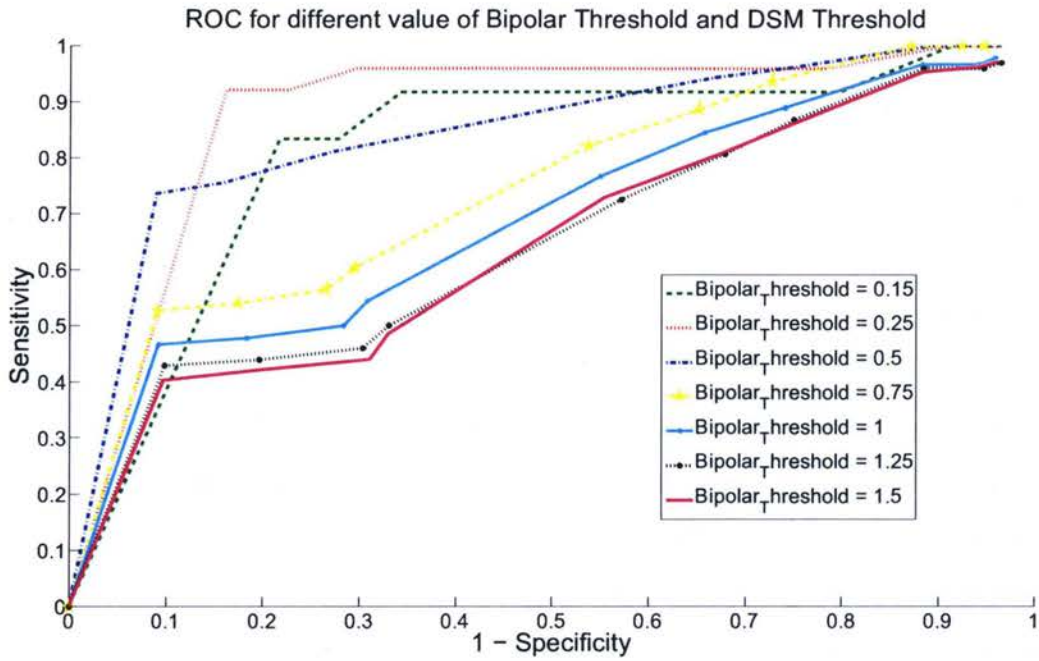

Figure 3.8: ROC Curve for different value of bipolar threshold and DSM threshold: Different values of unipolar threshold (ex. 10%, 25%, 30%, 45% and etc.) with a fixed bipolar threshold (ex. 0.125 mV, 0.25 mV, 0.5 mV and etc.) is used to draw each of these ROC curves. The best area under the curve is for the ROC curve shown in red with the elbow point of 25% of DSM threshold

Bipolar Threshold mV	Area Under the Curve AUC
0.15	0.794
0.25	0.862
0.5	0.824
0.75	0.716
1	0.669
1.25	0.631
1.5	0.625

Table 3.3: Area Under the Curve of the Optimal Value (25% DSM Threshold).

of the most negative slope were calculated (minimum dV/dt). The ability of unipolar virtual electrogram to define the areas of scarring was assessed with ROC curve (Figure 3.9). The ROC curve was the result of bipolar threshold by looking at different dV/dt threshold = [0.1, 0.2, 0.25, 0.28, 0.3, 0.4, 0.5, 0.6, 0.75, 0.8, and 0.9]. In detail, a fixed bipolar threshold (E.g. 0.5mV) was used to define the areas of low voltage detected by the contact bipolar electrograms. Then, in order to draw the ROC curve the set of dV/dt threshold was appointed. ROC therefore, represents a pattern of responding values expected for a particular bipolar threshold at the entire values of dV/dt threshold. As a result, dV/dt threshold of that could best describe the bipolar voltage defined scar was $0.25mV/s$. The resulted ROC curve is drawn in Figure 3.9.

3.5.3 ROC of unipolar filters in optimizing substrate prediction

The virtual electrograms were extracted from the EnSite system with the adjustment of different high−pass filter. Three values for the high−pass filter were chosen. 1 Hz which is the lowest value of the high−pass filter, 8 Hz which is the common value in RVOT VT mapping, and the last extreme 32 Hz. The ROC curve of all these three values were drawn which was the result of the bipolar threshold by looking at different DSM threshold (Figure 3.10). ROC curve resulted from the 2 Hz high−pass filter on the unipolar virtual

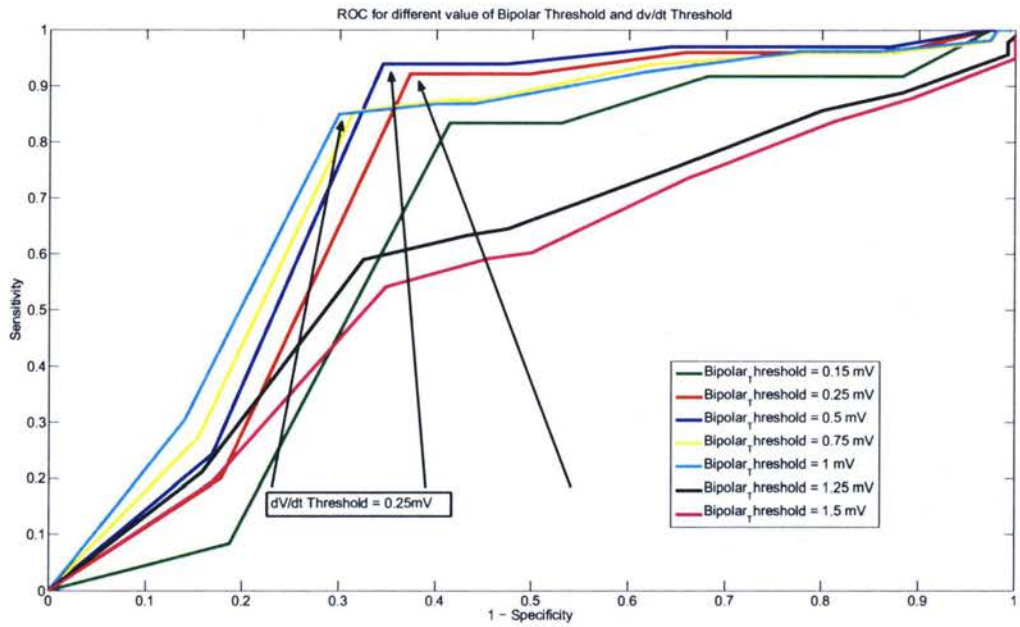

Figure 3.9: ROC for dV/dt of unipolar virtual electrogram vs bipolar threshold. The points along the diagonal indicate results that are no better than chance. When comparing test, the test with the largest area under the ROC curve is preferred, assuming that the goal is to balance the sensitivity and specificity. Bipolar threshold of 0.5mV has the largest area under the curve. This provided us a useful predictor for areas of substrate within the unipolar virtual electrogram.

electrogram has the largest area under the curve.

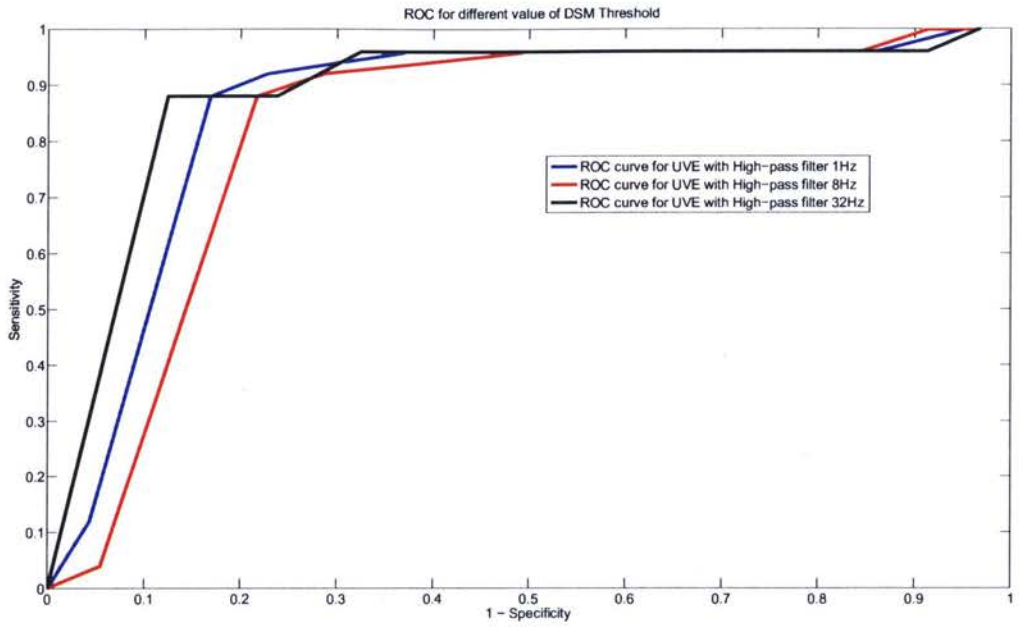

Figure 3.10: ROC for three values of high−pass filter The three set of high−pass filter is compared in this ROC curve. The best area under the curve was found to be for the 1 Hz. The AUC for 1 Hz, 8 Hz and 32Hz were as follows respectively 0.8369, 0.8056 and 0.8690.

3.6 Discussion

The ability to localize RVOT VT with sequential point to point mapping is restricted to a subset of patients with hemodynamically stable VT [63]. To overcome this limitation noncontact single beat activation mapping has been employed and has produced excellent ablation results [64]. However, the role of RVOT substrate in the initiation and maintenance of these arrhythmias has not been elaborated, and the combination of noncontact substrate and activation mapping may further improve ablation outcomes. To the best of our knowledge, this is the first study that determines the optimum settings for noncontact DSM to identify RVOT substrate with comparison to contact bipolar electrograms.

On the basis of the outcome of earlier clinical studies [65], [66] abnormal endocardium was defined as:

- scar (no identification electrograms or bipolar amplitude $< 0.05mV$ [67],[68]) and
- low−voltage endocardium with bipolar contact amplitude of $< 0.5mV$ [69], [67].

For the following reasons contact bipolar electrogram voltage was used as the benchmark for assessing RVOT substrate in this study:

(1) Bipolar contact electrograms remain the most commonly used and clinically established method to define the areas of abnormal endocardium [62] and arrhythmia mapping in the context of inherited and structural heart disease [66], [70], [71] and [72]. In human studies bipolar electrograms remain the electrophysiological gold standard for comparing other substrate assessment modalities, as assessment of tissue pathology is not possible.

(2) Most of the 3−D mapping systems including the EnSite system can import high quality structural information from CT or MR imaging studies [73]. Although both of these imaging modalities can detect areas of myocardial thinning consistent with prior infarction, delayed enhancement MRI can also provide excellent tissue differentiation allowing myocardial scar to be clearly recognized [74]. However, the role of advanced imaging techniques such as MR and PET to identify substrate have not been described for the RVOT.

Sivagangabalan et al. [62] demonstrated that noncontact DSM is comparable to the established CARTO contact system in differentiating normal myocardium and scar in chronic ovine model using rigorous method of direct comparison with transmural histology at plunge needle sites. DSM in that study was used to define post infarct LV scar, as opposed to evaluation of patchy endocardial substrate in structurally normal hearts within the current study. Further, the current study was able to compare significantly more unipolar virtual electrograms and bipolar electrogram points as both were collected on the same electroanatomic system. With the parameter settings we have defined, DSM can localize substrate within the RVOT with similar accuracy to contact bipolar electrograms.

Carrado et al. suggested that electroanatomic scar within the RVOT maybe an early

manifestation of arrhythmogenic right ventricular cardiomyopathy (ARVC) which was confirmed with endomyocardial biopsy [75]. A significant number of patients referred for RVOT tachycardia ablation may have this distinct entity. ARVC RVOT tachycardia is more difficult to ablate and results in poorer long term post ablation outcomes. This form of ARVC imitated idiopathic RVOT tachycardia and highlights the important role of accurate substrate mapping of the RVOT. The DSM parameters defined in our study provide the ability to combine noncontact activation mapping with accurate substrate identification, which may improve procedural success in the group of ARVC patients.

The conclusion of the above results and discussions will be carried out in Chapter 5. In that Chapter, the importance of the findings is also covered. The next Chapter studies the origin of electrical activation within the ventricular walls using the unipolar virtual electrograms. This will help localization of ventricular tachycardia and would finally help in successful ablation of focal arrhythmias.

Chapter 4

Signal Analysis for Cardiac Electrical Activation Studies in Canine Heart

THE purpose of the present thesis was to study the characteristics of the reconstructed unipolar electrograms generated by the EnSite system. This may distinguish the origin of electrical activation within the ventricular walls whether it is endocardial or epicardial. Activation sequence mapping has been used to understand the mechanisms of various ventricle rhythms and arrhythmias. As explained in Chapter 2 there exists wide variety of DSP methods and ideas for studying the endocardial vs epicardial electrical activation. An underlying assumption has been that the ventricle acts electrophysiologically as a two−dimensional surface. Therefore, investigators have recorded either from the epicardial or from the endocardial surface. Mapping of canine ventricle arrhythmia by extra−stimulation has occasionally demonstrated a focal activation pattern. Studies involving the mapping of ventricle fibrillation in humans have also shown similar focal patterns [76]. The purpose of this Chapter is:

1. To determine whether the epicardial and endocardial activation of canine right ventricle are concordant.

2. To relate any differences between the activation of the epicardium and endocardium to the underlying anatomy.

3. To determine whether these differences result in any re−entrant pathways outside the

epicardial or endocardial plane.

Clinical data using the noncontact mapping system suggest that characteristics of the reconstructed unipolar electrograms may predict the origin of electrical activation within the atrial and ventricular walls (endocardial vs epicardial origin.) This will facilitate the surgical treatment of these arrhythmias [77, 78, 79, 80, 81]. Understanding the complex ventricular arrhythmias result in more effective targeting of RF energy applications in patients with VTs [82, 83, 84, 64].

The advent of computer technology in the last twenty years allowed scientists to renew their efforts in the analysis of myocardial electrograms especially the virtual electrograms to improve the assessment of arrhythmias. Computer aided analysis has been carried out both in the time domain and in the frequency domain. Time domain techniques that rely on extracting features for classification directly from the electrogram, such as duration, are somewhat difficult to measure automatically [85]. On the other hand, signal analysis in the frequency domain reveals the spectral characteristics of the electrogram.

The combination of both results finally will help in a more effective targeting of RF energy applications in patients with atrial reentrant tachycardias and VTs [86]. Methods applied in this Chapter is found in the block diagram 4.1.

4.1 Database Analysis

In this Chapter, data was gathered from the right ventricle of a canine heart. This was done in St. Michael's Hospital in Toronto.

4.1.1 Model Preparation of the Canine Heart

The canine data was used to study whether some of the characteristics of reconstructed unipolar electrograms from the noncontact mapping can be used to detect epicardial electrical activation. The preparation and recording of the data was as follows:

The dog was anaesthetized with sodium pentobarbital (30 mg/kg IV) and maintained with 1−2% isoflurane. The protocol was approved by the Animal Care Committee of St

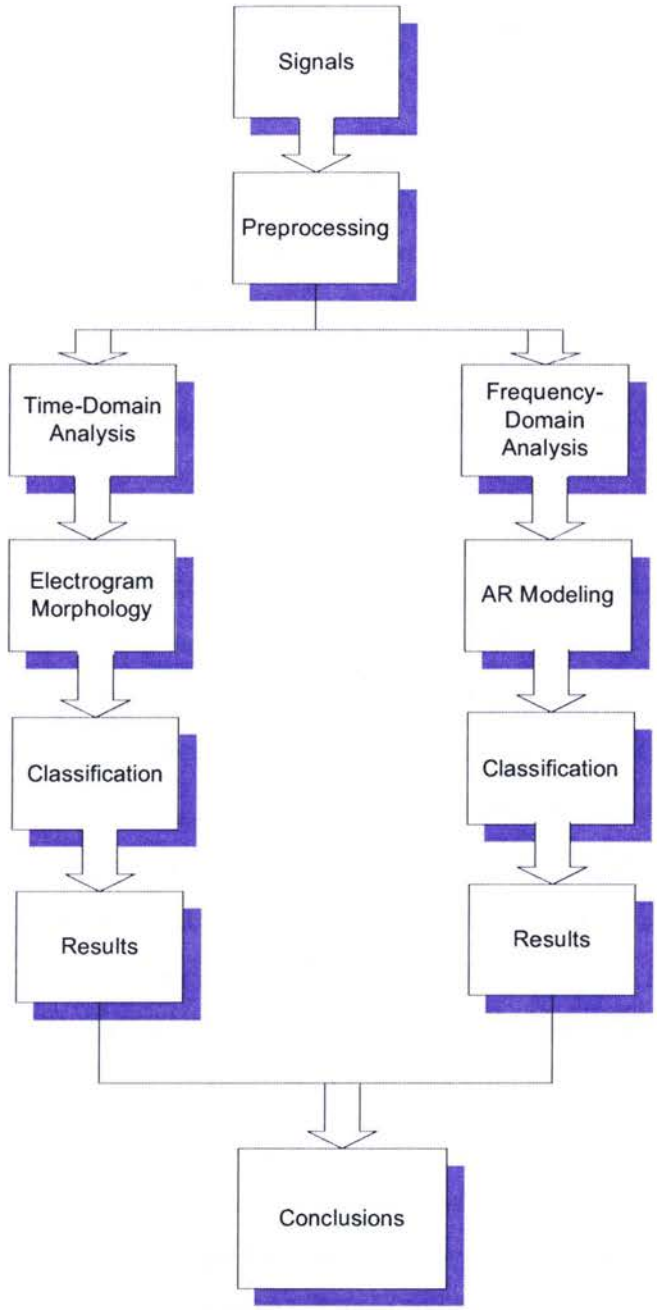

Figure 4.1: Proposed Method.

Michaels Hospital, Toronto, ON, Canada. The investigation conforms to the Guide for the Care and Use of Laboratory Animals, US National Institutes of Health (NIH Publication No. 85−23, revised 1996). Buprenorphine 0.3 mg IV was administered before starting any procedure. ECG leads I, II, and aVF and aortic blood pressure were monitored continuously using a VR12 physiological signal recorder (Electronics for Medicine, Pleasantville, NY, USA).

The technique of noncontact mapping which has been described in previous section was deployed in the right ventricle (RV). Activation clotting time was maintained over 250 seconds with the use of Heparin. An incorporated locator system was used in conjunction with fluoroscopy to position the conventional electrode catheter. By moving the ablation catheter around endocardium, multiple spatial points were identified; with this a 3−D geometry was generated. Simultaneous virtual unipolar electrograms were mathematically reconstructed and displayed on the anatomic model. A rectangular unipolar stimulus using basic drive cycle lengths of 350ms, 400ms and 600ms cycle length was used to pace the heart.

First, the pacing catheter was placed in different positions in the endocardium. The pacing amplitude was 0.5 mV to 0.9 V for different sites. The value was varied until the stimulus captured the ventricular conduction. The position of the pacing catheter was marked on the RV geometry. During the pacing, the noncontact array catheter records the endocardial electrograms for one minute. Following pacing several positions all around the RV, the pacing catheter was removed from the chamber and moved to the epicardium. For this iteration the pacing catheter was positioned on epicardial sites corresponding transmurally to the locations used on the endocardium. Figure 4.2 also shows an example of epicardially paced electrogram superimposed on the endocardially paced electrogram.

In order to capture the ventricular conduction and record it using the EnSite Array ^{TM} catheter, the amplitude of pacing was a bit higher than the endocardial pacing sites. The recording for each site was again 1 minute. The data set therefore consisted of two sets of virtual electrograms: one set was obtained during endocardially pacing recorded with MEA. The second data set was obtained during epicardially paced and also recorded with MEA.

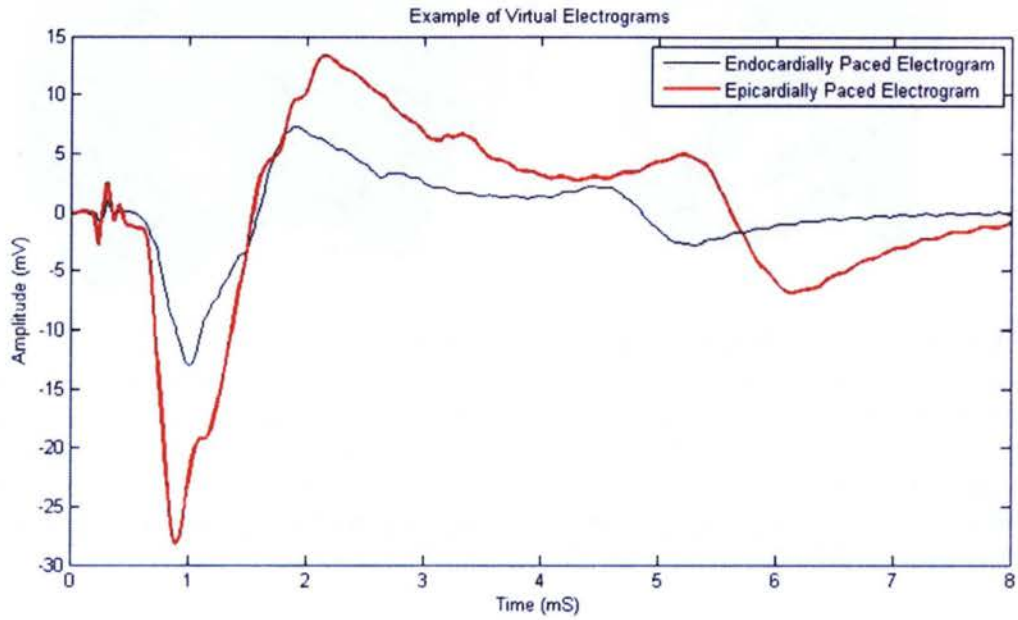

Figure 4.2: Example of Endocardially and Epicardially paced electrograms superimposed in one Plot

The detected electrograms by the MEA were amplified and digitally transferred to a computer workstation. Figure 4.3 shows the exact sites where the pacing took place.

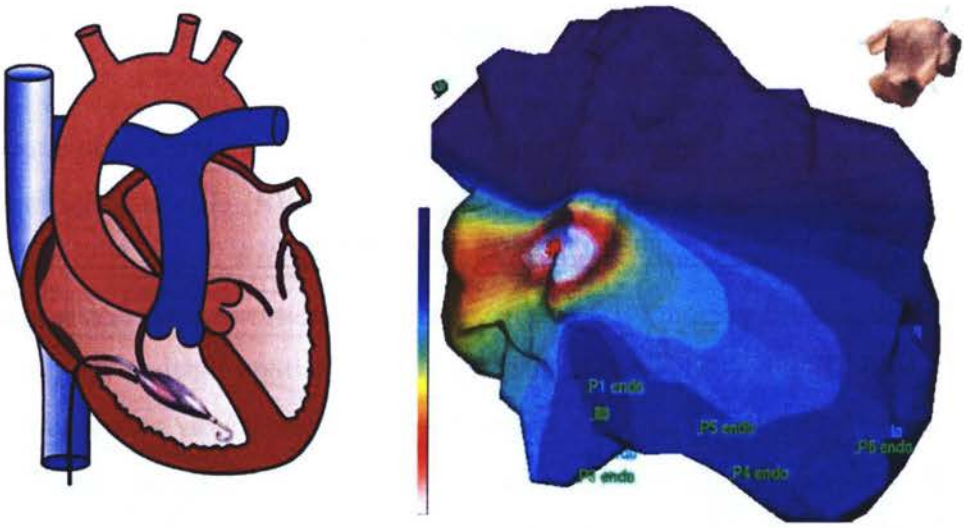

Figure 4.3: Figure on Left is the position of the EnSite Array in the RV; Figure on Right: Illustration of the geometry and positions of the paced areas. This is color−coded isopotential map which shows the range of voltages across the RV at a given time; this is created by moving the ablation catheter around the RV geometry. At a nominal setting the purple represents +5 mV (resting potential) and white represents $-5\ mV$ (depolarization). The worldview reference is a user−selected torso which shows the exact position of the MEA in the chamber. The six paced points are demonstrated in green.

4.1.2 Preprocessing

20 to 30 virtual electrogram recorded with both endocardial and epicardial pacing were selected for analysis and each data set was 4 seconds long. Since the pacing amplitude is different for endocardial and epicardial stimulus therefore to make the chosen features independent from varying pacing electrograms each sample of the signal was divided by the square root of the energy of the signal. Energy of the signal was calculated for each $V(t)$

electrogram with the following equation.

$$E = \sum_{t=0}^{t=4} |V(t)|^2 \tag{4.1}$$

The extracted signals were analyzed and the virtual electrograms for each of the endocardially paced and epicardially paced signals were overlaid. In order to isolate the individual heart beat, signals recorded had to be segmented first.

This segmentation was achieved manually (with approximately 780 samples in each segment) in such a way that, each segment had only one cycle of the virtual electrogram. Moreover, in order to measure and detect the parameters used in this study (explained in Section 4.2) the component between the pacing artifact and the depolarization part of virtual electrogram had to be segmented. This was done by having an imaginary line in mind (as base line) to separate the depolarization part from the rest of the signal. The example of the segmented signal can be found in Figure 4.4. The high pass−filter was set at 8 Hz; all other filters were not changed (low−pass filter at IC 150 Hz, AutoFocus off, Spatial Filter off).

4.2 Time−Domain Analysis of Electrograms

The analysis of intracardiac electrogram morphology has been proposed as a complementary method for accurate discrimination between endocardial and epicardial activation. The modern noncontact mapping system has significantly improved the understanding of complex atrial and ventricular arrhythmias by allowing the direct association of electrical activity at a particular location with the corresponding anatomic structures. In this study, the performance of a traditional time−domain method for electrogram interpretation was used to analyze filtered endocardial and epicardial paced waveforms.

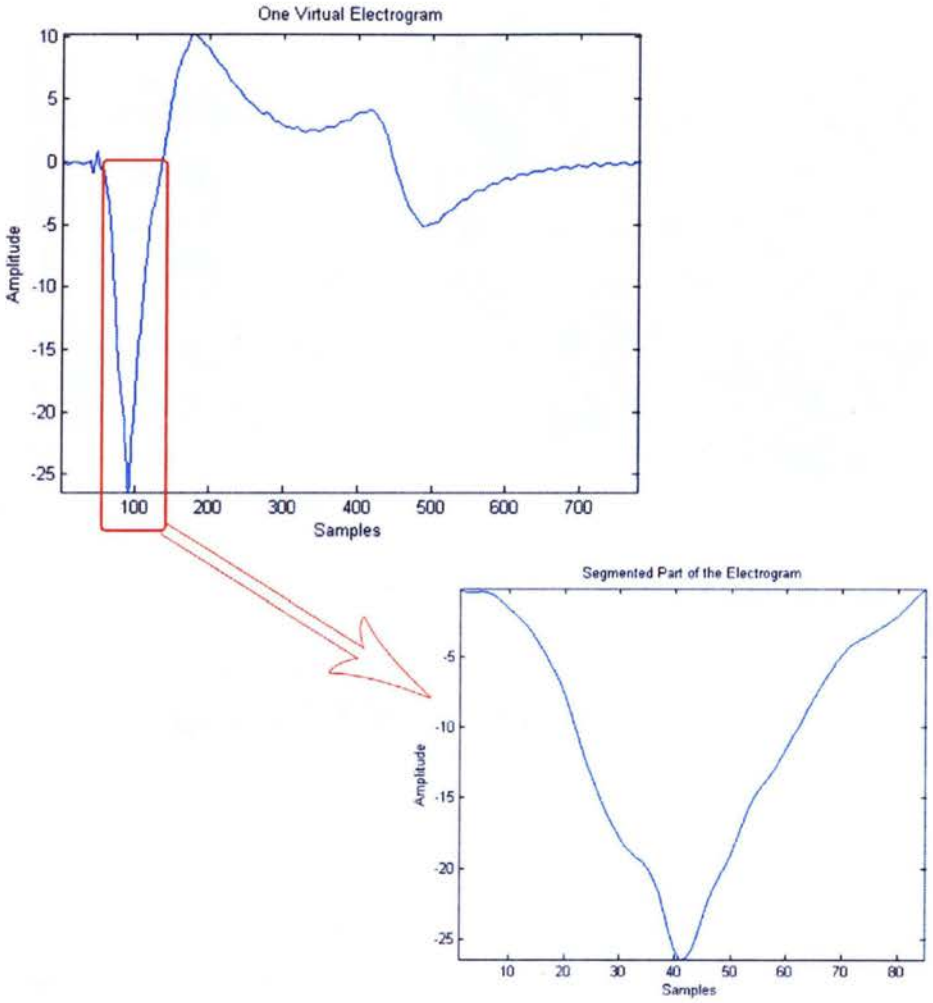

Figure 4.4: Example of the segmented electrogram.

4.2.1 Interpretation of Cardiac Electrograms

The objective for this part is to analyze the information contained in the morphologies of electrograms to predict the origination of cardiac activation in experimental setting. If we consider $V(t)$ to be an electrogram, the following measurements were obtained form each electrogram.

–Peak Negative Voltage (PNV) in (mV): The lowest negative point on the wave. The peak negative voltage indicates the maximum negative voltage of the wave.

–Maximal Negative dV/dt (mV/ms): Greatest amplitude difference in voltage. The measurement was made by computing difference in voltage between the two adjacent points and computing the slope (dV/dt) by dividing the difference in voltage by the difference in time between the two selected points.

$$dV/dt = \frac{V(t+h) - V(t)}{h} \tag{4.2}$$

where value of h close to zero will give a good approximation to the slope of the tangent line.

–Area Under the Curve (AUC) from baseline crossing of unipolar electrogram to maximal negative voltage and from negative voltage to the baseline crossing.

$$AUC = 2 * \sum_{t=0}^{PNV} V(t) \tag{4.3}$$

–Presence of an initial R–wave versus initial *QS* pattern: R–wave is the initial upward deflection of the *QRS complex*, following the Q–wave in the normal ECG and representing early depolarization of the ventricles. Clinicians mostly think of an acceptable R–wave to be ($\geq$ 5mV [87]).

–Duration: Electrogram duration assessed from baseline crossing of the unipolar electrogram to PNV (ms).

–Presence of low–amplitude depolarization preceding the spike of electrical activation of the local myocardium. When the mapping electrode is not in contact with the

myocardium (noncontact mapping case) if the electrogram is a far−field signal generated by tissue some distance from the recording electrode, then the initial negative slope of the recording is typically slow. This is known in literature as "Blue Ghost" [88].

Figure 4.5 shows an example of how the above features were calculated.

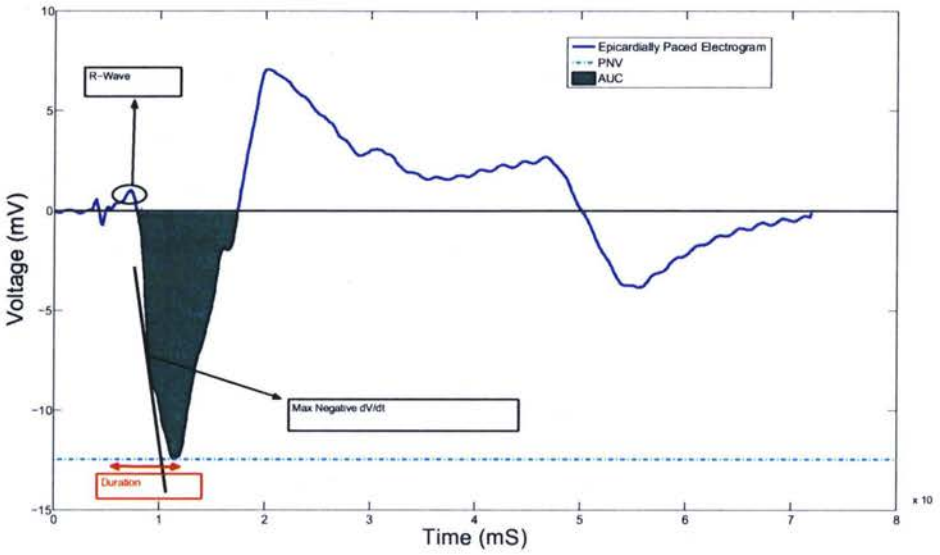

Figure 4.5: Unipolar virtual electrogram paced epicardially. Features described in the text are shown on this electrogram.

The following definitions of unipolar/bipolar waveforms were used:

- **RS:** one positive deflection followed by a negative deflection.
- **QS:** only one large negative deflection.
- **R:** only one large positive deflection.

4.2.2 t−Test

As explained in Chapter 2, t−Test analysis is appropriate in our case because we are comparing the average of the amplitude values of the two signals. In our case, endocardial and

epicardially paced signals. The result is presented in Table 4.2. If the noncontact mapping system revealed significant differences between the characteristics of endocardial or epicardial origin of activation, in Table 4.2 it is indicated as $p < 0.05$ or $p < 0.01$, otherwise non significant (NS).

4.2.3 ROC Analysis

ROC curves were constructed to assess sensitivity and specificity. True positive (TP) is when the specific feature of the signal truly classifies the signal as endocardially paced electrogram. If the feature of the signal classifies the signal to be endocardially paced while it is epicardially paced this is False positive (FP). True Negative (TN) is when the signal is epicardially paced and it is classified to be epicardially paced.

Given a classifier and a set of instances (the test set), a two−by−two confusion matrix can be constructed representing the dispositions of the set of instances as in Table 4.1.

Table 4.1: ROC Analysis.

	Endocardial	Epicardial
Endocardial	TP	FP
Epicardial	FN	TN
Total (in %)	100	100

The total area under the ROC curve is a measure of the performance of the diagnostic test since it reflects the test performance at all possible cut−off levels. The larger the area, the better the performance. The area under the ROC curves and their standard errors were derived as well.

4.2.4 Classification

In the previous section it was explained how the feature vectors consisting of time−domain analysis are constructed. In this section, these feature vectors are used as a descriptor for classification of unipolar virtual electrograms into endocardially or epicardially paced electrograms by the leave−one−out cross−validation method. In this method, one sample is excluded from the data−set and the classifier is trained with the remaining samples. Then the excluded signal is used as the test data and the classification accuracy is determined. This is repeated for all samples of the data−set. Since each signal is excluded from the training set in turn, the independence between the test and the training sets are maintained.

Leave−one−out cross validation has more subtle deficiencies for model selection. Shao (1995) [89] showed that in linear models, leave−one−out cross validation is asymptotically equivalent to AIC which is covered in Chapter 2. Leave−one−out should over fit in small samples [89].

4.2.5 Results

From the virtual electrograms, we analyzed peak negative voltage, max dV/dt, area under the depolarization curve and also detection of R−waves and low−amplitude depolarization. Analyzing the maximal negative voltage and duration from the onset of activation to the peak negative (-2 ± 1mV and 18.8 ± 6.2ms, respectively) exhibit fairly similar values to the epicardially paced electrograms ($-\ 3 \pm 5.3$mV and 22.2 ± 5.3ms, respectively). Maximal dV/dt of the endocardially paced electrograms (1.6 ± 0.2 mV/ms), however, was significantly different from epicardially paced electrograms ($P < 0.05$).

R−waves were observed on the earliest epicardially paced unipolar signals (80% of the times). The area under the curve for the depolarization division of the unipolar electrograms for the epicardially paced signals was wider ($P < 0.05$) than the endocardially paced signals. More than 60% of the virtual electrograms recorded for epicardially paced signals had the evidence of low−amplitude depolarization preceding the spike of electrical activity. Latency

between the pacing artifact and onset of the unipolar electrograms were studied and the result showed a significant difference between the epicardially and endocardially stimulated signals $P < 0.01$.

The result is summarized in Table 4.2. The data are given as mean ± SD.

Table 4.2: Electrocardiographic Parameters Analyzed

Case	Endocardial	Epicardial	t−Test
Latency	14.5±5.3*ms*	18.2±7.8 *ms*	$p < 0.01$
Duration	18.8±6.2 *ms*	22.2± 5.3 *ms*	NS
PNV	-2 ± 1 *mV*	-3 ± 5.3 *mV*	NS
Low Amp. Depo.	0 %	60%	$p < 0.05$
Max Neg. dV/dt	1.6±0.2 *mV/ms*	2.27±0.4 *mV/ms*	$p < 0.05$
AUC	881±36	1090±50.5	$p < 0.05$
R−Wave	0%	80%	$p < 0.01$

ROC curves were used to compare the potentially reliable criteria. Each of the variables had an area under the ROC curves significantly above 0.5 indicating that all were good tests of distinction of activation.

Table 4.3 below summarize the classification for the best discriminator found: Latency.

Table 4.3: Cross−validated: Linear discriminant analysis with leave−one−out method, % − Percentage of classification.

Method	Groups	Endocardial	Epicardial	Total
Cross−validated	Endocardial	131	19	150
	Epicardial	35	115	150
%	Endocardial	**87.3**	12.7	100
	Epicardial	23.3	**76.7**	100

4.3 Frequency−Domain Analysis

In this investigation we show that the frequency characteristics of the unipolar virtual electrograms recorded with EnSite system may help discern the epicardial origin of electrical

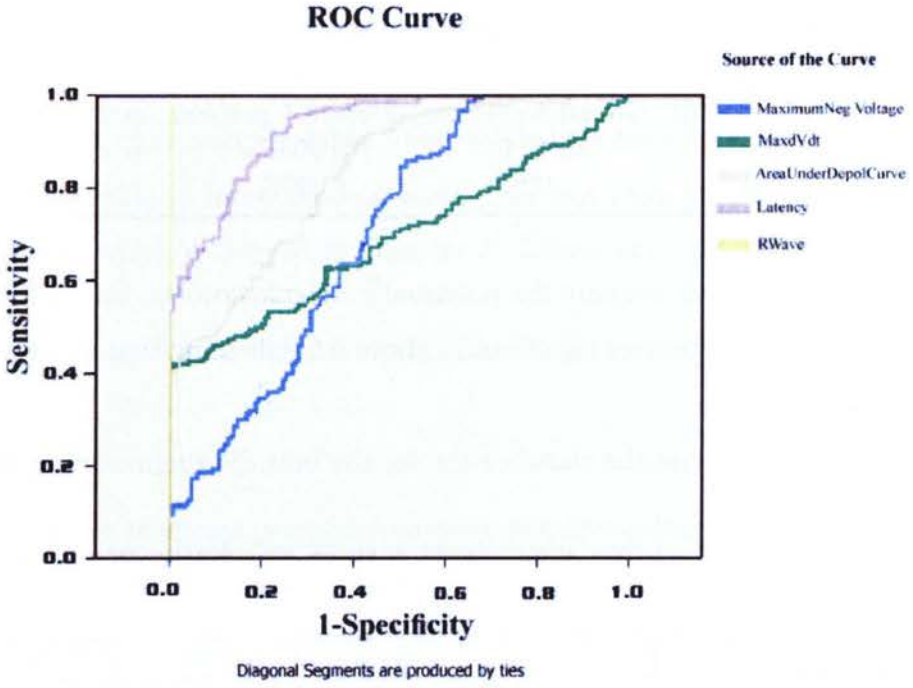

Figure 4.6: ROC curve results. The area under the ROC curve for R−wave was 1, latency was 0.932, area under the depolarization curve was 0.833, maximum negative voltage was 0.698 and maximum dV/dt was 0.692.

activation. This analysis based on FFT suffers from reduced frequency resolution and spectral leakage effects. To overcome this limitation the parametric modeling techniques such as AR, also referred to as all pole modeling, can be used. AR modeling provide parameters which could potentially be correlated with the physiological system producing the signals [43], [90], [91], [92]. AR modeling is a form of signal compression where the coefficients contain the information about the signal characteristics. Using the AR coefficients, cepstral analysis has also been applied to investigate the usefulness of it in the diagnostic assessment of endocardially paced vs. epicardially paced electrograms. Furthermore, classification performance of the the two features was investigated using LDA.

4.3.1 Autoregressive Coefficients

The frequency component of each segment were calculated with Fourier transform (FFT); the segments were multiplied point by point with a Hanning window to avoid edge discontinuities. The Burg method was used to compute the AR coefficients, and the model order was selected using the AIC criterion. The optimum model order was calculated to be 9. The AR coefficients with order $p = 9$ were normalized to be in the range of $-1 < a_1$ to $a_9 < 1$. The AR coefficients were calculated for all the pacing points from the virtual waveforms.

The FFT and the AR spectra for both the endocardially and epicardially paced electrograms is plotted in Figures 4.7 and 4.8, respectively. The power spectrum is plotted on right top corner. In this plot the frequency in Hz is plotted vs FFT magnitude in a logarithmic scale (dB). The AR coefficient is plotted in the bottom left corner with x−axis be the p number (model order) and y−axis to be the value for the AR coefficients.

Generally, the AR spectra either followed closely the FFT spectrum or formed the spectral envelope. In order to indicate that the AR model represents adequately the segmented electrogram, AR model validity was initially checked by a visual inspection of the residual periodogram. The order of the model must be chosen to guarantee that the residual (the error between the actual signal and the signal predicted by the model) is nearly white noise.

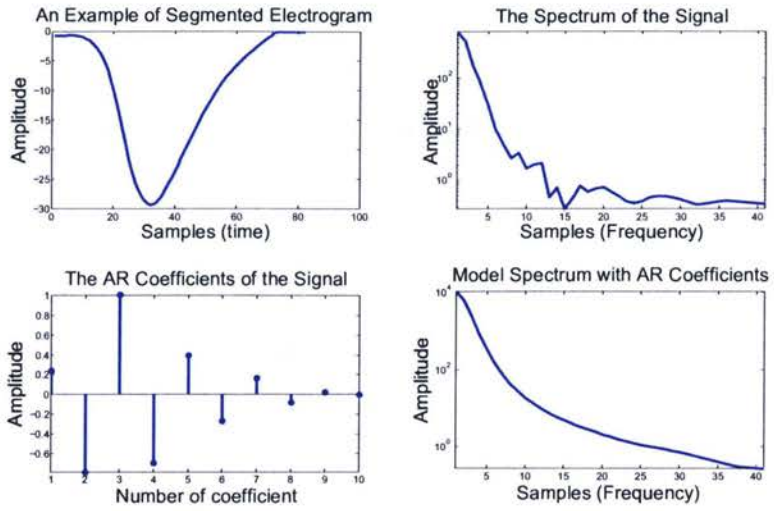

Figure 4.7: Figure on the top left is an example of a segmented electrogram which is Endocardially paced. The top right figure shows the FFT spectrum of the signal. The AR coefficient is plotted in bottom left corner. Bottom right is the spectral estimate using the AR coefficients.

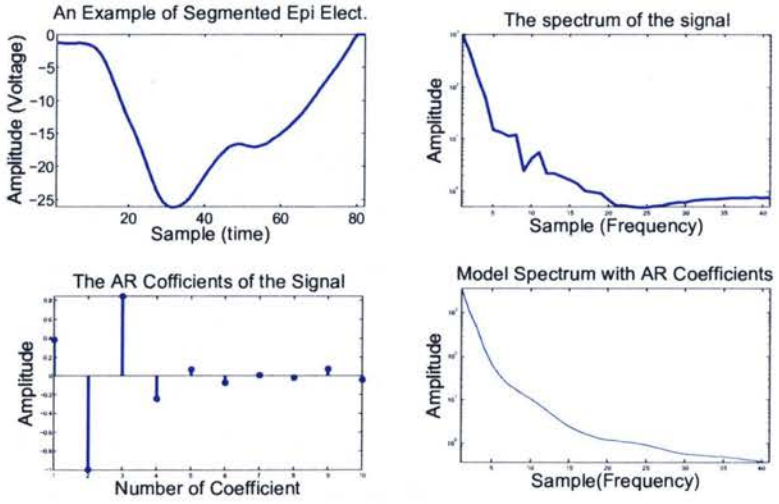

Figure 4.8: Figure on the top left is an example of a segmented electrogram which is Epicardially paced. The top right figure shows the FFT spectrum of the signal. The AR coefficient is plotted in bottom left corner. Bottom right is the spectral estimate using the AR coefficients.

The classification performance of the AR coefficients was examined by LDA as given in Table 4.4.

Table 4.4: Cross–validated: Linear discriminant analysis with leave–one–out method for AR coefficients, % – Percentage of classification.

Method	Groups	Endocardial	Epicardial	Total
Original	Endocardial	44	1	45
	Epicardial	9	51	60
%	Endocardial	**97.8**	2.2	100
	Epicardial	15	**85**	100
Cross–Validated	Endocardial	42	3	45
	Epicardial	11	49	60
%	Endocardial	**93.3**	6.7	100
	Epicardial	18.3	**81.7**	100

4.3.2 Cepstral Coefficients

The cepstral coefficients have additional advantage that one can derive from them a set of parameters which are invariant to any fixed frequency–response distortions introduced by the recording apparatus or the transition system. Therefore, cepstral coefficients improve the signal to noise ratio. Nine cepstral coefficients, c_1 to c_9 were determined directly from the estimated AR coefficients a_1 to a_9. Although cepstral coefficients are deduced from the AR coefficients, it is expected that the nonlinear characteristics of the transformation could lead to an improvement in signal classification using the former than the later. In literature cepstral coefficients provided better classification in speech [46], EMG [47], and vibroarthrogram (VAG) [93] signal analysis. In this we are interested in the parametric representation of the unipolar virtual electrogram that provides an accurate yet efficient representation of the signal to better differentiate the originate of electrical activation. LDA was again used to examine the classification performance of the cepstral coefficients. The result is shown in Table 4.5. It has also been reported that cepstral coefficients may show better separability

compared to the AR coefficient. However, as the result shown in Table 4.5 the cepstral coefficients did not improve the accuracy by a significant amount.

Table 4.5: Cross−validated: Linear discriminant analysis with leave−one−out method for cepstral coefficients, % − Percentage of classification.

Method	Groups	Endocardial	Epicardial	Total
Original	Endocardial	42	3	45
	Epicardial	15	45	60
%	Endocardial	**93.3**	6.7	100
	Epicardial	25	**75**	100
Cross−Validated	Endocardial	42	3	45
	Epicardial	15	45	60
%	Endocardial	**93.3**	6.7	100
	Epicardial	25	**75**	100

For each pacing sites, the average vector of 20 virtual electrogram for each feature set was computed and used as input to the classifier. Tables 4.4 and 4.5 summarize the highest diagnostic yield to be AR modeling to be 90%, followed by cepstral coefficients to be 82%.

Classification result for cepstral coefficient was identical for both the original group and cross validated group to be 82.9%. In this thesis, we have shown that AR spectral measure, AR coefficients as well as cepstral coefficients can be fed into a decision support system in order to improve the classification performance of each feature. It should be kept in mind that selecting the best classifier and best feature set is not necessarily the ideal choice because potentially valuable information contained in the less successful feature sets or classifier may be lost. Therefore, the combination of the results of the different features and the different classifiers increases the probability that the errors of the individual features or classifier may be compensated by the results of the rest [94].

4.3.3 Power Spectral Density(PSD)

The power spectral analysis was also applied to a typical ventricular depolarization. Power spectral density (PSD) is the average of Fourier transform magnitude squared over a large interval. PSD tells us where the average power is distributed as a function of frequency with the following Equation 4.4 [95]. Analysis of PSD (especially on electrocardiogram) has been subject of many investigators over the past few decades. The present study was designed to provide preliminary information regarding the spectral content of both endocardially and epicardially paced electrograms.

$$S_V(f) = \lim_{T\to\infty} E\left\{\frac{1}{2T}\left|\int_{-T}^{T} V(t)e^{-j2\pi ft}dt\right|^2\right\} \tag{4.4}$$

Four classification techniques utilizing spectral analysis were examined. The first classification technique was examining the peak frequency component (PFC) with the highest power as one feature to distinguish endocardial versus epicardial electrical activation. The second classification technique compared the frequency limit (cutoff frequency) below which 95% of total power is contained. Third and fourth classification is followed below.

Figure 4.9 represents PSD of both endocardially and epicardially paced electrogram in one plot. Looking at the graph what is immediately and clearly points is that endocardially paced electrograms reaches the maximum PSD value in the second ascent in frequencies between 50 to 70 Hz. However, the epicardially paced electrograms reach the maximum value for PSD in first ascent in frequencies between 30 to 50 Hz. And also the rate of change of power spectral density for epicardially paced electrogram is faster than the endocardially paced electrogram.

One more important result from Figure 4.9 is area under the PSD curve. The area under the PSD–frequency graph is equal to the mean square value of the signal or more precisely signal average power. Integrating the area under the PSD curve in Figure 4.9 shows that the average signal power of endocardially paced electrogram is greater than the epicardially paced electrogram.

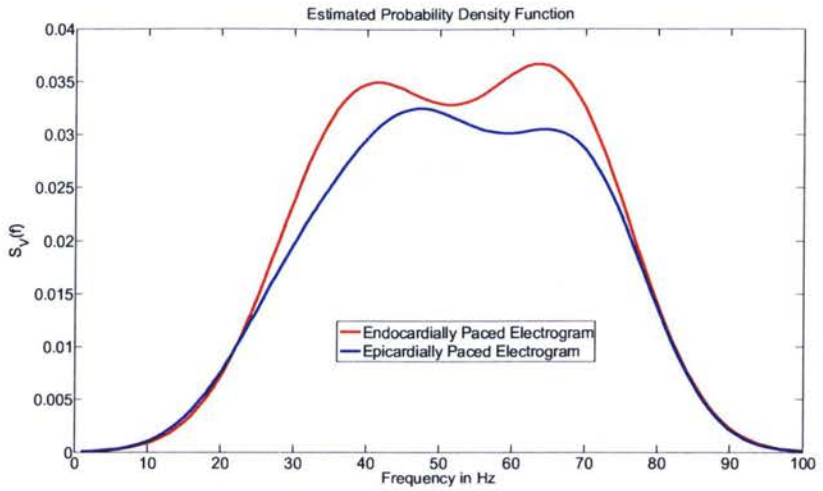

Figure 4.9: PSD of endocardially and epicardially paced electrogram of a segmented virtual electrogram.

4.4 Spectral Estimation

To date, spectral strain estimators introduced in the literature have been based on the DFT and are referred to as nonparametric methods because they make no assumptions about the underlying data (except stationarity). The rationale for investigating the use of parametric spectral estimation techniques stems from the fact that the Fourier transform operates on windowed data segments. Hence, this approach makes the implicit assumption that data outside the window are zero, which is an unrealistic assumption. The inherent consequence of this data windowing is smeared spectral estimates. In contrast, the use of a priori information may permit selection of a model that is an accurate approximation to that of the actual underlying (data−generating) process. Using this parametric based technique, it is hypothetically possible to obtain more accurate spectral estimates by incorporating this model−based approach and subsequently estimating the model parameters from the measured data [96].

Modern noncontact mapping technique allows for identifying arrhythmia focus without

the laborious sequential contact mapping techniques currently in practice. The endocardial and epicardial paced virtual electrograms from the juxtaposing sites allows for an estimate of the transfer function of the myocardium in different positions of the right ventricles of a canine heart. The transfer function estimation will aid in better mathematical modeling of myocardium and could be sensitive measure of myocardial homogeneity and arrhythmic foci localization.

The spectrum of the model was calculated using the Equation 4.5

$$P_{AR}(z) = \frac{1}{\left|1 + \sum_{k=1}^{p} \alpha_k e^{jkz}\right|^2} \tag{4.5}$$

The model spectrum was calculated for both endocardially and epicardially paced data.

$$P_{AR}(z) = \frac{1}{\alpha_0 + \alpha_1 z^{-1} + \alpha_2 z^{-2} + ... + \alpha_{p-1} z^{-p+1}} \tag{4.6}$$

4.4.1 Transfer Function Estimation

Koiwa et al. [97], studied the output signal from the contralateral portion of the left ventricle (LV), when a sinusoidal vibration was applied directly to the anterior epicardium in isolated canine LV, they showed an amplitude modulation with the cardiac contraction. Analyzing these signals, if we could draw an instantaneous LV transfer function curve then it will correlated to ventricular physical properties and its myocardial heterogeneity such as regional myocardial ischemia. If we could describe TFC of human LV, we might be able to estimate the physical properties of the LV. However, no reports have demonstrated the response of human LV or RV myocardium to vibration both from endo and epicardium. The aim of this study was to clarify whether we could vibrate the LV/RV noninvasively and to clarify the mode of vibration in human LV/RV myocardium.

If a model can be successfully fitted to a data stream, it can be transformed into the frequency domain instead of the data upon which it is based, producing a continuous and

smooth spectrum. After AR modeling was done on each segment the spectral estimation was calculated for both endocardially and epicardially paced electrograms, which was then used to derive the transfer function. Measured LV/RV transfer function is defined as the ratio of induced vibration in the LV/RV to input vibration, by applying an external mechanical vibration to the LV/RV epicardium. This transfer function has a resonance curve in relation to applied frequency. Its resonance frequency and the magnitude of the resonant peak are significantly influenced by ventricular pressure, which indicates that the resonance curve reflects the state of the ventricular cardiac muscle.

The transfer function was then calculated by dividing the spectrum of the epicardially paced data ($P_{AR\_Epi}(z)$) (the magnitude of Fourier transform of epicardially paced electrograms or input of our system) with the spectrum of endocardially paced data $P_{AR\_Endo}(z)$ (the magnitude of the Fourier transform of endocardially paced electrograms or output of our system) as shown in the Equation 4.7:

$$\text{TransferFunction} = \frac{\mathrm{P_{AR\_EPI}(z)}}{\mathrm{P_{AR\_ENDO}(z)}} \tag{4.7}$$

Using Equation 4.6 we would have the following:

$$H(z) = \frac{\beta_0 + \beta_1 z^{-1} + \beta_2 z^{-2} + ... + \beta_{p-1} z^{-p+1}}{\alpha_0 + \alpha_1 z^{-1} + \alpha_2 z^{-2} + ... + \alpha_{p-1} z^{-p+1}} \tag{4.8}$$

The important feature is that in the frequency domain, the input and output of a linear system are multiplicatively related via the transfer function. A full description of the transfer function includes both its magnitude and phase; in this thesis, however, we restrict our attention only to the magnitude. Transfer function completely characterizes the system and it may include the viscoelastic properties of the myocardium of the RV.

The transfer function of some of the paced points is illustrated in the following figures. The transfer function is a plot of the ratio of the amplitude spectrum for the epicardially paced electrogram to endocardially paced electrograms versus frequency. The shape of the curves in the figures has common characteristics which we interpret as low−pass like filter of the RV myocardium. By picking up different points and times within the cardiac recordings

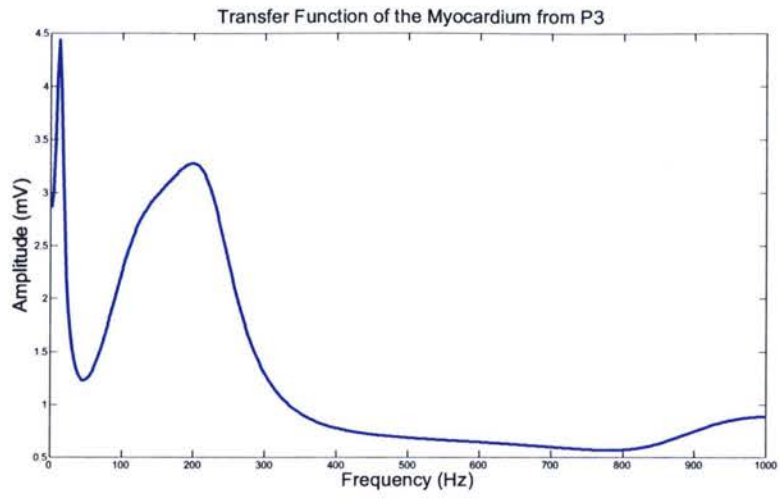

Figure 4.10: Transfer function plot of the myocardium from P3. X−axis is frequency and y−axis shows the magnitude response of the myocardium on P3.

we draw the transfer function and the results were analogous. This is shown in Figures 4.10 and 4.11.

The basic feature of these curves is that they are characterized by a single peak. The figures are consistent with results reported by Hashiguchi et al. [55]. They showed that the single peak configuration is seen in the physiological state of homogeneous myocardial perfusion. The result suggests the possibility of future use in modeling the human heart (especially the reentry circuit modeling of heart). Whole−ventricle models of electrical activity require the three−dimensional geometry of the ventricles, together with a description of the orientation of fibers. Because of inherent simplification of these models, they cannot provide any insight into the behavior and influence of specific ion channels and other intracellular processes on propagation because they are not included.

Hashiguchi et al. [55] computed the transfer function of the left ventricle and concluded two common characteristics. First, at low frequencies there is a gradually falling shape which was interpreted as a response of cardiac mass against local stiffness presented at the myocardium. Second, they also concluded that, at moderate frequencies a single smooth

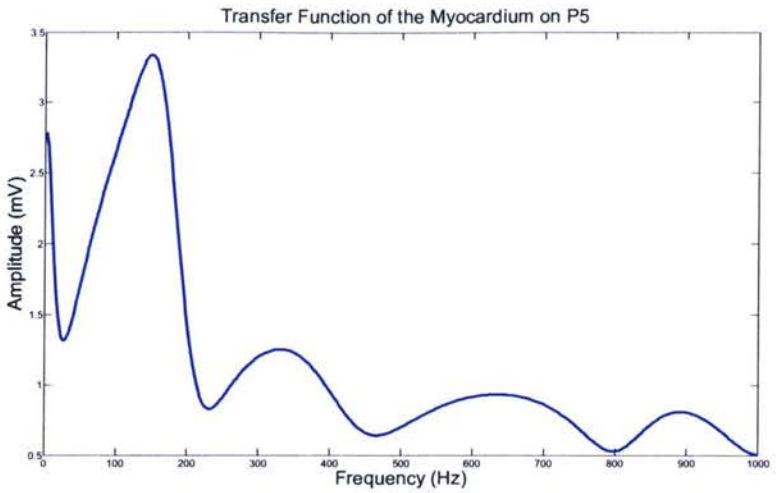

Figure 4.11: Transfer function of myocardium on P5.

peak exits.

Studying the basic characteristics of right ventricle instantaneous transfer function suggest the possibility of future use of this technique in the clinical setting, such as real−time monitoring of expansion of an ischemic region during open chest surgery. Real−time evaluation of the extent of regional damage is therefore important to assess for future use in diagnosis and treatment of functional loss.

4.4.2 Conclusion on Transfer Function Studies

We have presented time and frequency analysis as an efficient tool to estimate the transfer function of RV, in a canine model. This allows for a noncontact technique of identifying epicardial electrical activity. Further validation in humans may allow for a powerful technique to identify epicardial foci in patients using a simultaneous noncontact endocardial mapping tool.

4.5 Further Studies

Further studies was done on real electrograms which was recorded from the The Toby Hull Cardiac Fibrillation Management Laboratory, TGH. Again as was described before, the ability to automatically identify arrhythmias from ECG recordings is important for clinical diagnosis and treatment, as well as, for understanding the electrophysiological mechanisms of the arrhythmias. Therefore in this study the initial requirement of signal processing was first to look at the data and its spectrum and then, the frequency characteristics of the signal (e.g. stationary and nonstationary).

After looking at the characteristics the aim is to determine and quantify the ECG features which describe each arrhythmia in either frequency of time domain, and also to come up with quantifying features of heart abnormalities and arrhythmias. Below is the preparation for the data gathering, the analysis followed by the results and conclusions.

4.5.1 Langendorff Setup

Immediately after heart transplantation, heart was placed in cold tyerode's solution and transferred to the laboratory. Heart was perfused either through the aorta or selective cannulation of coronary arteries (retrograde perfusion). Tyrode's solution was used to perfuse the heart ($95\%O^2 - 5\%CO^2$). The tyrode's solution was passed through a roller pump that will propel it through an oxygenator and a thermostat to the heart. The flow rate was maintained between $0.5 - 0.75$ L/min. The perfusion pressure was maintained between $60 - 65$ $mmHg$ by adjusting the height of the reservoir. The temperature is maintained at $37°C$ and monitored continuously. Figure 4.12 is the langendorff setup in TGH.

4.5.2 Methodology

After a heart is brought to the TGH Lab, it is be placed in a sock with 112 electrodes, surrounding the heart as shown in Figure 4.13.

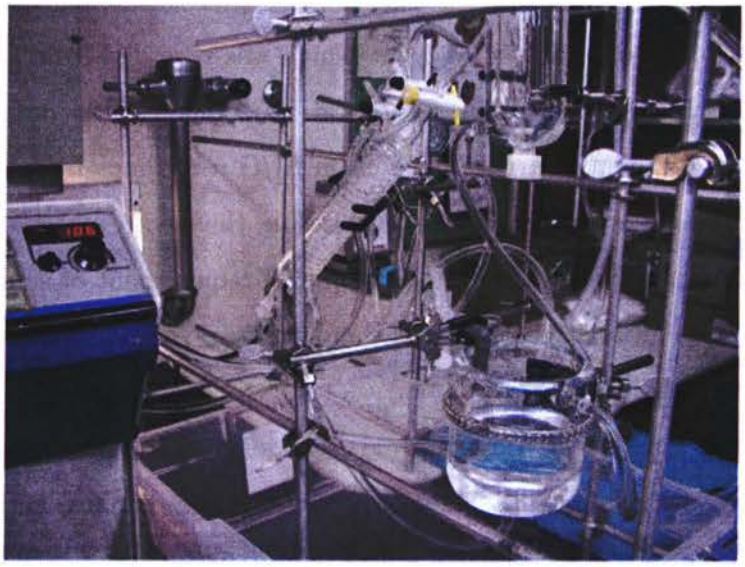

Figure 4.12: Langendorff Setup taken at the TGH Lab.

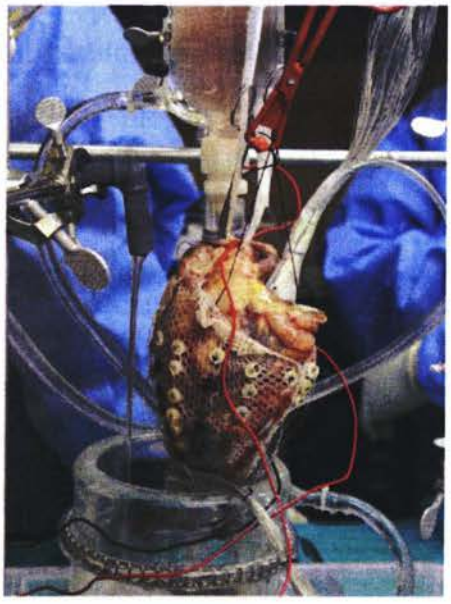

Figure 4.13: Prepared Langendorff Setup for One of the Human Heart Studies in TGH

All of these 112 electrodes have x−axis and y−axis coordinate information which can be scattered on a 2−D surface as shown in Figure 4.14. Each electrode will pick up a different measurement of heart activity from the surface of myocardium. These electrodes pick up all the electrical activities underneath of it during the whole experiment. In this project however, only 3 seconds of signal was chosen, which had 3000 samples (giving a 1 kHz sampling rate). 112 electrodes are numbered, row zero which has x−axis position of zero and y−axis of positive values will be positioned on the septum of myocardium for the reference that it is known which value is for which part of heart. Each row has 8 electrodes and there are 14 rows.

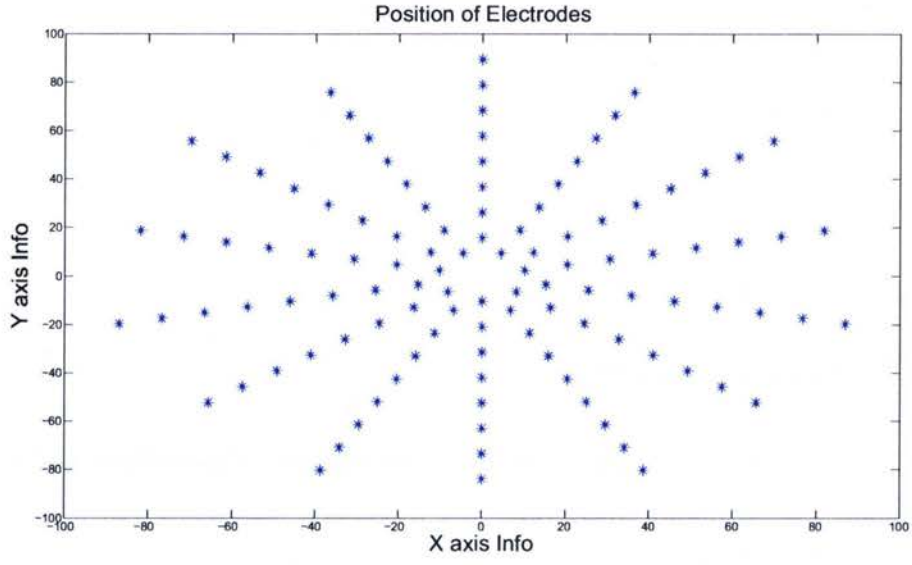

Figure 4.14: Position of the Sock Electrodes Mapped on a 2−D Surface

Figure 4.15 is an example of 11th row's third electrode which for simplicity of the rest of the project, the first 1000 samples of the signal is drawn as well.

For simplicity purposes, a GUI version of the 112 electrode was made which will have two inputs: the row number and the electrode number. After inputting the required electrode, the signal and its filter is drawn. As an example, the 83^{rd} electrode is redrawn here in the

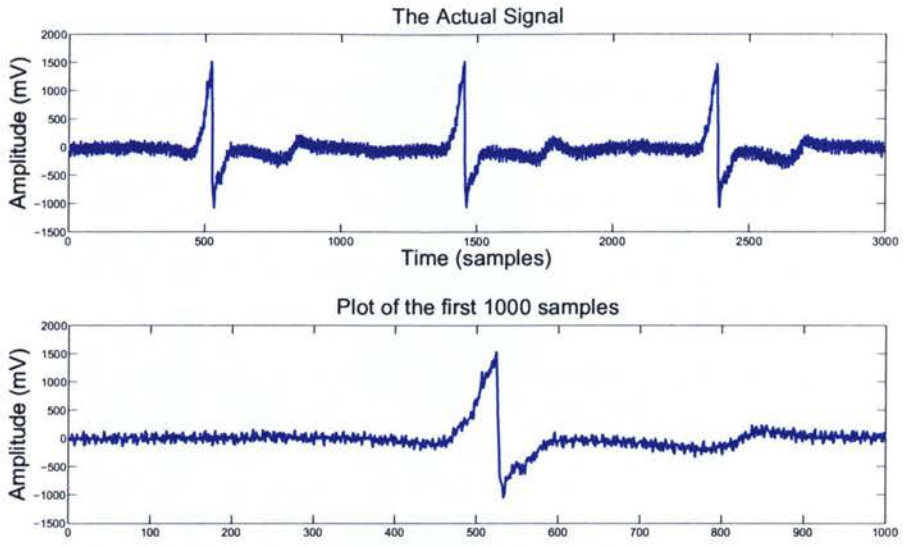

Figure 4.15: An Example of the Reading from one Electrode.

GUI (Figure 4.16).

The signal is noisy and needs to be filtered for further analysis. A low−pass Chebychev filter with order 9 was used. The FFT spectrum of the signal and filtered was drawn for comparative purposes in order to visualize the two spectra.

Each electrode can represent a different maximum magnitude as a specific frequency. In order to calculate the maximum magnitude, the frequency between 0.5 to 15 Hz was band-pass filtered. Then the FFT of the signal was calculated in order to pick up the maximum magnitude and its frequency. To give the higher frequencies some differences the graph was color coded with higher frequencies to be more reddish and lower frequencies to be bluish.

Figure 4.20 is called the DF map. In this project, in order to get the interpolated value first the circular interpolation was done. This is a very lengthy approach of interpolating the map. Circular interpolation will calculate the average of the two points and put the values in between the points. Assigning more points between two consecutive points gives the smoother color.

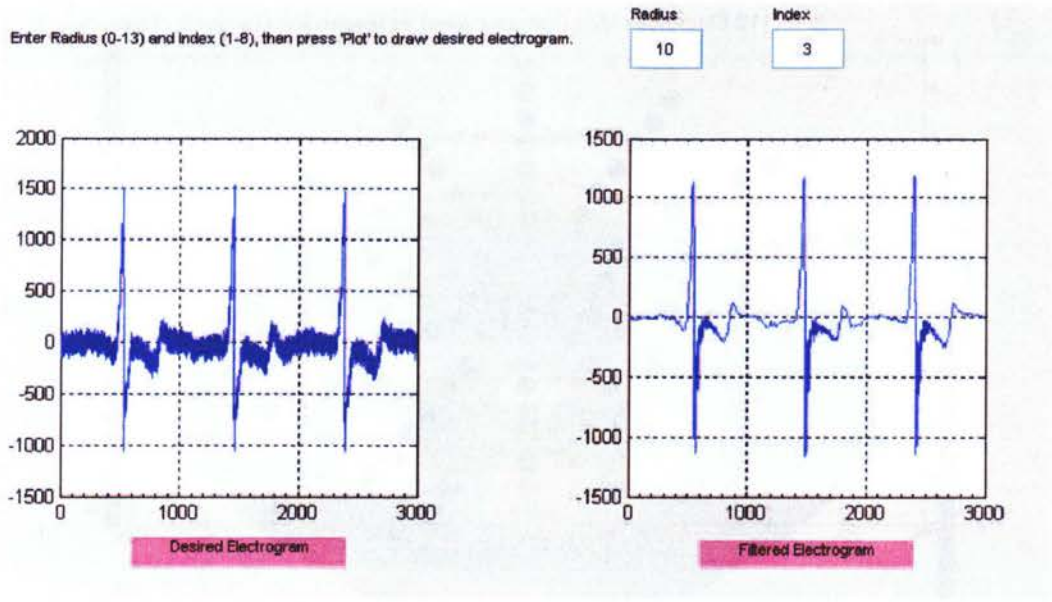

Figure 4.16: GUI Version of the 112 Electrodes

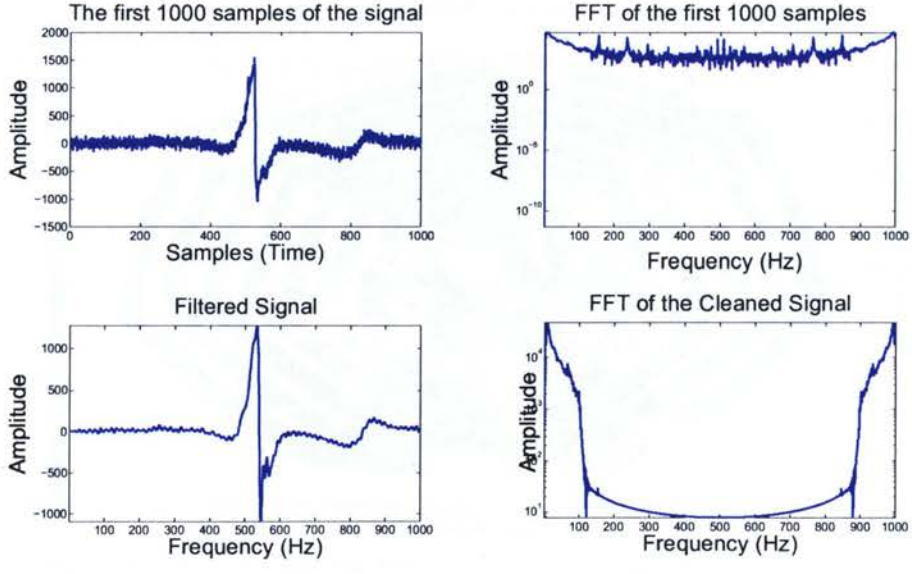

Figure 4.17: ECG electrograms and its spectrum.

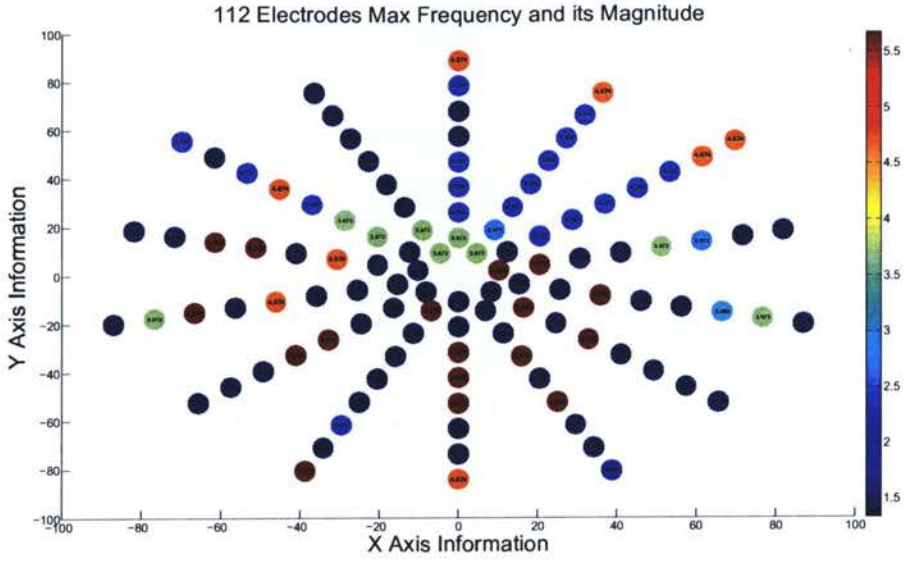

Figure 4.18: 112 Electrodes and its Maximum Frequencies.

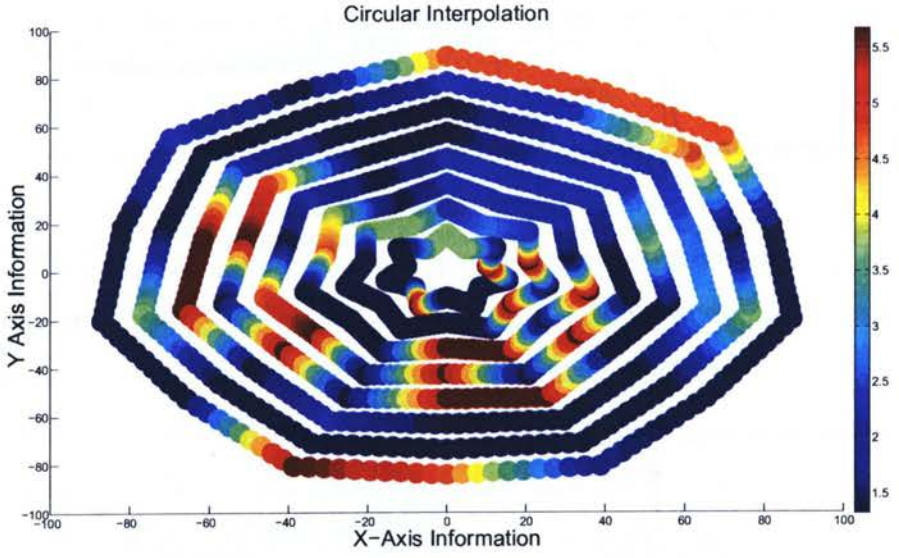

Figure 4.19: Circular Interpolation.

After circular interpolation, interpolation can be done row wise. Figure 10 is the final interpolation with first circular and then row wise.

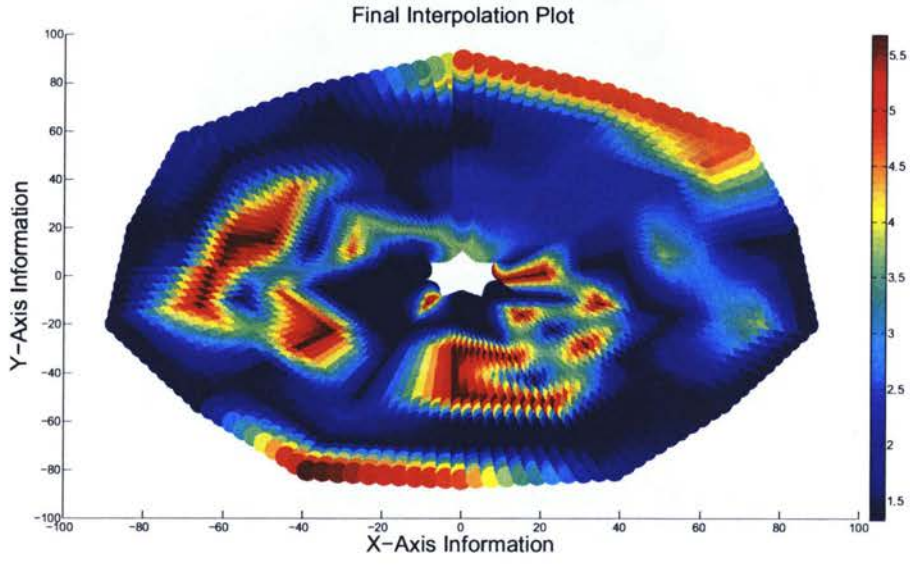

Figure 4.20: Final Interpolation of DF map.

Knowing the signal is non−stationary, there is a need to segment the signal into stationary components. The adaptive segmentation used was based on the recursive least square (RLS) algorithm. The goal of any adaptive filter such as the RLS algorithm is to find and track the optimum filter corresponding to the same signal operating environment with complete knowledge of the required statistics. The performance of such adaptive filters are evaluated using the concept of stability, speed of adaptation, quality of adaptation, and tracking capabilities. Therefore the distinguishing feature of the adaptive filters is that they can modify their response to improve their performance during operation without any intervention from the user [98]. The advantages as read from the literature is when using the lattice filter the statistical changes in the signal is reflected in the filter parameters, hence the segment boundaries can be detected by monitoring any one of the filter parameters such as mean squared error or reflection coefficients. According [99], the signal is passed twice to

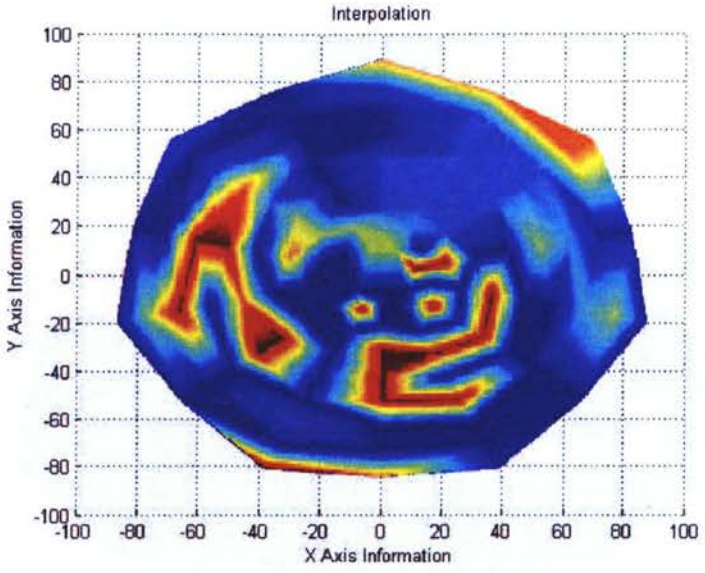

Figure 4.21: Complete Interpolation (Smooth Version).

the segmentation filter and at a particular time sample during the second pass if it is lesser than the threshold a primary segment boundary is marked. If the difference between a PSB and the previous PSB of the same signal is greater than or equal to the minimum desired segment length (700), the PSB is marked as a final segment boundary; if not, the PSB is deleted and the process continued until all the PSBs are tested.

After segmenting the signal into stationary components, now AR modeling was used to get the AR coefficients using Equation 4.9. The model order for AR modeling was 30 in this case. There is no straightforward way to determine the correct model order. As one increases the order of the model the root mean square (RMS) error generally decreases quickly up to some order and then more slowly. An order just after the point at which the RMS error flattens out is usually an appropriate order.

$$H(z) = \frac{G}{1 + \sum_{k=1}^{k=p} a[k] z^{-k}} \tag{4.9}$$

After getting the AR coefficients and averaging them because they would be different for different segments, using the Equation below the All Pole model of the system was generated. Poles of the AR model system could be extracted from the model transfer function by factorizing the denominator of Equation 4.9 [100]. In order to reduce the dimensions of the feature vector, dominant poles were used as they represent the dominant features of the signal in the spectral domain. Equation 4.9 may be factorized into individual pole contributions as follows:

$$H(z) = \frac{G}{|(z - b_1)(z - b_2)...(z - b_p)|} \tag{4.10}$$

where $b_1, b_2...b_p$ correspond to the complex poles of the transfer function $H(z)$.

Drawing the pole zero map, it is obvious that some of the poles are more dominant than others as shown in Figure 4.22. Dominant poles are the ones which have the maximum distance from the origin in the z−plane. These dominant poles will represent dominant peaks of the signal in the spectral domain, and could be used as parameters for constructing feature vectors [101].

The envelope of the spectrum of the signal using the AR coefficients was plotted as in Figure 4.23. As it is shown from the graph in Figure 4.24 the envelope of the spectrum of the signal using the AR coefficients is almost the same as the spectrum of the signal using FFT.

Detailed discussions and conclusions of these results can be found in Chapter 5.

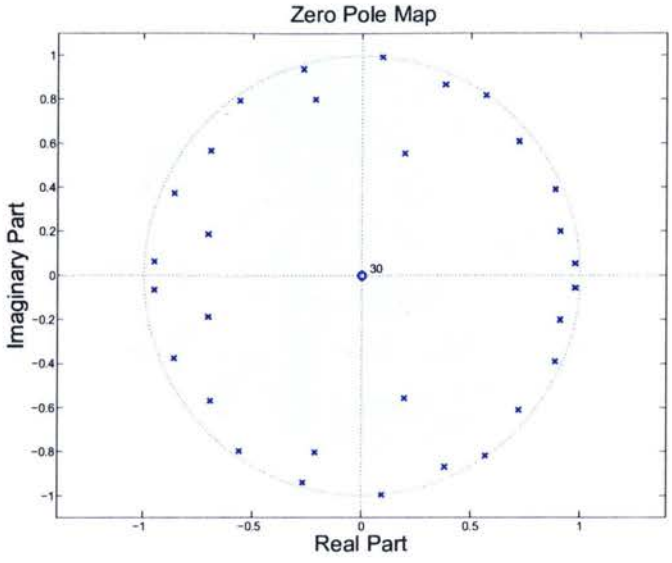

Figure 4.22: Pole Zero Map.

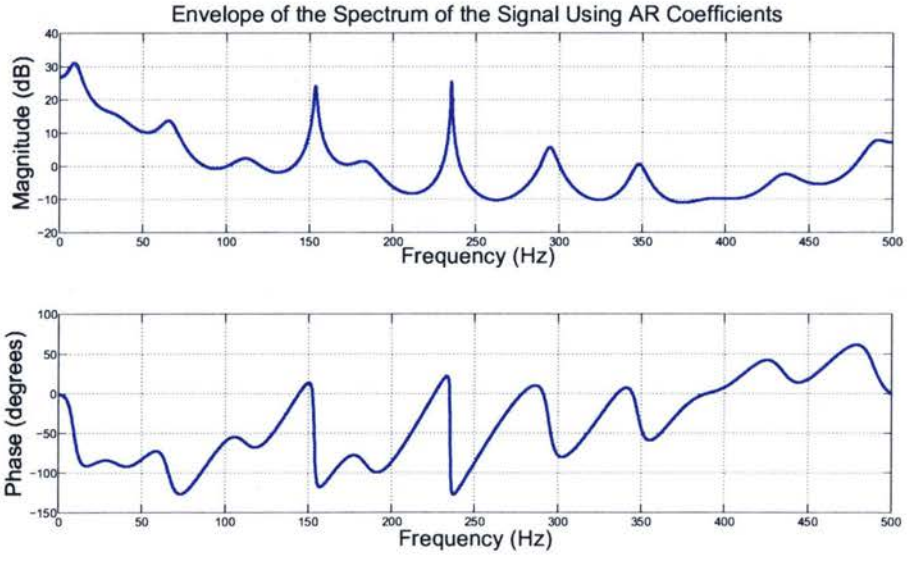

Figure 4.23: Envelope of the Spectrum Using AR Coefficients.

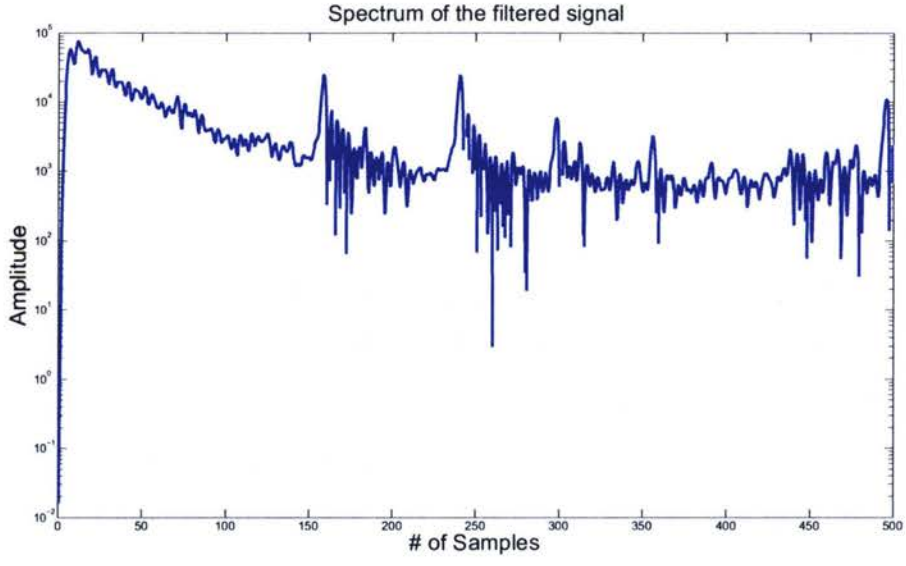

Figure 4.24: Spectrum of Filtered Signal.

Chapter 5

Conclusions

5.1 Discussion and Conclusion on Cardiac Studies

In the study of Chapter 3, in order to evaluate the ability of virtual electrograms to predict abnormal bipolar electrograms we tested the hypothesis of max dV/dt, filtering and optimized DSM threshold. This would hopefully allow, for better identification of abnormal myocardial substrate traditionally defined by contact bipolar mapping in human RVOT.

The DSM threshold for accurate substrate identification varies between species, cardiac chambers, and underlying pathology. Previous studies have used different DSM thresholds such as: threshold of $< 30\%$ in the human right atrium (RA). And Fontan used $< 50\%$ in the ovine left ventricle post infarct and later $< 34\%$ was used in the canine LV post infarct [60], [65], [102]. Defining DSM thresholds for clinical use in various scenarios will improve its utility. This study identifies a DSM threshold for substrate identification of the human RVOT which was reproducible across subjects in the study.

The first derivative of the unipolar electrogram (dV/dt) represents the velocity of local activation. The maximal negative dV/dt is used as a marker of local activation timing. dV/dt is dependent on the viability of local tissue and the speed of local conduction. In diseased states the slope of the unipolar electrogram is decreased, the duration prolonged and the maximal negative value of the derivative reduced. For substrate mapping these features provide additional details of tissue viability compared to electrogram voltage. In this study a dV/dt threshold of 0.25 mv/s identified bipolar defined substrate, and may have potential

role in substrate delineation.

Electrograms recorded in normally conducting atrial or ventricular myocardium possess spectral components in the mid range of 4 to 16 Hz; whereas electrogram in regions of slow conduction are composed of lower−frequency spectral components of 1 to 4 Hz. Spectral components associated with repolarization waves lie in the low end of the spectrum at 1 to 4 Hz. Thus, the high−pass filter must be adjusted between 1 and 32 Hz, helping to modulate the extent to which low−frequency signals are visible on the three−dimensional display. However, filtering out large repolarization waves by the high−pass filter may attenuate critical information contained in relevant signals of lower frequency and amplitude. For DSM construction in the RVOT, filtering unipolar virtual electrogram at 1 Hz produces the highest accuracy in comparison to contact bipolar electrograms.

Identification of true local activation or repolarization waves is essential to successful utilization of the EnSite system. This problem may be emphasized with unipolar, noncontact mapping because signals detected by the array initially are amplified to derive the endocardial map. Thus low−frequency noise, repolarization waves in the measure cavity will be magnified into larger signals on the reconstructed chamber. In the unipolar electrograms, signals associated with high conduction velocity possess a greater slope ($-dV/dt$), and thus are characterized by high−frequency spectral components ($>$ 32 Hz) electrograms recorded. The ratiometric design of DSM and the optimal filtering identified in this study overcome some of these limitations.

The major limitation of the noncontact system is the proximity accuracy of unipolar virtual electrogram. Beyond 40mm from the equator of the MEA the amplitude, timing, and morphology of unipolar virtual electrograms significantly decreased. This is an issue in large dilated aneurismal chambers but not of significance when mapping the RVOT as in the current study.

In this human in−vivo study of the right ventricular outflow tract we have demonstrated that when noncontact virtual unipolar electrograms are high pass filtered at 1 Hz, subject to dV/dt threshold of 25mV/s and to DSM threshold of 25% it provides substrate localization

comparable to contact bipolar electrogram mapping. Thus this strategy may provide an alternate rapid substrate mapping tool when used with optimal parameters. Therefore, the noncontact DSM tool can be used to identify RVOT substrate with a considerable degree of accuracy. Accurate noncontact identification of RVOT substrate may lead to improved patient ablation outcomes.

The next Section will cover the Conclusions on Chapter 4.

5.2 Conclusions on Cardiac Electrical Activity

5.2.1 Discussion and Conclusion of Time–Domain Analysis

Findings in this experiment is important if these results obtained in the present study:

- Are valid during the re–entrant and focal arrhythmias.
- Can correspond well with clinical findings.
- May help to determine if different characteristics is applicable to human ventricular tachycardia.

We have presented the electrographic parameters to analyze the difference between the endocardially paced and epicardially paced electrograms in this preliminary study. The morphologies of the unipolar electrograms generated by the noncontact mapping system allowed the discrimination of endocardial versus epicardial origin of electrical activation. R–wave appeared to be the best discriminant feature between endocardially and epicardially paced electrograms. From statistical results, it might be possible to identify possible parameters to be used to discriminate between epicardial and endocardial activation. We also believe the possibility that the combinations of these criteria might improve the perception over any single criterion. This may allow the detection of tachycardia that originates epicardially. It should be kept in mind that intracavitary maps deserve further studies, especially their performance should be evaluated in animal preparations of sustained VTs, as a preliminary step toward clinical trials.

The result of this experimental study with the intention to find different features to determine the origination of activation are in accordance with the findings derived from the clinical settings. The presence of initial R−wave had a positive predictive value of 0.8 for epicardial origin of electrical activation. This findings fit well to the meaning of the unipolar electrogram. The unipolar electrogram represents the intrinsic deflection at the given location it is recorded [103]. An initial R wave of the unipolar endocardial electrogram is resulted if the electrical wavefront from a myocardial and an epicardial focus travels in part toward the recording location. In contract to this, in theory an endocardial origin of activation results in a pure QS pattern at the location as all electrical forces are heading away from that location [104]. Therefore, according to this finding it may be stated that the noncontact mapping allows for identification of the origin of focal activation which would be useful in choosing the appropriate mode of energy delivery [105].

Electrograms obtained during epicardial simulation exhibited a significantly higher maximal negative voltage and maximal dV/dt than those reconstructed during endocardial simulation. Cardiac fiber orientation influences the maximal conduction velocity and maximal voltage of the electrical wavefront [106].

Latency between the pacing artifact and the beginning of the unipolar electrogram exhibited significant difference when compared according to pacing location in RV. This phenomenon is most probably related to thickness at the different pacing location chosen in this present study [107].

5.2.2 Discussion and Conclusion of Frequency−Domain Analysis

The frequency analysis of unipolar electrograms generated by noncontact mapping allows the discrimination of endocardially and epicardially paced electrograms. The decomposition of the signal using AR model of sufficient order produces residuals, thus allowing synthesis of statistically equivalent signals.

It will be clear that a classification scheme for clinical diagnosis can be evolved based on the pole−zero pattern of the signal models. The representation of the original signal by its

model, as proposed here, provides an efficient method to the hitherto related data handling problems of virtual electrograms for better discrimination of endocardial vs. epicardial activation pattern. We also believe that possibility of combination of the time−domain and frequency−domain characteristics would improve the perception over any single criterion.

Finding of this experiment may be discussed if these results obtained in the present study are still valid during the reentrant and focal arrhythmia. Further studies would help to determine if differing characteristics is applicable to human ventricular tachycardia.

5.2.3 Conclusion on Pole−Zero Map

In this Chapter, using the normal sinus rhythm data the signal and the spectrum of it were plotted. Two different ways were used to calculate the maximum frequency from the surface contact electrograms. The first way was using the FFT and then finding the maximum magnitude and its frequency. The second way, however, was first to segment the signal and get the AR coefficients and then calculate the dominant poles and draw the envelope spectrum of the signal. The two methods, gave similar values. There are two critical issues in AR modeling first is choosing the AR order of coefficients to model the signal. AR order should be appropriately chosen to make sure that the signal is approximated with high accuracy. Various model orders were tested to obtain the best accuracy in the modeled signal. In this thesis the model order was chosen on RMS algorithm as explained before. The second critical issue in AR modeling is the segmentation of parameters. This issue may be the cause of small error between using FFT or AR modeling to find the dominant frequency and its magnitude.

5.3 Future Work

Signal characteristics were studied both in the time and frequency domain to determine if some of the characteristics of reconstructed unipolar electrograms from the noncontact mapping system can be used to detect epicardial electrical activation in a canine heart. These

studies can be applied to in human heart. The reliability of these results should be tested in patients both during sinus rhythm and ventricular tachycardias. The impact of these studies would help electrophysiologists pin point the exact location of the tachyarrhythmias in patients.

And also, the efficacy of antitachycardia devices for the treatment of ventricular tachycardia medication depends upon the reliable identification of ventricular tachycardia. These criterium can be used in the VT detection algorithms used in automated external defibrillator (AED), which therefore implies algorithms that are accurate and easy to implement in hardware. High detection accuracy is suitable for real−time implementations in AEDs.

Publications

Journal Papers

- Elnaz Shokrollahi*, Vijay Chauhan, Imad Hameedullah, Karthikeyan Umapathy, Stephane Masse, Eugene Downar, Talha Farid, Krishnakumar Nair, Sridhar Krishnan, Kwaku Poku, Kumaraswamy Nanthakumar., "Noncontact and Contact Mapping: Criteria for Identifying Right Ventricular Outflow Tract Substrate", under review, *European Society of Cardiology (EP Europace)*, August 2009.

Conference Papers

- Elnaz Shokrollahi*, Sridhar Krishnan, Stephane Masse, Karthikeyan Umapathy, Luc Soucie, Talha Farid, Kumaraswamy Nanthakumar, "Efficacy of Noncontact Mapping in Detecting Epicardial Activation", In Proc., 31^{st} *Annual International Conference of the IEEE Engineering in Medicine and Biology Society (EMBC 2009)*, September 2009.

- Elnaz Shokrollahi*, Sridhar Krishnan, Stephane Masse, Karthikeyan Umapathy, Luc Soucie, Talha Farid, Kumaraswamy Nanthakumar, "Transfer Function Estimation of the Right Ventricle of Canine Heart", In Proc., *World Congress in Medical Physics and Biomedical Engineering (WC)*, September 2009.

Bibliography

[1] AED Headquarters. Sudden Cardiac Arrest kills more than 450,000 Americans each year. *http://www.aedhq.com*, 2007.

[2] Oregon Health and Science University. The heart's electrical conduction system. *http://www.ohsu.edu/health/health-topics*, 2008.

[3] Marschall S. Runge and M. Andrew Greganti. Physiology of the specialized conduction system. *http://www.us.elsevierhealth.com/*, 2008.

[4] Mayo Foundation for Medical Education and Research. Ventricular Arrhythmias. *http://www.revolutionhealth.com/*.

[5] ST. Jude Medical. EnSite Array ^{TM} Catheter. *http://www.sjmprofessional.com/*.

[6] Rajappan K. and Schilling R. J. Non-contact mapping in the treatment of ventricular tachycardia after myocardial infarction . *Journal of Interventional Cardial Electrophysiology*, 19(1):9–18, 2007.

[7] Douglas P. Zipes Ziad Issa, John M. Miller. Clinical arrhythmology and electrophysiology. *Elsevier Health Sciences*, 2008.

[8] William M.K. Trochim. Research Methods. *http://www.socialresearchmethods.net.*

[9] Richard Kirk. Congenial Heart Disease. *http://www.med.nus.edu.sg.*

[10] J.L. Huang, C.T. Tai, Y.J. Lin, B.H. Huang, K.T. Lee, S. Higa, Y. Yuniadi, Y.J. Chen, S.L. Chang, L.W. Lo, et al. Substrate mapping to detect abnormal atrial endocardium with slow conduction in patients with atypical right atrial flutter. *Journal of the American College of Cardiology*, 48(3):492–498, 2006.

[11] K. Rajappan and R.J. Schilling. Non-contact mapping in the treatment of ventricular tachycardia after myocardial infarction. *Journal of Interventional Cardiac Electrophysiology*, 19(1):9–18, 2007.

[12] Z.W. Liu, P. Jia, P.R. Ershler, B. Taccardi, R.L. Lux, D.S. Khoury, and Y. Rudy. Noncontact endocardial mapping: reconstruction of electrograms and isochrones from

intracavitary probe potentials. *Journal of cardiovascular electrophysiology*, 8(4):415–431, 1997.

[13] M. Shenasa, M. Borggrefe, and G. Breithardt. *Cardiac mapping*. Blackwell Pub, 2003.

[14] M.E. Josephson. *Clinical cardiac electrophysiology: techniques and interpretations*. Lippincott Williams & Wilkins, 2002.

[15] E. Delacretaz, K. Soejima, V.K. Gottipaty, C.B. Brunckhorst, P.L. Friedman, and W.G. Stevenson. Single catheter determination of local electrogram prematurity using simultaneous unipolar and bipolar recordings to replace the surface ECG as a timing reference. *Journal Of Pacing And Clinical Electrophysiology*, 24(4 Part 1), 2001.

[16] JMT De Bakker, RNW Hauer, and TA Simmers. Activation mapping: unipolar versus bipolar recording. *Cardiac Electrophysiology: From Cell to Bedside. Second Edition. WB Saunders, Philadelphia*, pages 1068–1078, 1995.

[17] S.K. Huang, S.K.S. Huang, M.A. Wood, and M.M. Scheinman. *Catheter ablation for cardiac arrhythmias*. Saunders, 2006.

[18] SR Spielman, EL Michelson, LN Horowitz, JF Spear, and EN Moore. The limitations of epicardial mapping as a guide to the surgical therapy of ventricular tachycardia. *Circulation*, 57(4):666–670, 1978.

[19] JM de Bakker, MJ Janse, FJ Van Capelle, and D. Durrer. Endocardial mapping by simultaneous recording of endocardial electrograms during cardiac surgery for ventricular aneurysm. *Journal of the American College of Cardiology*, 2(5):947–953, 1983.

[20] A. Harada, H.J.J.R. D'Agostino, RB Schuessler, JP Boineau, and JL Cox. Potential distribution mapping: new method for precise localization of intramural septal origin of ventricular tachycardia. *Circulation. Supplement*, 78(5):137–147, 1988.

[21] P.A. Friedman. Novel mapping techniques for cardiac electrophysiology, 2002.

[22] A.N. Tikhonov, V.I.A. Arsenin, and F. John. *Solutions of ill-posed problems*. VH Winston Washington, DC, 1977.

[23] E. Delacretaz, K. Soejima, V.K. Gottipaty, C.B. Brunckhorst, P.L. Friedman, and W.G. Stevenson. Single catheter determination of local electrogram prematurity using simultaneous unipolar and bipolar recordings to replace the surface ECG as a timing reference. *Journal Of Pacing And Clinical Electrophysiology*, 24(4 Part 1), 2001.

[24] D. Roy, HL Waxman, MG Kienzle, AE Buxton, FE Marchlinski, and ME Josephson. Clinical characteristics and long-term follow-up in 119 survivors of cardiac arrest: relation to inducibility at electrophysiologic testing. *The American journal of cardiology*, 52(8):969, 1983.

[25] ME Josephson, LN Horowitz, A. Farshidi, and JA Kastor. Recurrent sustained ventricular tachycardia. 1. Mechanisms. *Circulation*, 57(3):431–440, 1978.

[26] F. Morady, M. Harvey, SJ Kalbfleisch, R. El-Atassi, H. Calkins, and JJ Langberg. Radiofrequency catheter ablation of ventricular tachycardia in patients with coronary artery disease. *Circulation*, 87(2):363–372, 1993.

[27] KT Konings, CJ Kirchhof, JR Smeets, HJ Wellens, OC Penn, and MA Allessie. High-density mapping of electrically induced atrial fibrillation in humans. *Circulation*, 89(4):1665–1680, 1994.

[28] J. Sahadevan, K. Ryu, L. Peltz, C.M. Khrestian, R.W. Stewart, A.H. Markowitz, and A.L. Waldo. Epicardial mapping of chronic atrial fibrillation in patients preliminary observations. *Circulation*, 110(21):3293–3299, 2004.

[29] W.G. Stevenson and K. Soejima. Recording techniques for clinical electrophysiology. *Journal of Cardiovascular Electrophysiology*, 16(9):1017–1022, 2005.

[30] G. Bonneau, G. Tremblay, P. Savard, R. Guardo, A.R. LeBlanc, R. Cardinal, P.L. Page, and R.A. Nadeau. An integrated system for intraoperative cardiac activation mapping. *IEEE Transactions on Biomedical Engineering*, pages 415–423, 1987.

[31] FX Witkowski and PB Corr. An automated simultaneous transmural cardiac mapping system. *American Journal of Physiology- Heart and Circulatory Physiology*, 247(4):661–668, 1994.

[32] B. Taccardi, G. Arisi, E. Macchi, S. Baruffi, and S. Spaggiari. A new intracavitary probe for detecting the site of origin of ectopic ventricular beats during one cardiac cycle. *Circulation*, 75(1):272–281, 1987.

[33] Z. Mallat, A. Tedgui, F. Fontaliran, R. Frank, M. Durigon, and G. Fontaine. Evidence of apoptosis in arrhythmogenic right ventricular dysplasia, 1996.

[34] J. Zou, K. Cao, B. Yang, M. Chen, Q. Shan, C. Chen, W. Li, and D.E. Haines. Dynamic substrate mapping and ablation of ventricular tachycardias in right ventricular dysplasia. *Journal of Interventional Cardiac Electrophysiology*, 11(1):37–45, 2004.

[35] M.M. Scheinman. Patterns of catheter ablation practice in the United States: results of the 1992 NASPE survey. *Pacing and Clinical Electrophysiology*, 17(5):873–875, 1994.

[36]

[37] F. Voss, A. Bauer, S. Witte, H.A. Katus, and R. Becker. Can noncontact mapping distinguish between endo-and epicardial foci? *Clinical Research in Cardiology*, 97(10):734–741, 2008.

[38] K.C. Man, E.G. Daoud, B.P. Knight, M. Bahu, R. Weiss, A. Zivin, S.J. Souza, R. Goyal, S.A. Strickberger, and Morady E. Accuracy of the unipolar electrogram for identification of the site of origin of ventricular activation. *Journal of cardiovascular electrophysiology*, 8(9):974–979, 1997.

[39] R. Haberl, G. Jilge, R. Pulter, and G. Steinbeck. Spectral mapping of the electrocardiogram with Fourier transform for identification of patients with sustained ventricular tachycardia and coronary artery disease. *European Heart Journal*, 10(4):316–322, 1989.

[40] R. Haberl, G. Jilge, R. Pulter, and G. Steinbeck. Comparison of frequency and time domain analysis of the signal-averaged electrocardiogram in patients with ventricular tachycardia and coronary artery disease: methodologic validation and clinical relevance. *Journal of the American College of Cardiology*, 12(1):150–158, 1988.

[41] L. Ljung. *System identification: theory for the user*. Prentice-Hall, Inc. Upper Saddle River, NJ, USA, 1986.

[42] S. Mukhopadhyay and P. Sircar. Parametric modelling of ECG signal. *Medical and Biological Engineering and Computing*, 34(2):171–174, 1996.

[43] S.L. Marple Jr and W.M. Carey. Digital spectral analysis with applications. *The Journal of the Acoustical Society of America*, 86:2043, 1999.

[44] H. Akaike. A new look at the statistical model identification. *IEEE transactions on automatic control*, 19(6):716–723, 1974.

[45] PF Fougere. A solution to the problem of spontaneous line splitting in maximum entropy power spectrum analysis. *Journal of Geophysical Research*, 82:1051–1054, 1977.

[46] BS Atal. Effectiveness of linear prediction characteristics of the speech wave for automatic speaker identification and verification. *the Journal of the Acoustical Society of America*, 55:1304, 1974.

[47] W.J. Kang, J.R. Shiu, C.K. Cheng, J.S. Lai, H.W. Tsao, and T.S. Kuo. The application of cepstral coefficients and maximum likelihood method in EMG pattern recognition [movements classification]. *IEEE Transactions on Biomedical Engineering*, 42(8):777–785, 1995.

[48] SPSS Inc. SPSS advanced statistics user's guide. 1990.

[49] S. Mika, G. Ratsch, J. Weston, B. Scholkopf, and KR Mullers. Fisher discriminant analysis with kernels. In *Neural Networks for Signal Processing IX, 1999. Proceedings of the 1999 IEEE Signal Processing Society Workshop*, pages 41–48, 1999.

[50] K. Fukunaga. *Introduction to statistical pattern recognition*. Academic press, 1990.

[51] O. Chapelle, V. Vapnik, O. Bousquet, and S. Mukherjee. Choosing multiple parameters for support vector machines. *Machine Learning*, 46(1):131–159, 2002.

[52] CJ Wolfkiel and BH Brundage. Transfer-function analysis of UFCT myocardial time-density curvesby time-varying recursive least squares analysis. *IEEE Transactions on Biomedical Engineering*, 41(1):69–76, 1994.

[53] C.M. Coulam, H.R. Warner, E.H. Wood, and J.B. Bassingthwaighte. A transfer function analysis of coronary and renal circulation calculated from upstream and downstream indicator-dilution curves. *Circulation Research*, 19(5):879–890, 1966.

[54] Y. Koiwa, R. Hashiguchi, T. Ohyama, S. Isoyama, S. Satoh, H. Suzuki, and T. Takishima. Measurement of instantaneous viscoelastic properties by impedance-frequency curve of the ventricle. *American Journal of Physiology- Heart and Circulatory Physiology*, 250(4):672–684, 1986.

[55] R. Hashiguchi, Y. Koiwa, T. Ohyama, T. Takagi, J. Kikuchi, JP Butler, and T. Takishima. Dependence of instantaneous transfer function on regional ischemic myocardial volume. *Circulation research*, 63(6):1003–1011, 1988.

[56] H. Free. Endocardial mapping and ablation of tachycardia guided by noncontact balloon catheter mapping system. *CMJ*, 6:909–913, 2002.

[57] DM Cassidy, JA Vassallo, FE Marchlinski, AE Buxton, WJ Untereker, and ME Josephson. Endocardial mapping in humans in sinus rhythm with normal left ventricles: activation patterns and characteristics of electrograms. *Circulation*, 70(1):37–42, 1984.

[58] D.J. Callans, J.F. Ren, J. Michele, F.E. Marchlinski, and S.M. Dillon. Electroanatomic left ventricular mapping in the porcine model of healed anterior myocardial infarction Correlation with intracardiac echocardiography and pathological analysis, 1999.

[59] F.E. Marchlinski, D.J. Callans, C.D. Gottlieb, and E. Zado. Linear ablation lesions for control of unmappable ventricular tachycardia in patients with ischemic and nonischemic cardiomyopathy, 2000.

[60] F. Voss, H. Steen, A. Bauer, E. Giannitsis, H.A. Katus, and R. Becker. Determination of myocardial infarct size by noncontact mapping. *Heart Rhythm*, 2007.

[61] L.A. Chinitz and J.S. Sethi. How to perform noncontact mapping. *Heart Rhythm*, 3(1):120–123, 2006.

[62] G. Sivagangabalan, J. Pouliopoulos, K. Huang, J. Lu, M.A. Barry, A. Thiagalingam, D.L. Ross, S.P. Thomas, and P. Kovoor. Comparison of Electroanatomic Contact and Noncontact Mapping of Ventricular Scar in a Postinfarct Ovine Model With Intramural Needle Electrode Recording and Histological Validation. *Circulation: Arrhythmia and Electrophysiology*, 1(5):363, 2008.

[63] R.J. Schilling, N.S. Peters, and D.W. Davies. Simultaneous endocardial mapping in the human left ventricle using a noncontact catheter comparison of contact and reconstructed electrograms during sinus rhythm, 1998.

[64] P.A. Friedman, S.J. Asirvatham, S. Grice, M. Glikson, T.M. Munger, R.F. Rea, W.K. Shen, A. Jahanghir, D.L. Packer, and S.C. Hammill. Noncontact mapping to guide ablation of right ventricular outflow tract tachycardia. *Journal of the American College of Cardiology*, 39(11):1808–1812, 2002.

[65] P. Jais, D.C. Shah, M. Haissaguerre, M. Hocini, J.T. Peng, A. Takahashi, S. Garrigue, P. Le Metayer, and J. Clementy. Mapping and ablation of left atrial flutters, 2000.

[66] I.H. Stevenson, P.M. Kistler, S.J. Spence, J.K. Vohra, P.B. Sparks, J.B. Morton, and J.M. Kalman. Scar-related right atrial macroreentrant tachycardia in patients without prior atrial surgery: electroanatomic characterization and ablation outcome. *Heart Rhythm*, 2(6):594–601, 2005.

[67] A. Thiagalingam, E.M. Wallace, C.R. Campbell, A.C. Boyd, V.E. Eipper, K. Byth, D.L. Ross, and P. Kovoor. Value of noncontact mapping for identifying left ventricular scar in an ovine model, 2004.

[68] P. Della Bella, A. Pappalardo, S. Riva, C. Tondo, G. Fassini, and N. Trevisi. Noncontact mapping to guide catheter ablation of untolerated ventricular tachycardia, 2002.

[69] RM Gulrajani. The forward and inverse problems of electrocardiography. *IEEE Engineering in Medicine and Biology Magazine*, 17(5):84–101, 1998.

[70] R. Mandapati, E.P. Walsh, and J.K. Triedman. Pericaval and periannular intra-atrial reentrant tachycardias in patients with congenital heart disease. *Journal of cardiovascular electrophysiology*, 14(2):119–125, 2003.

[71] H. Nakagawa, N. Shah, K. Matsudaira, E. Overholt, K. Chandrasekaran, K.J. Beckman, P. Spector, J.D. Calame, A. Rao, C. Hasdemir, et al. Characterization of Reentrant Circuit in Macroreentrant Right Atrial Tachycardia After Surgical Repair of Congenital Heart Disease Isolated Channels Between Scars Allow HFocal Ablation, 2001.

[72] B.A. Love, K.K. Collins, E.P. Walsh, and J.K. Triedman. Electroanatomic characterization of conduction barriers in sinus/atrially paced rhythm and association with intra-atrial reentrant tachycardia circuits following congenital heart disease surgery. *Journal of Cardiovascular Electrophysiology*, 12(1):17–25, 2001.

[73] V.Y. Reddy, Z.J. Malchano, G. Holmvang, E.J. Schmidt, A. d'Avila, C. Houghtaling, R.C. Chan, and J.N. Ruskin. Integration of cardiac magnetic resonance imaging with

three-dimensional electroanatomic mapping to guide left ventricular catheter manipulation Feasibility in a porcine model of healed myocardial infarction. *Journal of the American College of Cardiology*, 44(11):2202–2213, 2004.

[74] R.J. Kim, D.S. Fieno, T.B. Parrish, K. Harris, E.L. Chen, O. Simonetti, J. Bundy, J.P. Finn, F.J. Klocke, and R.M. Judd. Relationship of MRI delayed contrast enhancement to irreversible injury, infarct age, and contractile function, 1999.

[75] D. Corrado, C. Basso, L. Leoni, B. Tokajuk, P. Turrini, B. Bauce, F. Migliore, A. Pavei, G. Tarantini, M. Napodano, et al. Three-dimensional electroanatomical voltage mapping and histologic evaluation of myocardial substrate in right ventricular outflow tract tachycardia. *Journal of the American College of Cardiology*, 51(7):731, 2008.

[76] JL Cox, TE Canavan, RB Schuessler, ME Cain, BD Lindsay, C. Stone, PK Smith, PB Corr, and JP Boineau. The surgical treatment of atrial fibrillation. II. Intraoperative electrophysiologic mapping and description of the electrophysiologic basis of atrial flutter and atrial fibrillation. *The Journal of thoracic and cardiovascular surgery*, 101(3):406–426, 1991.

[77] C.C. Gornick, S.W. Adler, B. Pederson, J. Hauck, J. Budd, and J. Schweitzer. Validation of a new noncontact catheter system for electroanatomic mapping of left ventricular endocardium. *Circulation*, 99(6):829–835, 1999.

[78] A. Kadish, J. Hauck, B. Pederson, G. Beatty, and C. Gornick. Mapping of atrial activation with a noncontact, multielectrode catheter in dogs. *Circulation*, 99(14):1906–1913, 1999.

[79] N.S. Peters, W.M. Jackman, R.J. Schilling, G. Beatty, and D.W. Davies. Human left ventricular endocardial activation mapping using a novel noncontact catheter. *Circulation*, 95(6):1658–1660, 1997.

[80] L. Gepstein, G. Hayam, and S.A. Ben-Haim. A novel method for nonfluoroscopic catheter-based electroanatomical mapping of the heart In vitro and in vivo accuracy results. *Circulation*, 95(6):1611–1622, 1997.

[81] T.I. Betts, P.R. Roberts, S.A. Aelen, and J.M. Morgan. Radiofrequency ablation of idiopathic left ventricular tachycardia at the site of earliest activation as determined by noncontact mapping. *Journal of Cardiovascular Electrophysiology*, 11(10):1094–1101, 2000.

[82] T. Paul, A.T.D. Blaufox, and J.P. Saul. Non-contact mapping and ablation of tachycardia originating in the right ventricular outflow tract. *Cardiology in the Young*, 12(03):294–297, 2006.

[83] P.C. Dorostkar, JIE Cheng, and M.M. Scheinman. Electroanatomical mapping and ablation of the substrate supporting intraatrial reentrant tachycardia after palliation for complex congenital heart disease. *Pacing and Clinical Electrophysiology*, 21(9):1810–1819, 1998.

[84] Friedman PL Stevenson WG, Delacretaz E. Identification and ablation of macro reentrant ventricular tachycardia with the CARTO electroanatomical mapping system. *Pacing and Clinical Electrophysiology*, 21:1445–1456, 1998.

[85] E. Stålberg, S. Andreassen, B. Falck, H. Lang, A. Rosenfalck, and W. Trojaborg. Quantitative analysis of individual motor unit potentials: a proposition for standardized terminology and criteria for measurement. *Journal of clinical neurophysiology*, 3(4):313, 1986.

[86] S. Willems, C. Weiss, R. Ventura, R. Ruppel, Tim Risius, M. Hoffmann, and T. Meinertz. Catheter ablation of atrial flutter guided by electroanatomic mapping (CARTO): a randomized comparison to the conventional approach. *Journal of Cardiovascular Electrophysiology*, 11(11):1223–1230, 2000.

[87] M. Kroll, T. Kriebel, B. Windhagen-Mahnert, B. Franzbach, C. Jux, M. Zutz, J. Tebbenjohanns, and T. Paul. Differentiation by Electrogram Characteristics Using the Noncontact Mapping System. *Pacing and Clinical Electrophysiology*, 26(10):1970–1978, 2003.

[88] W. Whitwam, S. Rule, and S.M. Narayan. Noncontact mapping of small pulmonary artery potentials preceding ectopy from the right ventricular outflow tract. *Heart Rhythm*, 4(7):959–963, 2007.

[89] J. Shao. An asymptotic theory for linear model selection. *Statistica Sinica*, 7:221–242, 1997.

[90] JM Mendel. Tutorial on higher-order statistics (spectra) in signal processingand system theory: theoretical results and some applications. *Proceedings of the IEEE*, 79(3):278–305, 1991.

[91] C.L. Nikias and A.P. Petropulu. *Higher-order spectra analysis: a nonlinear signal processing framework.* Prentice Hall, 1993.

[92] CL Nikias and JM Mendel. Signal processing with higher-order spectra. *IEEE Signal Processing Magazine*, 10(3):10–37, 1993.

[93] RM Rangayyan, S. Krishnan, GD Bell, CB Frank, and KO Ladly. Parametric representation and screening of knee jointvibroarthrographic signals. *IEEE Transactions on Biomedical Engineering*, 44(11):1068–1074, 1997.

[94] C.S. Pattichis and A.G. Elia. Autoregressive and cepstral analyses of motor unit action potentials. *Medical Engineering and Physics*, 21(6-7):405–419, 1999.

[95] S.K. Mitra. Digital signal processing: a computer-based approach. 1998.

[96] K. Hoyt, F. Forsberg, and J. Ophir. Investigation of parametric spectral estimation techniques for elasticity imaging. *Ultrasound in medicine & biology*, 31(8):1109–1121, 2005.

[97] Y. Koiwa, R. Hashiguchi, T. Ohyama, S. Isoyama, S. Satoh, H. Suzuki, and T. Takishima. Measurement of instantaneous viscoelastic properties by impedance-frequency curve of the ventricle. *American Journal of Physiology- Heart and Circulatory Physiology*, 250(4):672–684, 1986.

[98] J.R. Treichler, C.R. Johnson Jr, and M.J. Larimore. *Theory and design of adaptive filters*. Wiley-Interscience New York, NY, USA, 1987.

[99] S. Krishnan, RM Rangayyan, GD Bell, CB Frank, and KO Ladly. Recursive least squares-lattice based adaptive segmentation, and autoregressive modeling of nonstationary vibroarthrographic signals. In *Proc. Canadian Conf. Electrical and Computer Engineering*, pages 339–342.

[100] D.G. Manolakis, V.K. Ingle, and S.M. Kogon. *Statistical and adaptive signal processing*. McGraw-Hill Boston, 2000.

[101] S. Tavathia, R.M. Rangayyan, and C.B. Frank. Analysis of knee vibration signals using linear prediction. *IEEE Transactions on Biomedical Engineering*, 39(9):959, 1992.

[102] D.J. Abrams, M.J. Earley, S.C. Sporton, P.M. Kistler, M.A. Gatzoulis, M.J. Mullen, J.A. Till, S. Cullen, F. Walker, M.D. Lowe, et al. Comparison of noncontact and electroanatomic mapping to identify scar and arrhythmia late after the Fontan procedure. *Circulation*, 115(13):1738, 2007.

[103] T. Paul, J.P. Moak, C. Morris, and A. Garson. Epicardial mapping: how to measure local activation? *Pacing and Clinical Electrophysiology*, 13(3):285–292, 1990.

[104] M. Kroll, T. Kriebel, B. Windhagen-Mahnert, B. Franzbach, C. Jux, M. Zutz, J. Tebbenjohanns, and T. Paul. Origin of electrical activation within the right atrial and left ventricular walls: differentiation by electrogram characteristics using the noncontact mapping system. *Pacing and clinical electrophysiology: PACE*, 26(10):1970, 2003.

[105] L.L. Skrumeda and R. Mehra. Comparison of standard and irrigated radiofrequency ablation in the canine ventricle. *Journal of cardiovascular electrophysiology*, 9(11):1196–1205, 1998.

[106] DE Roberts, LT Hersh, and AM Scher. Influence of cardiac fiber orientation on wavefront voltage, conduction velocity, and tissue resistivity in the dog. *Circulation Research*, 44(5):701–712, 1979.

[107] D.S. Khoury, B. Taccardi, R.L. Lux, P.R. Ershler, and Y. Rudy. Reconstruction of endocardial potentials and activation sequences from intracavitary probe measurements Localization of pacing sites and effects of myocardial structure. *Circulation*, 91(3):845–863, 1995.